EFFICIENT PRODUCTION OPTIMIZATION USING FLOW NETWORK MODELS

A Thesis

by

PONGSATHORN LERLERTPAKDEE

Submitted to the Office of Graduate Studies of
Texas A&M University
in partial fulfillment of the requirements for the degree of

MASTER OF SCIENCE

August 2012

Major Subject: Petroleum Engineering

Efficient Production Optimization Using Flow Network Models

EFFICIENT PRODUCTION OPTIMIZATION USING FLOW NETWORK MODELS

A Thesis

by

PONGSATHORN LERLERTPAKDEE

Submitted to the Office of Graduate Studies of
Texas A&M University
in partial fulfillment of the requirements for the degree of

MASTER OF SCIENCE

Approved by:

Co-Chairs of Committee,	Eduardo Gildin
	Behnam Jafarpour
Committee Member,	Shankar Bhattacharyya
Head of Department,	Daniel Hill

August 2012

Major Subject: Petroleum Engineering

ABSTRACT

Efficient Production Optimization Using Flow Network Models. (August 2012)

Pongsathorn Lerlertpakdee, B.Eng., Chulalongkorn University

Co-Chairs of Advisory Committee: Dr. Eduardo Gildin
Dr. Behnam Jafarpour

Reservoir simulation is an important tool for decision making and field development management. It enables reservoir engineers to predict reservoir production performance, update an existing model to reproduce monitoring data, assess alternative field development scenarios and design robust production optimization strategies by taking into account the existing uncertainties. A big obstacle in automating model calibration and production optimization approaches is the massive computation required to predict the response of real reservoirs under proposed changes in the model inputs. To speed up reservoir response predictions without compromising accuracy, fast surrogate models have been proposed. These models are either derived by preserving the physics of the involved processes (e.g. mass balance equations) to provide reliable long-range predictions or are developed based solely on statistical relations, in which case they can only provide short-range predictions due to the absence of the physical processes that govern the long-term behavior of the reservoir.

We present an alternative solution that combines the advantages of both statistics-based and physics-based methods by deriving the flow predictions in complex two-dimensional models from one-dimensional flow network models. The existing

injection/production wells in the original model form the nodes or vertices of the flow network. Each pair of wells (nodes) in the flow network is connected using a one-dimensional numerical simulation model; hence, the entire reservoir is reduced to a connected network of one-dimensional simulation models where the coupling between the individual one-dimensional models is enforced at the nodes where network edges intersect. The proposed flow network model provides a useful and fast tool for characterizing inter-well connectivity, estimating drainage volume between each pair of wells, and predicting reservoir production over an extended period of time for optimization purposes.

We estimate the parameters of the flow network model using a robust training approach to ensure that the flow network model reproduces the response of the original full model under a wide range of development strategies. This step helps preserve the flow network model's predictive power during the production optimization when development strategies can change at different iterations. The robust networks training and the subsequent production optimization iterations are computationally efficient as they are performed with the faster flow network model. We demonstrate the effectiveness and applicability of our proposed flow network modeling approach to rapid production optimization using two-phase waterflooding simulations in synthetic and benchmark models.

DEDICATION

To my family and friends

ACKNOWLEDGEMENTS

I would like to thank my committee chairs, Dr. Gildin and Dr. Jafarpour and my committee member, Dr. Bhattacharyya, for their guidance and support throughout the course of this research.

Thanks also to my friends and colleagues who always help me when I have any problem, and the department faculty and staff for making my time at Texas A&M University a great experience. I also want to extend my gratitude to PTT Exploration and Production Public Company Limited, my employer, who provided the scholarship and supported me throughout my graduate program.

Finally, thanks to my family for their encouragement and to my girlfriend for her patience and love.

NOMENCLATURE

β_c	unit conversion factor for the flow terms
k	total permeability
k_x	permeability in the direction along the flow path
k_y	permeability in the direction perpendicular to the flow path
A_x	cross-sectional area perpendicular to the direction of flow
k_r	relative permeability of the interested phase to the total permeability
k_{rw}	relative permeability to the water phase
k_{ro}	relative permeability to the oil phase
μ_w	water viscosity
μ_o	oil viscosity
B_w	water formation volume factor
B_o	oil formation volume factor
p_w	water phase pressure
p_o	oil phase pressure
γ_w	water gravity or density
γ_o	oil gravity or density
Z	elevation from the datum
h	well-block thickness
Δx	incremental distance in flow direction / grid block dimension in the direction along the flow path

Δy	grid block dimension in the direction perpendicular to the flow path
V_b	bulk volume of the interested control volume
α_c	unit conversion factor for the accumulation terms
ϕ	porosity
S_w	water saturation in the pore volume
S_o	oil saturation in the pore volume
p_{cow}	oil-water capillary pressure
$q_{w_{sc}}$	source/sink term of the water phase, measured at the standard condition
$q_{o_{sc}}$	source/sink term of the oil phase, measured at the standard condition
${T_{wx_{i,j}}}^n$	transmissibility of water at location (i,j) evaluated at time-step n
${T_{ox_{i,j}}}^n$	transmissibility of oil at location (i,j) evaluated at time-step n
d_{wp_i}	coefficient of pressure difference in the accumulation term in water equation of cell i
d_{ws_i}	coefficient of saturation difference in the accumulation term in water equation of cell i
d_{op_i}	coefficient of pressure difference in the accumulation term in cell i oil equation
d_{os_i}	coefficient of saturation difference in the accumulation term in cell i oil equation
WI	Peaceman's well index

μ	viscosity of the interested phase
B	formation volume factor of the interested phase
r_o	equivalent wellbore radius
r_w	actual wellbore radius
s	skin factor
p_o	well-block pressure
p_{wf}	wellbore flowing pressure
q	flow rate in standard condition
T^n	transmissibility matrix evaluated at the current time-step
D^n	accumulation matrix evaluated at the current time-step
Q^{n+1}	source/sink vector evaluated using new time-step pressure but with the well index evaluated at the current time-step
X^{n+1}	state vector of the new time-step
X^n	state vector of the current time-step
$wcut$	water cut
nw	total number of wells
na	total number of connections
nx	number of grids in each connection (user defined)
ng	total number of grids in the system
$ObjFn$	objective function value to be minimized (scalar)
$g(m)_n$	model response from the flow network model using the n^{th} control trajectory (vector of length no)

m	parameters to be varied (vector of length np), $dy\ and\ k$ of each grid
d_{obs_n}	observed data from the full-order model using the nth control trajectory (vector of length no)
W_n	weight matrix of the nth realization (square matrix of dimension $no \times no$)
$J(u^n)$	objective function in production optimization, NPV of the project
u^n	control trajectory, how each well is controlled
$FOPR^n$	field oil production rate at time-step n
$FWPR^n$	field water production rate at time-step n
$FWIR^n$	field water injection rate at time-step n
i_{op}	income for each barrel of oil production
c_{wp}	cost for each barrel of water production
c_{wi}	cost for each barrel of water injection
Δt^n	time interval at time-step n
b	discount factor

TABLE OF CONTENTS

Page

Page

LIST OF FIGURES

Page

Page

Page

LIST OF TABLES

Page

INTRODUCTION AND LITERATURE REVIEW

Introduction

Our days of easily producible oil and gas are over. Increasing recovery of the fossil fuel by only a small percentage can significantly affect the accumulation of the reserves and the profitability of the current and future assets, especially given the current global economic and environmental demands and concerns.

Development in diverse areas in petroleum engineering such as drilling, enhanced oil recovery (EOR), and data management allowed some improvements in recovery process. In addition, the oil and gas companies realize that the introduction of fast and more accurate reservoir management concepts can yield more recovery. To this end, efficient optimization methods can leverage these gains.

With the natural production mechanism, oil recovery efficiency can be as low as 5-15%. In some cases, where reservoirs are in contact with natural aquifers or big gas caps, they would help maintain reservoir pressure and hence improving production. However, in the absence of these pressure supports, a pressure maintenance program should be designed by either gas or water injection. This is indeed the most common practice in the industry. This secondary recovery could raise the recovery factor to be higher, average of 35-45%. After the field is maturely developed under secondary production mechanism, tertiary recovery or enhanced oil recovery technique could be

---

This thesis follows the style of *SPE Journal*.

implemented to squeeze additional 5-15% of oil in place. In all these cases, it can be seen that some of the hydrocarbons are still left underground. Some of these secondary and tertiary recoveries are related to fluid injection, which has two main mechanisms, namely pressure maintenance and sweep effect. The latter one is quite difficult to manage without a proper tool.

Modern workflow processes can provide a better decision making tool by integrating geological and geophysical knowledge with the historical and real-time production data. These data can be used to build a more accurate reservoir model, which in turn, can be used as a tool to improve the production strategies. With the aid of the modern powerful computers, these workflows could be a great tool for petroleum engineers to better understand the reservoir dynamics, and hence efficiently develop the underground resources.

Recently, the idea of closed loop reservoir management (CLRM) has gained more attention. It is shown to be beneficial to the overall oil-field operation and reservoir development. Many researches are concentrated on this idea (Jansen et al. 2005; Jansen et al. 2008). The overall concept of CLRM is illustrated in Figure 1.

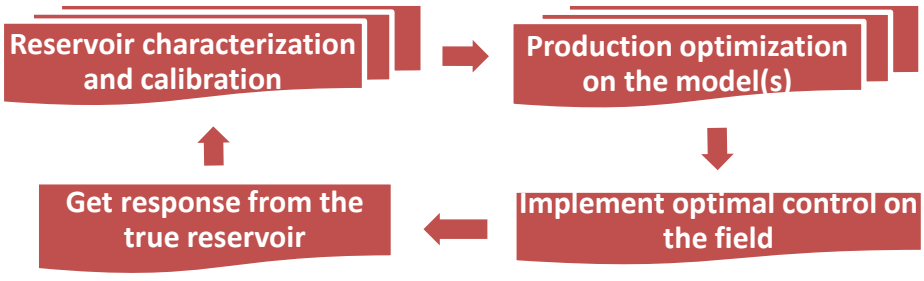

Figure 1: Simplified closed loop reservoir management idea

Petroleum engineers normally deal with limited amount of data. Data that normally have good areal coverage like seismic data, which characterizing how the subsurface structure looks or sometimes also implies the fluid type contained in the structure, would have high uncertainty. The other types of data like well logs or other well related data can be measured quite accurately, but it only covers a very small portion of the reservoir. Combining these data together, sometimes with dynamic data like well testing, the reservoir models can be constructed. The reservoir is discretized into many small grid blocks containing information like porosity and permeability. These data are normally only available at the well location, which is very sparse relative to the reservoir size. In the grid blocks where there is no hard data, these parameters are assigned with the aid of geostatistical technique. There are many models that can give the same injection/production response, and the 'real' subsurface reservoir is actually unknown; therefore, many models are normally built and assessed to cover the uncertainties.

These models need to be calibrated to the production history. This is to make sure that the model can reproduce the response from the reservoir using the same control input. The ability to reproduce the response from the reservoir would imply the predictive capability of the model to be further used for prediction or production optimization. History matching is notoriously known to be an ill-posed problem; many solutions can give the similar quality of match. Hence, multiple realizations also exist in the process. The process could be automated using the optimization algorithms.

Once the models are built and calibrated, taking the uncertainties into account, optimal control theory can play an important role in finding the best production strategy (Alhuthali et al. 2007; Brouwer and Jansen 2002; van Essen et al. 2006; Jansen et al. 2008). This process is also normally automated by mathematical algorithms. The objective of production optimization could be maximizing oil production, penalizing water production and water injection, or maximizing NPV of the project, taking into account of discounted income, capital cost, and operating cost. In addition, optimization can also be used to find the optimal location to drill the well. This is known as the well placement problem. The optimization processes itself is an iterative method, which requires many simulation runs, could be as many as hundreds or thousands, or more, to get to the optimal solution.

Basically, multiple geological models are built to account for the uncertainties. Each of them is calibrated to the production history. The predictive model is then used for production optimization to find the optimal production strategy. Once it is implemented in the field, the discrepancy between the actual response and prediction is used to update the models. It is called in the closed loop reservoir management because the feedback from the real field is used in to improve the model prediction capability, and hence more precise production strategy can be found and implemented to improve the recovery.

Motivation

From the idea of CLRM introduced previously, it can be seen that the history matching and production optimization are very computationally demanding processes.

Especially when it is implemented in the uncertainty quantification paradigm, many simulation runs are required to evaluate the model responses with respect to the changes in the model inputs. This sometimes makes it impossible to apply the CLRM concept to the 'real world' problem where the reservoir model is defined by millions of grid blocks. In this case, each simulation run could take hours or days to be completed.

In order to overcome this computational burden, many initiatives in reduced-order modeling have been researched. A central objective is to speed up the simulation runs. Some of the reduced-order modeling techniques are derived by preserving the physics of the involved processes, e.g. mass balance equations, to provide reliable long-term predictions. These methods involve the use of mathematical manipulation to obtain the problem of smaller size. This complex mathematical manipulation could be quite difficult to understand. Some methods require information from the full-order model to be used in model construction. On the other hand, some reduced-order models are developed on the more simplified physics; some are even based solely on the statistical relationship between inputs and outputs. In this case, they can only provide the short-term predictions due to the absence of the physical processes that govern the long-term behavior of the reservoir. However, one of the advantages of this type of model is that it can be built from only injection/production data. Many research projects (Cardoso and Durlofsky 2010; Sayarpour 2008; van Doren et al. 2006; Weber 2009) have applied the reduced-order modeling for production optimization.

In this thesis, the goal is to obtain reduced-order models that can combine the strengths of both approaches in an optimal fashion. The developed reduced-order models

will be used as surrogate models for a more efficient production optimization. The idea is to define the model based on the input-output, i.e. production-injection relationship. In this case, the physics of flow in porous media will be simplified, but not totally ignored, such that the long term prediction capability is preserved.

Literature Review

Recently, the oil and gas industry has started deploying reduced-order modeling into the production optimization process. Many papers about the application of reduced-order modeling in production optimization are available. Selected papers will be discussed in this section.

van Doren et al. (2006) utilize the reduced-order model for production optimization. Proper orthogonal decomposition (POD), also known as principal component analysis, is used to generate the low-order models using snapshots of states from the forward simulation using the original high-order models. The authors then utilize reduced-order model for production optimization.

For the POD model reduction, the concept is to project the original model states into the lower order subspace. It can be viewed as a projection of the original large state space model onto the smaller dimensional space. This is done so that the overall energy of the system is maintained at 90-100% of the original model.

They demonstrate the method for production optimization in the waterflood problem. They use adjoint-based optimal control methodology to perform optimization on the low-order model. The results are then verified with the original high-order model. The process is repeated if it is necessary to do so. If the result of optimization on the

low-order model is applied on the high-order model and is found not to be optimal, then the model reduction would be performed using the new snapshots from the verification run, and the production optimization would also be repeated. They call the implementation framework a 'nested approach'. Basically, the simulated states from the low-order model are almost identical to the high-order model when the control trajectory is the same as the one used in the high-order model. However, if the control is extremely altered, the structures of the states of the high-order model are less well represented by the reduced-order model.

In summary, van Doren et al. (2006) suggest that the procedure is very good for reservoir models with dominant large-scale geological features. It will be less beneficial to use the method with the reservoir models with small correlation length.

POD can reduce the dimension of the problem significantly. However, Cardoso and Durlofsky (2010) point out that the degree of speed-up is limited in the standard procedure of POD for nonlinear problems. The standard POD procedure works at the level of the linear solver. However, the computational efforts for some operations, e.g. construction of Jacobian matrix, are not reduced at all. To overcome this problem, they applied the linearization procedure, specifically the trajectory piecewise linearization (TPWL), to the governing equations in addition to the reduced-order modeling using POD. In other words, they applied the POD framework on the linearized system.

The method works by pre-determining the states and converged Jacobian matrices, which are determined in the training simulation runs. A basis matrix is then constructed from the states, saved from training simulation runs, using POD. This basis

matrix is then used to calculate the reduced states and reduced Jacobian matrices. In the subsequent simulation runs, new states can be obtained by linear expansions around the previously pre-determined reduced states and Jacobians. This procedure is computationally efficient because it is conducted in the reduced space. It has shown significant improvement in term of speed-up, compared to the standard POD procedure.

In summary, these afore mentioned reduced-order modeling techniques are considered to be the physical-based type. The speed-up is gained from mathematical manipulation. In order to use these methods, the full order reservoir model is assumed to be known.

Some other model reduction techniques are developed based on the more simplified physics, in particular, based on the wells/reservoirs input-output relationships. The Capacitance-Resistance Model (CRM) is developed to describe interactions between injectors and producers in the reservoirs. More detail about the CRM development and its application can be found in Sayarpour (2008) and Weber (2009).

CRM is an input-output model that can be developed from only the injection/production data. The total injection rates are considered to be the input signals, while the total production rates are considered to be the output signals. The method is derived from the equivalency between the porous media flow and the electrical network models, so that the electrical potential is converted into voltage or current in a resistor-capacitor circuit. It is initially developed using multivariate linear regression with diffusivity filters. The model has been improved continuously. It is also used as a tool to perform production optimization to increase recovery by manipulating injection rates.

The advantage of the model is that reservoir performance predictions can be done very quickly. In the CRM model, the production responses are given in total liquid production rates. Water and oil can be differentiated using the separate fractional flow models. Hence, if there is no water-breakthrough in the production history, CRM will predict the reservoir performance without any water production.

From the previous discussions, it can be seen that some reduced-order modeling techniques depend on mathematical manipulation, which is sometimes difficult to understand and not familiar by most petroleum engineers. Some of them require only simple data such as injection/production data, but might not be accurate for long-term prediction.

Considering both the pros and cons of each technique, an alternative method that combines the strengths of each approach is proposed. It must be rapid, easy to understand, and require less data. Furthermore, prior knowledge of the reservoir can be used to improve the predictive power of the model.

Scope of Study

This work proposes an alternative to the existing reduced-order modeling techniques. The proposed technique will not only speed up the calculations, but will maintain the long-term prediction capabilities. The reduced-order models will be used as surrogate models in production optimization processes. In addition, the mathematical formulation is derived from finite difference method, which is standard in reservoir simulation.

The main idea is to build models based on the injection/production information. Instead of trying to define all the spatial properties, like porosity and permeability, only relationships between the output behavior of the reservoir from the given input production strategy are investigated and used in the processes. To do this, each pair of wells is connected with a one-dimensional finite difference reservoir simulation model. Since every well is connected to one another, a network of one-dimensional reservoir models is obtained. The important parameters that govern the fluid flow in each connection are how much fluid is contained in the drainage area in that specific connection and the reservoir quality, which will dictate the pressure drop along the flow path. It can be seen that the spatial reservoir model is transformed into the flow network model with much fewer parameters. The same physics of flow in porous media are still maintained, but the physical dimension is reduced.

Unlike the conventional reservoir models, the parameters in the flow network models depend very much on the dynamic status of reservoirs. Hence, the models need to be calibrated to the production data generated from the full-order models. Assuming full access to the full-order models, one can generate any responses from the full-order models; these do not have to be the same as one in the production history. In this case, the models will be used to perform production optimization, in which the models will be prescribed with wide ranges of control trajectories, i.e. how to control the injectors and producers. It would be better to have models that are less sensitive to the control trajectory. This can be achieved by calibrating the models against multiple sets of control trajectories.

The calibrated flow network models can be used as surrogate models for a much less expensive production optimization. Basically, once the full-order models are characterized and calibrated to the real production data, the flow networks, reduced-order models, are generated and calibrated against the full-order models. The flow network models, instead of the full-order models, will be used to perform production optimization. The CLRM idea in Figure 1 can be replaced by Figure 2. To illustrate how the idea works, a few synthetic field examples will be demonstrated.

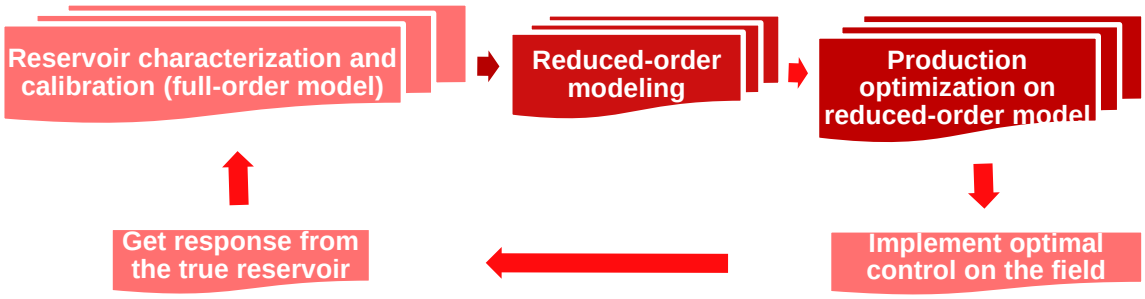

Figure 2: Simplified closed loop reservoir management using surrogate model in production optimization

MODEL CONSTRUCTION

In conventional reservoir simulation models, the reservoir is discretized into many grid blocks; each of them is defined by spatial properties, e.g. porosity and permeability. Each block is considered as the control volume, which has fluid flowing in and out. The physics of flow involves mass balance of fluid in the control volume, flow equation, which dictates flow between grids, and equation of states of the fluid. Grid connections are defined by their spatial location relative to the others.

In this work, the flow network model is introduced. The existing injection/production wells in the original model form the nodes or vertices of the flow network. Each pair of wells (nodes) in the flow network is connected using a one-dimensional numerical simulation model; hence, the entire reservoir is reduced to a connected network of one-dimensional simulation models, where the coupling between the individual one-dimensional flow models is enforced at the nodes where network edges intersect. The proposed network model provides a useful and fast tool for characterizing inter-well connectivity, estimating drainage volume between each pair of wells, and predicting reservoir production over an extended period of time for optimization purposes.

In this section, the basic governing equations of the subsurface flow will be covered; only two-phase oil-water fluid model is used in this work. First, the basic equations for one-dimensional simulation model are shown. Then, how the conventional model can be modified to get the flow network model is discussed.

Basic Flow Equations

Multiphase flow in petroleum reservoir involves the simultaneous flow of oil, water, and gas. This multiphase flow transports multiple fluid components. In the case of black oil models, the fluid components are oil, water, and gas. Oil and water are assumed to be immiscible; hence, there is no mass transfer between these two phases. Gas can be soluble in oil, but not in water. Therefore, the gas component can occur in both oil and gas phases. The portion of gas soluble in oil is generally called solution gas. In this research, only two-phase oil-water flow is studied.

The physics of fluid flow in porous media can be described by three major equations, namely mass conservation, flow equation, and equation of states. Full derivation would not be shown here. Only some equations that are used to create the flow network model concept are shown. More detail derivation can be found in reservoir simulation text books (Aziz and Settari 1979; Ertekin et al. 2001). Basically, the interpretation of these equations is that the difference of fluid flowing in and out of the control volume is equal to the rate of accumulation of that fluid in the control volume. The two-phase flow equations of water and oil in one-dimensional flow are described in equations (1) and (2).

$$\frac{\partial}{\partial x}\left[\beta_c k_x A_x \frac{k_{rw}}{\mu_w B_w}\left(\frac{\partial p_w}{\partial x} - \gamma_w \frac{\partial Z}{\partial x}\right)\right]\Delta x = \frac{V_b}{\alpha_c}\frac{\partial}{\partial t}\left(\frac{\phi S_w}{B_w}\right) - q_{w_{sc}} \quad \textbf{(1)}$$

$$\frac{\partial}{\partial x}\left[\beta_c k_x A_x \frac{k_{ro}}{\mu_o B_o}\left(\frac{\partial p_o}{\partial x} - \gamma_o \frac{\partial Z}{\partial x}\right)\right]\Delta x = \frac{V_b}{\alpha_c}\frac{\partial}{\partial t}\left(\frac{\phi S_o}{B_o}\right) - q_{o_{sc}} \quad \textbf{(2)}$$

where

β_c is a unit conversion factor for the flow terms

k_x is a permeability in the direction along the flow path

A_x is the cross-sectional area perpendicular to the direction of flow

k_{rw} is the relative permeability to the water phase

k_{ro} is the relative permeability to the oil phase

μ_w is the water viscosity

μ_o is the oil viscosity

B_w is the water formation volume factor

B_o is the oil formation volume factor

p_w is the water phase pressure

p_o is the oil phase pressure

γ_w is the water gravity or density

γ_o is the oil gravity or density

Z is the elevation from the datum

Δx is the incremental distance in flow direction

V_b is the bulk volume of the interested control volume

α_c is the unit conversion factor for the accumulation terms

ϕ is the porosity

S_w is the water saturation in the pore volume

S_o is the oil saturation in the pore volume

$q_{w_{sc}}$ is the source/sink term of the water phase, measured at the standard condition

$q_{o_{sc}}$ is the source/sink term of the oil phase, measured at the standard condition

In equations (1) and (2), there are four unknowns, namely oil phase pressure (p_o), water phase pressure (p_w), oil saturation (S_o), and water saturation (S_w). Hence, an additional two equations are required to solve the above system. These two equations are the saturation equation, which limits the total saturation to be unity, and the capillary pressure equation, which relates the water pressure to the oil pressure. The two equations are given in equations (3) and (4), respectively.

$$S_w + S_o = 1 \quad \textbf{(3)}$$

$$p_{cow} = p_o - p_w \quad \textbf{(4)}$$

For this research, capillary and gravity effects are neglected. They are explicitly expressed in equations (5) and (6), respectively.

$$p_{cow} = 0 \rightarrow p_o = p_w \quad \textbf{(5)}$$

$$\frac{\partial Z}{\partial x} = 0 \quad \textbf{(6)}$$

The number of unknowns is reduced down from four to two. In this case, oil phase pressure and water saturation are selected as unknowns for the system of equations. Hence, the previous flow equations can be written as equations (7) and (8).

$$\frac{\partial}{\partial x}\left[\beta_c k_x A_x \frac{k_{rw}}{\mu_w B_w}\left(\frac{\partial p_o}{\partial x}\right)\right]\Delta x = \frac{V_b}{\alpha_c}\frac{\partial}{\partial t}\left(\frac{\phi S_w}{B_w}\right) - q_{w_{sc}} \quad \textbf{(7)}$$

$$\frac{\partial}{\partial x}\left[\beta_c k_x A_x \frac{k_{ro}}{\mu_o B_o}\left(\frac{\partial p_o}{\partial x}\right)\right]\Delta x = \frac{V_b}{\alpha_c}\frac{\partial}{\partial t}\left(\frac{\phi(1 - S_w)}{B_o}\right) - q_{o_{sc}} \quad \textbf{(8)}$$

The terms, on the left hand side of equations (7) and (8), account for the flow into and out of the control volume of the two phases, while the first terms, on the right hand side, account for the rate of accumulation of both phases in the control volume. The

second terms, on the right hand side, represent external source and sink terms. They are for the injection into and production from the reservoir using the injectors and producers.

Finite Difference Discretization

Previously, the partial differential equations (p.d.e.) describing the oil-water flow in porous media are shown. In some cases, where further simplification can be made, the p.d.e. can be solved with analytical techniques. However, for some 'real world' applications, this becomes a daunting, if not impossible, task. One of the most popular techniques that can be used to solve the p.d.e. is the finite difference technique. The reservoir p.d.e. is discretized in both time and space to obtain the algebraic equations that can be solved simultaneously. Discretization of the p.d.e. is shown next.

To begin with, discretization of the flow terms in space is manipulated. By looking at the left hand side term in the water flow equation, equation (7), the discretization in space becomes:

$$\frac{\partial}{\partial x}\left[\beta_c k_x A_x \frac{k_{rw}}{\mu_w B_w}\left(\frac{\partial p_o}{\partial x}\right)\right]\Delta x = \left[\beta_c k_x A_x \frac{k_{rw}}{\mu_w B_w}\left(\frac{\partial p_o}{\partial x}\right)\right]_{i+\frac{1}{2}} - \left[\beta_c k_x A_x \frac{k_{rw}}{\mu_w B_w}\left(\frac{\partial p_o}{\partial x}\right)\right]_{i-\frac{1}{2}} \quad \textbf{(9)}$$

Here, the term called transmissibility of water, T_{wx}, is introduced as shown in equation (10). The transmissibility contains the geometrical factor of the flow between the two adjacent grids, and the pressure and saturation dependent parameters like formation volume factor, viscosity, and the relative permeability.

$$T_{wx} = \beta_c k_x A_x \frac{k_{rw}}{\mu_w B_w} \quad \textbf{(10)}$$

We can re-arrange equation (9) and use the definition of the water transmissibility to obtain equations (11) and (12).

$$\frac{\partial}{\partial x}\left[\beta_c k_x A_x \frac{k_{rw}}{\mu_w B_w}\left(\frac{\partial p_o}{\partial x}\right)\right]\Delta x = \left[\beta_c \frac{k_x A_x}{\Delta x}\frac{k_{rw}}{\mu_w B_w}\left(p_{o_{i+1}} - p_{o_i}\right)\right] + \left[\beta_c \frac{k_x A_x}{\Delta x}\frac{k_{rw}}{\mu_w B_w}\left(p_{o_{i-1}} - p_{o_i}\right)\right] \quad \textbf{(11)}$$

$$\frac{\partial}{\partial x}\left[\beta_c k_x A_x \frac{k_{rw}}{\mu_w B_w}\left(\frac{\partial p_o}{\partial x}\right)\right]\Delta x = \left[T_{wx_{i+\frac{1}{2}}}\left(p_{o_{i+1}} - p_{o_i}\right)\right] + \left[T_{wx_{i-\frac{1}{2}}}\left(p_{o_{i-1}} - p_{o_i}\right)\right] \quad \textbf{(12)}$$

For the oil equation, the discretization can be done in a similar fashion. Transmissibility of the oil phase would be used instead of water. Thus, the flow term of oil phase in equation (8) can be written as in equation (13).

$$\frac{\partial}{\partial x}\left[\beta_c k_x A_x \frac{k_{ro}}{\mu_o B_o}\left(\frac{\partial p_o}{\partial x}\right)\right]\Delta x = \left[T_{ox_{i+\frac{1}{2}}}\left(p_{o_{i+1}} - p_{o_i}\right)\right] + \left[T_{ox_{i-\frac{1}{2}}}\left(p_{o_{i-1}} - p_{o_i}\right)\right] \quad \textbf{(13)}$$

For the first terms on the right hand side of equations (7) and (8), i.e. the accumulation terms, discretization in time can be done as in equations (14) and (15).

$$\frac{V_b}{\alpha_c}\frac{\partial}{\partial t}\left(\frac{\phi S_w}{B_w}\right) = \frac{V_b}{\alpha_c \Delta t}\left[\left(\frac{\phi S_w}{B_w}\right)^{n+1} - \left(\frac{\phi S_w}{B_w}\right)^{n}\right] \quad \textbf{(14)}$$

$$\frac{V_b}{\alpha_c}\frac{\partial}{\partial t}\left(\frac{\phi(1-S_w)}{B_o}\right) = \frac{V_b}{\alpha_c \Delta t}\left[\left(\frac{\phi(1-S_w)}{B_o}\right)^{n+1} - \left(\frac{\phi(1-S_w)}{B_o}\right)^{n}\right] \quad \textbf{(15)}$$

The accumulation terms in equations (14) and (15) can be further expanded. This expansion is non-unique; it can be done in many forms. For this research, the final forms are given in equations (16) and (17).

$$\frac{V_b}{\alpha_c}\frac{\partial}{\partial t}\left(\frac{\phi S_w}{B_w}\right) = \frac{V_b}{\alpha_c \Delta t}\left[\left[\frac{\emptyset'}{B_w^n} + \emptyset^{n+1}\left(\frac{1}{B_w}\right)'\right] S_w^n (p_o^{n+1} - p_o^n) + \left(\frac{\emptyset}{B_w}\right)^{n+1}(S_w^{n+1} - S_w^n)\right] \quad \textbf{(16)}$$

$$\frac{V_b}{\alpha_c}\frac{\partial}{\partial t}\left(\frac{\phi(1 - S_w)}{B_o}\right) = \frac{V_b}{\alpha_c \Delta t}\left[\left[\frac{\emptyset'}{B_o^n} + \emptyset^{n+1}\left(\frac{1}{B_o}\right)'\right](1 - S_w^n)(p_o^{n+1} - p_o^n) - \left(\frac{\emptyset}{B_o}\right)^{n+1}(S_w^{n+1} - S_w^n)\right] \quad \textbf{(17)}$$

The derivatives, with respect to pressure, of porosity and the inverse of the formation volume factor can be determined by numerical perturbation as shown in the equations (18) and (19).

$$\emptyset' = \frac{(\emptyset^{n+1} - \emptyset^n)}{(p^{n+1} - p^n)} \quad \textbf{(18)}$$

$$\left(\frac{1}{B_w}\right)' = \frac{\left(\left(\frac{1}{B_w}\right)^{n+1} - \left(\frac{1}{B_w}\right)^n\right)}{(p^{n+1} - p^n)} \quad \textbf{(19)}$$

Finally, the partial differential equations of water and oil, in the equations (7) and (8), can be transformed into the following algebraic equations as shown in equations (20) and (21) , respectively.

$$T_{wx_{i+\frac{1}{2},j}}\left(p_{o\,i+1,j}-p_{o\,i,j}\right)+T_{wx_{i-\frac{1}{2},j}}\left(p_{o\,i-1,j}-p_{o\,i,j}\right)$$
$$=\frac{V_b}{\alpha_c\Delta t}\left[\left[\frac{\emptyset'}{B_w^n}+\emptyset^{n+1}\left(\frac{1}{B_w}\right)'\right]S_w^n(p_o^{n+1}-p_o^n)\right. \quad \textbf{(20)}$$
$$\left.+\left(\frac{\emptyset}{B_w}\right)^{n+1}(S_w^{n+1}-S_w^n)\right]-q_{wsc}$$

$$T_{ox_{i+\frac{1}{2},j}}\left(p_{o\,i+1,j}-p_{o\,i,j}\right)+T_{ox_{i-\frac{1}{2},j}}\left(p_{o\,i-1,j}-p_{o\,i,j}\right)$$
$$=\frac{V_b}{\alpha_c\Delta t}\left[\left[\frac{\emptyset'}{B_o^n}+\emptyset^{n+1}\left(\frac{1}{B_o}\right)'\right](1-S_w^n)(p_o^{n+1}-p_o^n)\right. \quad \textbf{(21)}$$
$$\left.-\left(\frac{\emptyset}{B_o}\right)^{n+1}(S_w^{n+1}-S_w^n)\right]-q_{osc}$$

For the source and sink terms, which represent the flow into and out of the reservoir by injection and production wells, the sign convention is defined such that mass going into the reservoir is positive, and negative otherwise. In general, injection wells can be controlled by specifying either injection rate or bottom-hole injection pressure. Producers are mostly controlled either by specifying liquid production rate or bottom-hole producing pressure. In the case of rate control, the rate term can be directly included into the algebraic equations. On the other hand, for wells that are controlled by

injection or production bottom-hole pressure, a well model is needed to couple the well production rate, well bottom-hole flowing pressure, and well-block pressure together.

There exist many well models that can be used. Peaceman's well index (Peaceman 1983), one of the most popular well models, is used for this research. Peaceman defines the equivalent wellbore radius. At this radius, the steady-state pressure in the reservoir is equal to the well-block pressure. The equivalent wellbore radius can be calculated using equation (22).

$$r_0 = 0.28\frac{\left\{\left[\left({ky}/{kx}\right)^{\frac{1}{2}}(\Delta x)^2\right] + \left[\left({kx}/{ky}\right)^{\frac{1}{2}}(\Delta y)^2\right]\right\}^{\frac{1}{2}}}{\left(\frac{ky}{kx}\right)^{1/4} + \left(\frac{kx}{ky}\right)^{1/4}} \quad \textbf{(22)}$$

where

k_x is the permeability in the direction along the flow part

k_y is the permeability in the direction perpendicular to the flow path.

Δx is the grid block dimension in the direction along the flow path

Δy is the grid block dimension in the direction perpendicular to the flow path

In this research, the goal is to develop the network of one-dimensional flow models. Hence, only one-dimensional flow is investigated. Peaceman's well model can be simplified as shown in equation (23).

$$r_0 = 0.14[(\Delta x)^2 + (\Delta y)^2]^{\frac{1}{2}} \quad \textbf{(23)}$$

From the equivalent wellbore radius obtained above, the injection/production rate and injection/production pressure relationship can be established by using the well index. It is given in equations (24) and (25).

$$WI = -\frac{2\pi\beta_c k k_r h}{\mu B[\ln(r_o/r_w) + s]} \quad \textbf{(24)}$$

$$q = WI(p_o - p_{wf}) \quad \textbf{(25)}$$

where

WI is the Peaceman's well index

β_c is the unit conversion for the flow term

k is the total permeability

k_r is the relative permeability of the interested phase to the total permeability

h is the well-block thickness

μ is the viscosity of the interested phase

B is the formation volume factor of the interested phase

r_o is the equivalent wellbore radius

r_w is the actual wellbore radius

s is the skin factor

p_o is the well-block pressure

p_{wf} is the wellbore flowing pressure

q is the interested phase flow rate in standard condition

From the algebraic equations of water and oil, equations (20) and (21), either implicit or explicit formulation can be obtained. In the case that flow terms, on the left

hand side of the equations, are evaluated at the old time-steps, i.e. the pressure on the flow terms are evaluated at the old time-steps, the method is considered as an explicit formulation. On the other hand, if the new time-steps are used, it would be considered as an implicit formation. The explicit and implicit formulation can be written as in equations (26) and (27), using the arguments evaluated at $\{n\}$ and $\{n+1\}$ respectively.

$$T_{wx}{}^{n,n+1}_{i+\frac{1}{2},j}\left(p_{o\,i+1,j}-p_{o\,i,j}\right)^{n,n+1}+T_{wx}{}^{n,n+1}_{i-\frac{1}{2},j}\left(p_{o\,i-1,j}-p_{o\,i,j}\right)^{n,n+1}$$
$$=\frac{V_b}{\alpha_c\Delta t}\left[\left[\frac{\emptyset'}{B_w^n}+\emptyset^{n+1}\left(\frac{1}{B_w}\right)'\right]S_w^n(p_o^{n+1}-p_o^n)\right. \tag{26}$$
$$\left.+\left(\frac{\emptyset}{B_w}\right)^{n+1}(S_w^{n+1}-S_w^n)\right]-q_{wsc}$$

$$T_{ox}{}^{n,n+1}_{i+\frac{1}{2},j}\left(p_{o\,i+1,j}-p_{o\,i,j}\right)^{n,n+1}+T_{ox}{}^{n,n+1}_{i-\frac{1}{2},j}\left(p_{o\,i-1,j}-p_{o\,i,j}\right)^{n,n+1}$$
$$=\frac{V_b}{\alpha_c\Delta t}\left[\left[\frac{\emptyset'}{B_o^n}+\emptyset^{n+1}\left(\frac{1}{B_o}\right)'\right](1-S_w^n)(p_o^{n+1}-p_o^n)\right. \tag{27}$$
$$\left.-\left(\frac{\emptyset}{B_o}\right)^{n+1}(S_w^{n+1}-S_w^n)\right]-q_{osc}$$

The advantage of the explicit formulation is its speed. At each time-step, each grid block pressure and saturation can be solved explicitly. However, the explicit formulation is considered to be only conditionally stable. The stability of the explicit formulation depends on the grid size and time-step size.

In the implicit formulation, it can be seen that the flow terms on the left hand side of the equations are evaluated at the new time-steps. Hence, the pressure and saturation solution of each grid block would also depend on its neighbors. In this case, the equations of each grid block must be solved simultaneously. It is more computational demanding compared to the explicit formulation. However, its advantage over the explicit formulation is that it is unconditionally stable. Therefore, it is more practical in 'real world' problems.

This research is mainly concentrated in the waterflood problem; hence, the implicit formulation is used for the fact that it allows more flexibility in selecting the grid size and time-step.

After the p.d.e. is discretized, the resulting algebraic equations must be solved. Various choices of how to solve these equations are available, e.g. fully implicit, implicit pressure explicit saturation (IMPES), sequential implicit, and semi-implicit. Obviously, the most powerful solution method is the fully implicit. However, it is more computationally demanding. In this project, the lagging coefficients method, i.e. semi-implicit, is used to solve the algebraic equations. The pressure and saturation unknowns on the left hand side of the equations are evaluated at the new time-steps; however, the nonlinear terms that depend on the pressure and saturation are evaluated based on the pressure and saturation of the current time-steps. This makes the algebraic equations in each time-step become linear. Hence, they can be solved directly, not iteratively. Equations (26) and (27) are modified to be solved with the lagging coefficients solving technique. Equations (28) and (29) are repeated here for the sake of completeness.

$$T_{wx_{i+\frac{1}{2},j}}{}^{n}\left(p_{o\,i+1,j}-p_{o\,i,j}\right)^{n+1}+T_{wx_{i-\frac{1}{2},j}}{}^{n}\left(p_{o\,i-1,j}-p_{o\,i,j}\right)^{n+1}$$

$$=\frac{V_b}{\alpha_c\Delta t}\left[\left[\frac{\emptyset'}{B_w^n}+\emptyset^n\left(\frac{1}{B_w}\right)'\right]S_w^n(p_o^{n+1}-p_o^n)+\left(\frac{\emptyset}{B_w}\right)^n(S_w^{n+1}-S_w^n)\right] \quad \textbf{(28)}$$

$$-{q_{wsc}}^{n+1}$$

$$T_{ox_{i+\frac{1}{2},j}}{}^{n}\left(p_{o\,i+1,j}-p_{o\,i,j}\right)^{n+1}+T_{ox_{i-\frac{1}{2},j}}{}^{n}\left(p_{o\,i-1,j}-p_{o\,i,j}\right)^{n+1}$$

$$=\frac{V_b}{\alpha_c\Delta t}\left[\left[\frac{\emptyset'}{B_o^n}+\emptyset^n\left(\frac{1}{B_o}\right)'\right](1-S_w^n)(p_o^{n+1}-p_o^n)\right. \quad \textbf{(29)}$$

$$\left.-\left(\frac{\emptyset}{B_o}\right)^n(S_w^{n+1}-S_w^n)\right]-{q_{osc}}^{n+1}$$

In order to simplify notations, one can define the following parameters as shown in equations (30) to (33). The coefficients of the accumulation terms are re-defined:

$$d_{wp}=\frac{V_b}{\alpha_c\Delta t}\left[\frac{\emptyset'}{B_w^n}+\emptyset^{n+1}\left(\frac{1}{B_w}\right)'\right]S_w^n \quad \textbf{(30)}$$

$$d_{ws}=\frac{V_b}{\alpha_c\Delta t}\left(\frac{\emptyset}{B_w}\right)^{n+1} \quad \textbf{(31)}$$

$$d_{op}=\frac{V_b}{\alpha_c\Delta t}\left[\frac{\emptyset'}{B_o^n}+\emptyset^n\left(\frac{1}{B_o}\right)'\right](1-S_w^n) \quad \textbf{(32)}$$

$$d_{os}=-\frac{V_b}{\alpha_c\Delta t}\left(\frac{\emptyset}{B_o}\right)^n \quad \textbf{(33)}$$

With the new definition of the coefficients of the accumulation terms, equations (28) and (29) can be rewritten as equations (34) and (35).

$$T_{wx_{i+\frac{1}{2},j}}{}^{n}\left(p_{o\,i+1,j}-p_{o\,i,j}\right)^{n+1}+T_{wx_{i-\frac{1}{2},j}}{}^{n}\left(p_{o\,i-1,j}-p_{o\,i,j}\right)^{n+1}$$
$$=d_{wp_i}(p_o^{n+1}-p_o^n)+d_{ws_i}(S_w^{n+1}-S_w^n)-{q_{wsc}}^{n+1} \quad \textbf{(34)}$$

$$T_{ox_{i+\frac{1}{2},j}}{}^{n}\left(p_{o\,i+1,j}-p_{o\,i,j}\right)^{n+1}+T_{ox_{i-\frac{1}{2},j}}{}^{n}\left(p_{o\,i-1,j}-p_{o\,i,j}\right)^{n+1}$$
$$=d_{op_i}(p_o^{n+1}-p_o^n)-d_{os_i}(S_w^{n+1}-S_w^n)-{q_{osc}}^{n+1} \quad \textbf{(35)}$$

Once the equations are established for each grid block, they can be rearranged and written in the matrix form as shown in equation (36).

$$T^nX^{n+1}=D^n(X^{n+1}-X^n)-Q^{n+1} \quad \textbf{(36)}$$

where

T^n is the transmissibility matrix evaluated at the current time-step

D^n is the accumulation matrix evaluated at the current time-step

Q^{n+1} is the source/sink vector evaluated using new time-step pressure but with the well index evaluated at the current time-step

X^{n+1} is the state vector of the new time-step

X^n is the state vector of the current time-step

In order to illustrate the matrix structure, a one-dimensional two-phase simulation model of the system with 5 grids is explicitly compiled. The transmissibility matrix is illustrated in equation (37), while the accumulation matrix is shown in equation (38).

$$T^n = \begin{bmatrix}
-T_{wx_{1+\frac{1}{2}}} & 0 & T_{wx_{1+\frac{1}{2}}} & 0 & & & & & & \\
-T_{ox_{1+\frac{1}{2}}} & 0 & T_{ox_{1+\frac{1}{2}}} & 0 & & & & & & \\
T_{wx_{2-\frac{1}{2}}} & 0 & -\left(T_{wx_{2-\frac{1}{2}}} + T_{wx_{2+\frac{1}{2}}}\right) & 0 & T_{wx_{2+\frac{1}{2}}} & 0 & & & & \\
T_{ox_{2-\frac{1}{2}}} & 0 & -\left(T_{ox_{2-\frac{1}{2}}} + T_{ox_{2+\frac{1}{2}}}\right) & 0 & T_{ox_{2+\frac{1}{2}}} & 0 & & & & \\
 & & T_{wx_{3-\frac{1}{2}}} & 0 & -\left(T_{wx_{3-\frac{1}{2}}} + T_{wx_{3+\frac{1}{2}}}\right) & 0 & T_{wx_{3+\frac{1}{2}}} & 0 & & \\
 & & T_{ox_{3-\frac{1}{2}}} & 0 & -\left(T_{ox_{3-\frac{1}{2}}} + T_{ox_{3+\frac{1}{2}}}\right) & 0 & T_{ox_{3+\frac{1}{2}}} & 0 & & \\
 & & & & T_{wx_{4-\frac{1}{2}}} & 0 & -\left(T_{wx_{4-\frac{1}{2}}} + T_{wx_{4+\frac{1}{2}}}\right) & 0 & T_{wx_{4+\frac{1}{2}}} & 0 \\
 & & & & T_{ox_{4-\frac{1}{2}}} & 0 & -\left(T_{ox_{4-\frac{1}{2}}} + T_{ox_{4+\frac{1}{2}}}\right) & 0 & T_{ox_{4+\frac{1}{2}}} & 0 \\
 & & & & & & T_{wx_{5-\frac{1}{2}}} & 0 & -T_{wx_{5-\frac{1}{2}}} & 0 \\
 & & & & & & T_{ox_{5-\frac{1}{2}}} & 0 & -T_{ox_{5-\frac{1}{2}}} & 0
\end{bmatrix} \quad \textbf{(37)}$$

$$D^n = \begin{bmatrix}
d_{wp_1} & d_{ws_1} & & & & & & & & \\
d_{op_1} & d_{os_1} & & & & & & & & \\
 & & d_{wp_2} & d_{ws_2} & & & & & & \\
 & & d_{op_2} & d_{os_2} & & & & & & \\
 & & & & d_{wp_3} & d_{ws_3} & & & & \\
 & & & & d_{op_3} & d_{os_3} & & & & \\
 & & & & & & d_{wp_4} & d_{ws_4} & & \\
 & & & & & & d_{op_4} & d_{os_4} & & \\
 & & & & & & & & d_{wp_5} & d_{ws_5} \\
 & & & & & & & & d_{op_5} & d_{os_5}
\end{bmatrix} \quad \textbf{(38)}$$

Because the coefficients of the flow terms (transmissibility) and accumulation terms are evaluated at the current time-step, equation (36) can be rearranged such that it can be linearly solved for the pressure and saturation in the next time-step as shown in equations (39) and (40).

$$T^n X^{n+1} = D^n (X^{n+1} - X^n) - Q^{n+1} \quad \textbf{(39)}$$

$$(T^n - D^n) X^{n+1} = -D^n X^n - Q^{n+1} \quad \textbf{(40)}$$

In the case that the sources or sinks are specified by flow rates at the standard condition, they can be included into the equations by directly specifying the specific phase flow rate in the matrix equation. The injection into the grid is taken as positive sign, while the production out of the grid is taken as the negative sign. In the case that liquid rate is specified, water flow rate can be determined by the ratio of well index of

water and the sum of well index of both phases as shown in equation (41). Oil flow rate can be determined by the difference between liquid and water flow rate.

$$wcut = \frac{WI_w}{WI_w + WI_o} \tag{41}$$

In the case that wells are specified by flowing bottom-hole pressure, the flow terms in the matrix Q can be replaced by equations (42) to (45). Note that the well index is evaluated at the current time-step.

$$q_{o_i} = WI_{o_i}^{\ n}\left(p_{o_i}^{\ n+1} - p_{wf_i}\right) \tag{42}$$

$$q_{o_i} = WI_{o_i}^{n} p_{o_i}^{n+1} - WI_{o_i} p_{wf_i} \tag{43}$$

$$q_{w_i} = WI_{w_i}^{\ n}\left(p_{o_i}^{\ n+1} - p_{wf_i}\right) \tag{44}$$

$$q_{w_i} = WI_{w_i}^{\ n} p_{o_i}^{\ n+1} - WI_{w_i}^{\ n} p_{wf_i} \tag{45}$$

To this end, equation (40) has to be modified accordingly. The transmissibility matrix can be modified to include the negative of the product of the well index and the well-block pressure, while the left-hand side of the equation can be modified to include the negative of the product of the well index and the well flowing pressure. Then, the linear system of equations can then be solved directly.

To solve the resulting system of linear equations, two main classes of method can be used. The first class is the direct method, e.g. Gaussian elimination and LU decomposition. Because the matrix is very sparse and has specific features, it can be efficiently solved by direct method for the small scale system. However, for the large scale problem, iterative methods would be considered to be more appropriate. GMRES, conjugate gradient, and bi-conjugate gradient are examples of the iterative methods.

Flow Network Models

In the previous subsection, the construction of a one-dimensional finite difference reservoir simulation is discussed. In this part, the methodology used to transform multi-dimensional models into the flow network models is described.

As mentioned earlier, fluid flow in the reservoir is affected by interaction between wells and corresponding flow paths. In the proposed flow network modeling, a multi-dimensional reservoir is reduced to a connected network of one-dimensional simulation models, in which the coupling between the individual one-dimensional models is enforced at the well-block, where edges of each network intersect. Figure 3 illustrates the transformation of flow in the two-dimensional domain of a two-well problem into the one-dimensional flow domain.

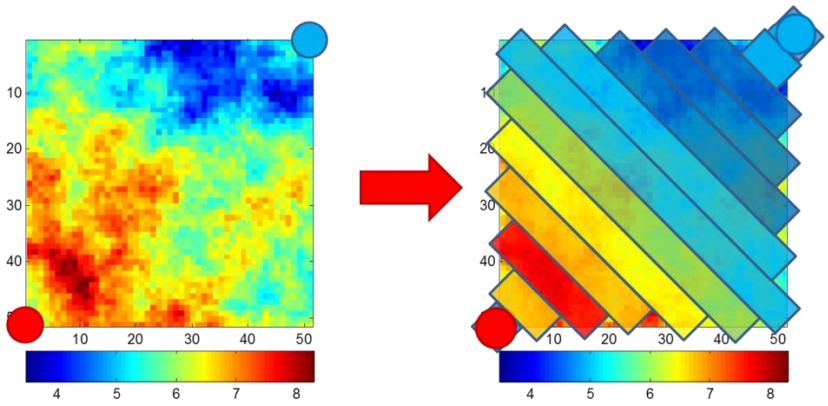

Figure 3: Problem transformation from 2D model to 1D model

In Figure 3, the wells are located at the diagonally opposite corners of the heterogeneous reservoir. The heterogeneity is shown by different shades of colors, which

represent the logarithmic value of permeability in each grid block. On the right hand side, the two wells are connected by one-dimensional grids with a similar color scale. This simple example illustrates the idea of reducing the problem from two to one dimension.

In order to illustrate a more complex problem with a bigger set of wells, the inverted-5-spot waterflood problem is shown in Figure 4.

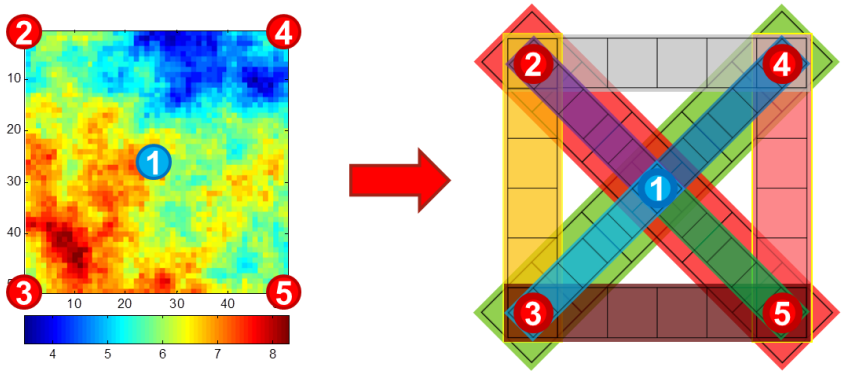

Figure 4: Problem transformation from spatial model to network model

In the flow network model, the physics of the flow is still described by three main components, namely mass conservation, flow equation, and the equation of states. The problem is formulated as a grid base simulation, and thus, it can be solved using finite difference methodology similar to what is previously described in the one-dimensional problem. The main difference stems from the fact that, in flow network model, the input-output relationship is dictated by the interaction between wells via the network of one-dimensional models, not the detailed spatial multi-dimensional model.

Basic Flow Network Examples

This part describes how to construct the flow network model for simple cases, which consist of only few wells in the systems. In the more complex cases, the flow network models can be constructed in a similar way. Figure 5 shows the simplified flow network model with 2, 3, and 4 wells, respectively. Note that physical dimensions and other important properties of grid blocks are not reflected in the figure.

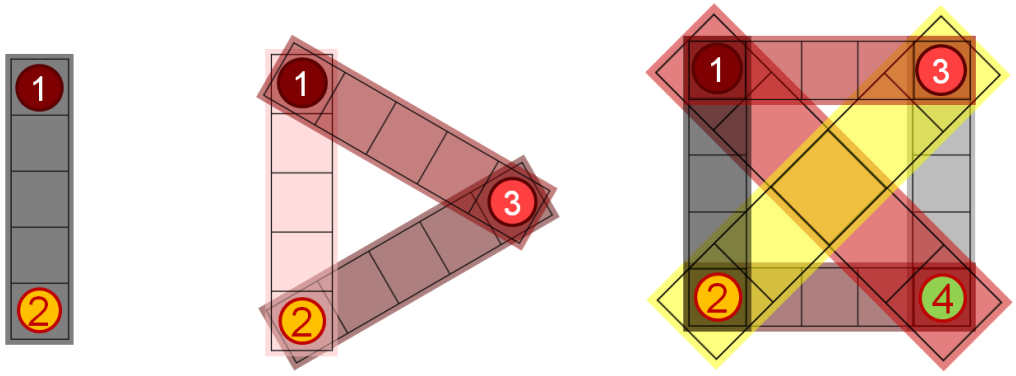

Figure 5: Simple flow network for 2, 3, and 4 well problems

In the two-well case, the structure of the flow network model is exactly the same as the finite difference flow equation previously described. One single connection will connect the two wells together. In this case, the number of grids in the connection is arbitrarily defined to be five, as shown in the left picture in Figure 5.

For the three-well problem, three connections are required to connect every well together, i.e. the first connection links well number 1 and 2, the second connection links well 1 and 3, and the last connection connects well 2 and 3. In the same way, each

connection is defined to have five grids. Because each connection will share the same grids at the well-blocks, the total number of grids would be $3 + (5 - 2) \times 3 = 12$ grids.

Extending this idea to the four wells case, every well has to be connected to one another. Therefore, $3 + 2 + 1 = 6$ connections are required. As before, each connection has five grids; hence, the system would consist of $4 + (5 - 2) \times 6 = 22$ grids.

In summary, the number of connections and number of grids can be determined using the formulas given in equations (46) and (47).

$$na = \frac{nw(nw - 1)}{2} \quad \textbf{(46)}$$

$$ng = nw + na(nx - 2) \quad \textbf{(47)}$$

where

nw is the total number of wells

na is the total number of connections

nx is the number of grids in each connection (user defined)

ng is the total number of grids in the system

Matrix Set-Up

As mentioned in the previous subsection, the connectivity between each grid is different from conventional reservoir simulation with the orthogonal gridding system. In the conventional one-dimensional reservoir simulation problem, the transmissibility matrix is tri-diagonal for single-phase flow, or tri-block-diagonal for multi-phase flow. For the two-dimensional or three-dimensional single-phase flow, the transmissibility matrix is penta-diagonal and hepta-diagonal, respectively. In the flow network models,

the main structure is the tri-block-diagonal matrix. In addition to the main diagonal terms, there are off-diagonal terms that account for the connection between any two grids that are not numbered next to each other. The shape of the transmissibility matrix depends on how the grid numbering is defined. Although the matrix of the flow network model would have higher bandwidth, its main advantage stems from the fact that the number of grid blocks can be significantly reduced. In addition, the transmissibility and accumulation matrices are sparse; thus, they can be stored and solved efficiently.

Grid Numbering

Similar to the conventional simulation model, grids can be numbered in various ways. The numbering system can have an effect on the simulation efficiency if the direct method is used to solve the linear equation. In this section, the following example in Figure 6 is used to depict the grid numbering methodology used in this research. This numbering methodology is by no means optimized. This inverted-5-spot waterflood example is also used as a tool to demonstrate how to set up the flow network model in the following part. In this case, the system consists of 1 injector in the middle, which floods oil into each of the 4 producers at each corner of the square 2D reservoir. Based on the given formula, a total of 10 connections is used to link all the wells together. Each connection is arbitrarily defined to have 6 grids. The total of 45 grids is obtained in this flow network.

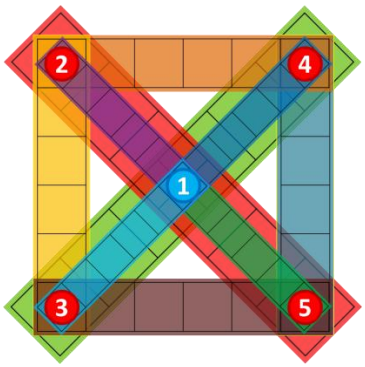

Figure 6: Flow network model for inverted-5-spot waterflood problem

In Figure 6, different colors represent the different connections between each pair of wells. However, at each well-block grid, many connections share the same grid block; hence, it is only considered as one single grid block for each well. In each connection, the well with the smaller number, according to our gridding system, is considered as the head of the connection, while the well with the bigger number is the tail of the connection. The connection between wells one and two is considered as the first connection. Then, the connections from well one-to-three, one-to-four, and one-to-five would be the second, third, and fourth connections, respectively. Then, the two-to-three, two to four, and two-to-five would be the fifth, sixth, and seventh. Analogously, three-to-four and three-to-five will be the eighth and ninth. The last one would be the connection for wells four and five. Figure 7 illustrates how each well is connected to one-another. The same color arrows in Figure 7 represent the connections with the same head.

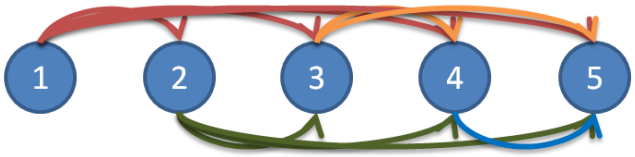

Figure 7: Definition of connection

As depicted by Figure 7, there are many different connections, and each of them can be viewed as a separate one-dimensional simulation model. To combine these connections as a flow network model, the global grid numbering is required. For the first connection, the grid numbering is given as shown in Figure 8.

Figure 8: Grid numbering for connection number 1

Note that each well-block is given with a number from 1 to *nw*; *nw* is 5 in this case. Then, grid numbering for the grids without a well would be given from the first to the last connection, sequentially. Each connection will have 4 more grids in addition to the two well-block grids at the head and tail location of each connection. The other main connections that connect the injector and producers are the second, third, and fourth connections. Grid numbering of these connections is presented in Figure 9.

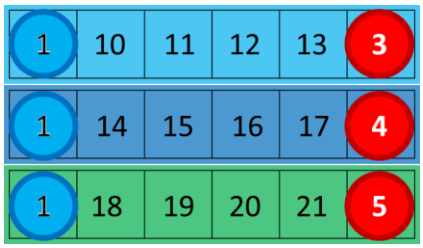

Figure 9: Grid numbering for connection number 2, 3, and 4

The fifth to the tenth connections are connections between producers and producers. Grid numbering of these connections can be found in Figure 10.

Figure 10: Grid numbering for connection number 5 to 10.

Transmissibility

Similar to the conventional finite difference reservoir simulation models, the connectivity of adjacent grids is defined by transmissibility terms. In the conventional models, the south, east, north, west, top, and bottom transmissibility terms define the

connection between each grid. However, in the network models, transmissibility terms are defined differently as shown in equation (48).

$$T(a,b,c,d) = Transimissibility\ between\ any\ two\ grids \quad \textbf{(48)}$$

Where

a is the well number in the head of the connection

b is the well number in the tail of the connection

c is the local grid number

d is the local grid number

The transmissibility terms of any two grids can be indexed by specifying the well number at the head and tail of that connection, and the two grids that are being investigated. For example, $T(1,2,5,6)$ is the transmissibility of the grid number 5 and 6 in the connection between wells 1 and 2.

One may observe that the grids in the middle of the connection are only connected to the two adjacent grids, while the well-block grids, both head and tail grids, have more than two connections. In this specific problem, there are five wells; hence, each well-block is connected to the other four wells. Therefore, the well-block grids would have 4 connections. For example, well number 1 has four connections; the well-block grid of well number 1 will have four transmissibility terms, namely $T(1,2,1,2), T(1,3,1,2), T(1,4,1,2)$ and $T(1,5,1,2)$. An additional example for well number 2 has $T(1,2,5,6), T(2,3,1,2), T(2,4,1,2)$, and $T(2,5,1,2)$. Figure 11 illustrates connection number 1 and its transmissibility terms.

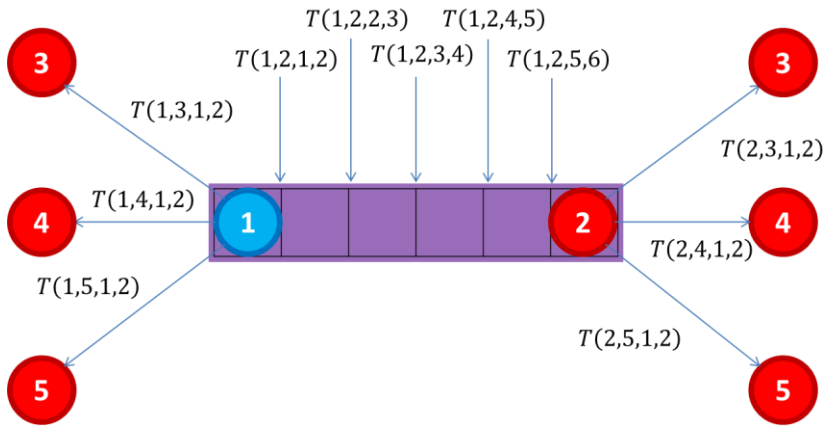

Figure 11: Transmissibility between each grid in connection between well 1 and 2

Transmissibility in the other connection can be referenced in a similar way. To clarify the idea, one more example presenting the connection between well 3 and well 5 is given in Figure 12.

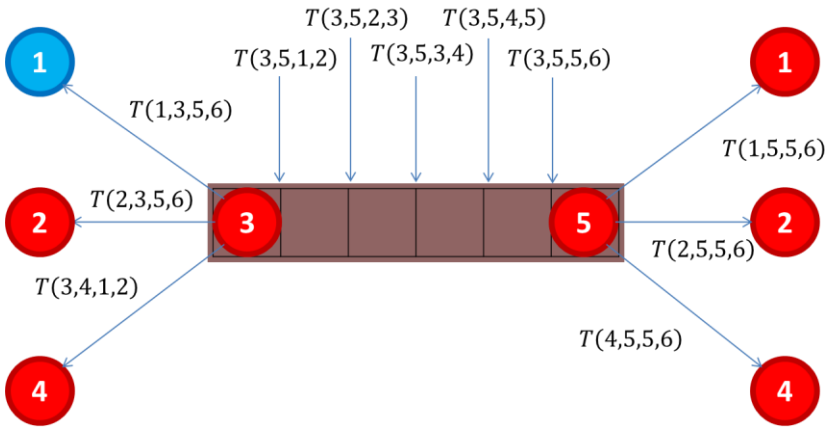

Figure 12: Transmissibility between each grid in connection between well 3 and 5

Transmissibility and Accumulation Matrices

The transmissibility (T) and accumulation(D) matrices of the flow network model are illustrated in Figure 13 and Figure 14 respectively.

Overall, it can be seen that the transmissibility matrix (T), shown in Figure 13, is very sparse. The main part can be viewed as a tri-block-diagonal matrix. The non-diagonal terms account for the connection of the well-blocks and the adjacent grid blocks that are not numbered as its neighboring grids. The accumulation matrix (D), shown in Figure 14, is a block-diagonal matrix.

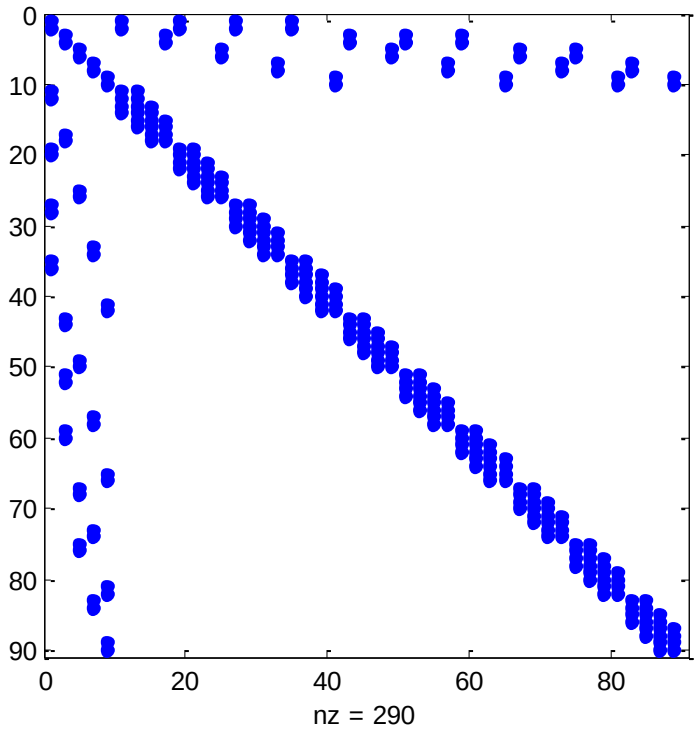

Figure 13: The structure of transmissibility matrix

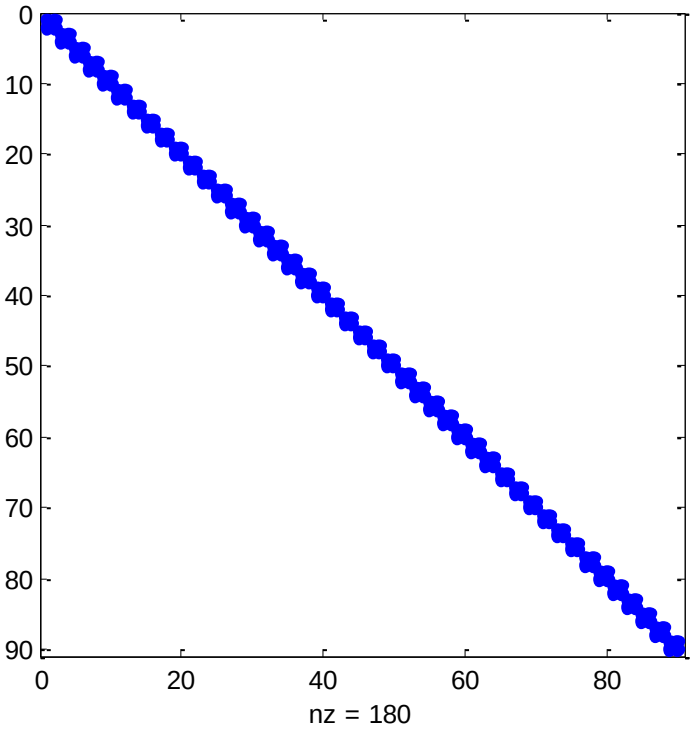

Figure 14: The structure of accumulation matrix

In this section, the construction of a flow network model and its mathematical formulation are given. Differences between the flow network model and the conventional reservoir model are pointed out. In the next section, how to make this flow network model be the predictive model to be further used for production optimization is discussed.

MODEL CALIBRATION

In the previous section, the concept of how to construct the flow network model is given. Basically, it is very similar to the finite difference reservoir simulation model, but the wells are connected and interacted via a network of one-dimensional reservoir simulation models, instead of the multi-dimensional reservoir model. The flow network model would be used to replace the full-order model in production optimization part of the CLRM as shown in Figure 2. Once the full-order model is constructed and history matched, it will be used to generate the production responses for the flow network model calibration. The main task discussed in this section is how to tune the parameters in the flow network model to match the responses from the full-order model. Note that they could be different from the actual production history.

Some of the required data for the flow network model is very similar to that for the conventional model. Fluid properties, namely PVT and viscosity models are the same as those used in the conventional model. For the rock properties like relative permeability, the same relative permeability curve as the one in the conventional model is used. However, by doing so, modeling error caused by dimension reduction will be introduced. The use of pseudo-relative permeability functions would potentially help to mitigate these errors. Since this thesis deals with the conceptual modeling of the flow network and given that it is the early stage of the model development, original relative permeability curves are used without modification.

In addition to the previously mentioned parameters, porosity and grid physical dimension dictate how much fluid is contained in the drainage area between each pair of wells, while the permeability will dictate how much pressure drop is caused by fluid flowing from one point to the other. To get the predictive flow network model, these parameters have to be tuned such that the flow network model can reproduce the response from the full-order model.

Because the full-order model is known, information like average porosity, permeability, and initial fluid in-place can always be extracted and used as a good initial guess and constraints in the flow network calibration.

Initialization of Calibration Process

The task here is to describe the flow network model using a minimal number of parameters. The parameters that will be varied in each grid are grid dimension in the direction perpendicular to the flow path (dy) and grid permeability (k).

For the other parameters, namely $dx, dz, and\ porosity$, the prior knowledge in the full-order model can be used as a guide. For the two-dimensional flow domain, dx of each grid can be defined such that the sum of dx in that specific connection is equal to the actual distance between that pair of wells. For dz, its value would be equal to the reservoir thickness. Porosity also has an effect on the fluid volume in each drainage area. In our case, only dy would be varied to affect the fluid volume in the connections, while porosity and other grid block dimensions will be kept constant. The porosity value of grids in the flow network model is the average porosity of the full-order model.

In addition to the main idea above, each connection is divided into three main parts. The first part is the well-block in the head position of the connection. The second one is well-block at the tail position. The last one is the grids in the middle of the connection that carry most of fluid in the drainage area. Only the three sets of parameters are tuned, not each single grid, in each connection. This way, the number of parameters in the flow network model calibration is minimized.

As this research is mainly concentrated on fluid displacement problems, the waterflood problems; most of the fluid is expected to be carried in the connection between injectors and producers, not between the producers and producers. Hence, the calibration can be initialized such that more fluid is in the connections between injectors and producers. For permeability, we can start with the average permeability of the field.

Calibration Objective Function

Similar to the history matching problem, where the full-order model parameters are tuned to match the response of the true reservoir, the flow network model parameters will be varied to minimize the mismatch between the flow network model and the full-order model responses.

For injectors, if the water injection rate is controlled, the injecting bottom-hole pressure is considered as observed data, and vice-versa. Similarly for producers, if producing bottom-hole pressure is specified, observed data is the oil and water production rate. In the case that producers are controlled by specifying the liquid production rate, observed data is the oil production rate, water production rate, and well producing bottom-hole pressure.

The frequency of the observed data, generated by the full-order model, and the flow network model responses has to be the same in order to reconcile the same dynamics. In this research, the responses are generated and compared every ten days.

To calibrate the model, the objective function that is a measurement of the mismatch between the full-order model and the flow network model responses is defined as shown in equation (49). It can be viewed as the Euclidean norm of the weighted mismatch between the full-order model and the flow network model responses.

$$ObjFn = (g(m) - d_{obs})^T W (g(m) - d_{obs}) \quad \textbf{(49)}$$

where

$ObjFn$ is the objective function value to be minimized (scalar)

$g(m)$ is the responses from the flow network model (vector of length no)

m is the parameters to be varied (vector of length np), $dy\ and\ k$ of grids

d_{obs} is the observed data from the full-order model (vector of length no)

W is the weight matrix (square matrix of dimension $no \times no$)

Note that the weight matrix can be as simple as the identity matrix. It could be a diagonal matrix with each diagonal element reflecting the confidence or uncertainty in the observed data of that specific term of mismatch.

Prior knowledge from the full-order model can be utilized to better pose the problem. For example, the linear equality constraint can be imposed on the dy to make the flow network model preserve the total pore volume of the full-order model. In addition, to make the problem more stable, lower and upper bounds can be prescribed to limit the range of the practical value of each parameter.

Optimization Algorithm Used in Model Calibration

The objective of the model calibration process is to minimize the mismatch between observed data and model response. Optimization algorithms can be employed in order to handle the mathematics associated with the minimization process. Many optimization algorithms are available (Griva et al. 2009).

Some of these production optimization algorithms are gradient-based methods like steepest descent, which requires only the first order derivative information. The Newton algorithm would be more sophisticated, but requires Hessian, the second order derivative information. This makes it more computationally expensive. Quasi-Newton methods are something in between; they estimate the Hessian using different techniques. A major drawback of these gradient-based methods is that it might get stuck in the local optimum.

Some other techniques are available for global optimization. These include simulated annealing, evolutionary algorithm, and swarm-based optimization algorithm, among others. These algorithms are even more computationally demanding.

In this study, our primary objective is to demonstrate the construction and utilization of the flow network model, not to find the best method to calibrate the model. Therefore, only gradient-based methods are considered and used.

Implementation

To demonstrate the framework to calibrate or train the flow network model, the flow network model is coded in MATLAB®. The full-order model response is generated using commercial software, namely ECLIPSE. The calibration process was done using 'fmincon' keyword in MATLAB®. The objective function is basically the weighted Euclidean norm of the mismatch vector. The overall workflow is shown in Figure 15.

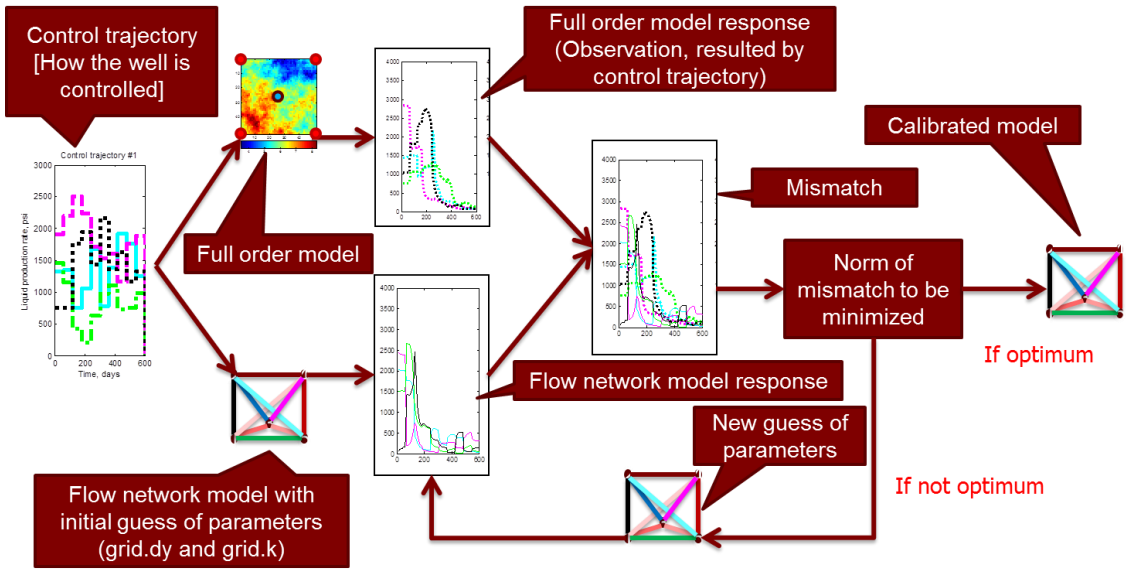

Figure 15: The framework of standard model calibration

The gradient of the objective function with respect to each calibration parameter is required. In this study, it is calculated by numerical perturbation, considering that each simulation run can be done rapidly. It is required to run simulations as many times as the number of calibration parameters.

Further study can improve the efficiency by deploying the gradient calculation using adjoint formulation or using other efficient techniques.

Robust Training

Similar to the history matching problem of the conventional reservoir model, the inverse problem is ill-posed; there might be so many non-unique solutions that can yield a response similar to the observed data. However, each of them would give different prediction.

In the case that data, used in the calibration, is generated from one single realization of the control trajectory, the flow network model might be able to reproduce the response of the full-order model, in which the wells are controlled by that specific control trajectory. However, when the calibrated flow network model is prescribed with other control trajectories, it might no longer be able to produce the same response as the full-order model. In other words, the flow network model might lose its prediction capability if the control trajectory is altered from the one that is used to train the model.

The primary goal of this research is to develop a flow network model such that it can be used as a surrogate model to perform production optimization. In production optimization, the control is varied to find the optimal production strategy. According to the defined objective, if the flow network model is sensitive to the control trajectory, the resulting control might be inaccurate. In the worst case scenario, the obtained optimal control might give a worse result than the initial guess.

To avoid this problem, ‘robust training’ can be used. Robust training is basically a model calibration against multiple sets of control trajectories. This is very similar to

idea of robust optimization. van Essen et al. (2006) has successfully used the robust optimization to find the optimal waterflooding strategy under uncertainty in the geological modeling. In our application, multiple realizations of production responses can be generated from different control trajectories, expected and allowed in the production optimization. The flow network model is then calibrated against these realizations of responses instead of one single set of responses.

The objective function of the flow network model calibration could be modified to minimize the expected value of the Euclidean norm of the weighted mismatch between the flow network model and full-order model response with respect to each control trajectory. In other words, the mean of the objective function of each single realization is minimized. The robust training objective function is modified to be equation (50).

$$RobustObjFn = E\left[\left(g(m)_n - d_{obs_n}\right)^T W_n\left(g(m)_n - d_{obs_n}\right)\right] \quad \textbf{(50)}$$

where

$g(m)_n$ is the response from the flow network model using the nth control trajectory

m is the parameters to be varied (grid dimension and permeability)

d_{obs_n} is the observed data from the full-order model using the nth control trajectory

W_n is the weight matrix of the nth realization

Note that the full-order model is only needed to generate responses with respect to different control trajectories. Therefore, it is run only as many times as the number of realizations of control trajectories desired in the robust training framework. During the process, only the flow network model with the updated parameters is run to match the

pre-determined full-order model responses. Hence, the process can be implemented efficiently. The product of the robust training is one single calibrated flow network model that is less sensitive to the control trajectories.

The predictive power of the resulting model on one specific control might not be as good as doing standard calibration on that specific control trajectory. However, the model is relatively good for the wider range of control that is expected in the production optimization. Overall, the robust model calibration is illustrated in Figure 16.

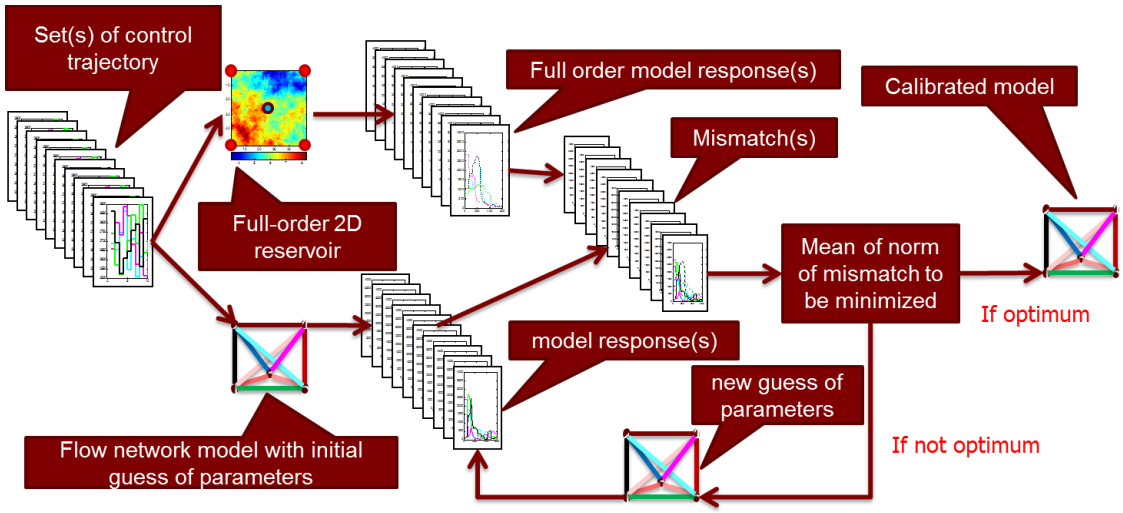

Figure 16: The framework of robust model calibration technique

For clarity, robust training is not a requirement for the flow network model calibration. Ideally, robust training can yield the result that is less sensitive to the control trajectory. However, in some cases, standard calibration against one single control trajectory might be good enough. It is very problem dependent.

Training Control Trajectories Data

As mentioned previously, the flow network model parameters have to be tuned to match the flow network model responses with the full-order model responses. Different from the history matching problem, where the full-order model parameters are tuned to match the full-order model responses with the real production history of the field, production responses can be generated from the full-order model using any control trajectory. However, the question is which kind of data is a good training data for the flow network model. Although it might not be optimal, the main idea here is to generate the training data using the ranges of control trajectories that are allowed in the real field operation. This allowable range of control would also be the constraints in the production optimization.

In each realization, the control trajectory has two dimensions, namely wells and control-steps. Ideally, the training data should cover the whole space of the possible control. In this case, the Latin Hypercube Sampling (L.H.S.) technique is employed to construct each realization.

For the waterflooding problem, one of the key objectives is to maintain the reservoir pressure. Therefore, the off-take should be controlled to be relatively equal to the in-take of the reservoir. In other words, field liquid production has to be relatively equal to the field water injection.

Depending on how wells are controlled, if injectors are controlled by injection rate, and producers are controlled by bottom-hole flowing pressure, the field is automatically operated at the voidage replacement ratio of one, i.e. in-take is equal to

off-take. The average reservoir pressure is mainly dictated by ranges of bottom-hole flowing pressure of the producers. On the other hand, if injectors are controlled by bottom-hole injection pressure, and producers are controlled by liquid production rate, the voidage replacement ratio is still unity, but the average reservoir pressure becomes dictated by the injection pressure. In the case that both injectors and producers are controlled by rate, there is no guarantee that the voidage replacement ratio would be unity, unless the equality constraint is applied to force the field water injection rate to be equal to the field liquid production rate. Lastly, if both injectors and producers are controlled by bottom-hole pressure, the voidage replacement ratio is unity, and the average reservoir pressure is between the injection and production pressure.

To generate the training data in the case that either injectors or producers, or both, are controlled by bottom-hole pressure, each well control trajectory can be generated using the L.H.S. technique without any modification. However, for the cases that both injectors and producers are controlled by liquid production rate, either injectors or producers are initially put on bottom-hole pressure control to observe the expected range of flow rate based on the allowable bottom-hole pressure. Then, L.H.S. is implemented to sample injection or production rates for each injector or producer, based on the ranges of flow rates from the bottom-hole pressure control simulations. The flow rates of each well are then scaled to have an approximate voidage replacement ratio of unity. If the scaled flow rates violate the allowable ranges of control, then they are re-sampled until they comply with all the constraints.

In addition, the training data should be at least equal to or longer than the expected range of production optimization. It should also be long enough to have sufficient pore volume of injection at the end of the production period. This is to make sure that every well has a reasonable period of production after water-breakthrough. Based on our experience, this would give a better model.

In the real applications, the process should be designed backward from production optimization to model calibration. For illustration, if the model is to be optimized for 400 days, it should be trained with the similar injection/production control but with longer production time to achieve more pore volume of injection, 600 days for example. The closer the training data to the expected condition in the production optimization, the better predictability of the model is expected.

PRODUCTION OPTIMIZATION

The ultimate goal of this research is to have a robust and fast tool to be utilized in finding the optimum production strategy that would help the operators make a better decision on the day-to-day field operations, or even in the real-time basis under the closed loop reservoir management concept. Brouwer and Jansen (2002) and Jansen et al. (2008) demonstrated the idea of using reservoir simulation as a tool to optimize the waterflood operation using optimal control theory. van Essen et al. (2006) showed the idea of doing robust optimization of waterflooding field under uncertainty of the geological models.

The idea is to utilize the reduced-order models, the flow network models in this case, to perform production optimization instead of the full-order models. This is similar to what van Doren et al. (2006) does with the reduced-order model using proper orthogonal decomposition, and Cardoso and Durlofsky (2010) use the trajectory piecewise linearization (TPWL) model for production optimization.

Basically, the production optimization problem can be interpreted as finding the control trajectory that would minimize or maximize the specified objection function. This could be to maximize the net present value (NPV) of the project, ultimate oil recovery, minimize water production, or delay water breakthrough.

As suggested previously in the flow network model calibration, there are many optimization algorithms that could automate the process. However, for this research, the gradient-based optimization method is used.

Assumption

Since this research is concentrated in the waterflood problem, one of the goals is to maintain a relatively constant reservoir pressure. A voidage replacement ratio of unity is desired. In the case that either injectors or producers are controlled by bottom-hole pressure, this condition would be achieved automatically. In the case that both of them are controlled by flow-rate, this voidage replacement ratio of unity should be imposed as a constraint in the selection of the feasible control trajectory. This constraint is expressed as shown in equation (51).

$$\sum_{i=1}^{np} q_{prod_i} = \sum_{j=1}^{ni} q_{inj_j} \quad \textbf{(51)}$$

This can simply be interpreted as the allocation of injection and production rate of each well to achieve the optimal condition. The oil price is assumed to be $100 per barrel, the cost to handle the produced water and inject water is assumed to be $10 per barrel. No discount factor is imposed in this demonstration.

Objective Function and Mathematical Formulation

In this research, the objective of production optimization is to maximize the NPV of the project. NPV is a function of field oil production, field water production, field water injection, their associated cost and sale price, and the discount factor at each time-step. The objective function is shown in equation (52).

$$J(u^n)$$

$$= \sum_{n=t0}^{n=te} \left(\frac{FOPR^n(u^n) * i_{op} - FWPR^n(u^n) * c_{wp} - FWIR^n(u^n) * c_{wi}}{(1-b)^T} \right) \Delta t^n \quad \textbf{(52)}$$

where

$J(u^n)$ is the NPV of the project

u^n is the control trajectory

$FOPR^n$ is the field oil production rate at time-step n

$FWPR^n$ is the field water production rate at time-step n

$FWIR^n$ is the field water injection rate at time-step n

i_{op} is income for each barrel of oil production

c_{wp} is the cost for each barrel of water production

c_{wi} is the cost for each barrel of water injection

b is the discount factor

Δt^n is the time interval at time-step n

T is number of time intervals for discounting

From the objective function shown above, it can be seen that field oil production rate, field water production rate, and field water injection rate depend on the well control trajectory. The input-output relationship is basically defined by the reservoir simulation run. This optimization problem can be expressed as shown in equation (53).

$$\max_{u^n \in U} J(u^n) = \phi(x^N) + \sum_{n=1}^{n=N-1} (L^n(x^{n+1}, u^n)) \quad \textbf{(53)}$$

Subject to

$$f(x^{n+1}, x^n, u^n, m) = 0 \quad \textbf{(54)}$$

$$x_{init} = x_o \quad \textbf{(55)}$$

$$Au = b \quad \textbf{(56)}$$

$$lb \leq u \leq ub \quad \textbf{(57)}$$

where

$\phi(x^N)$ is the terminal cost

L^n is the function of states vector $x^{n+1}$and control input vector u^n

Equation (54) is the reservoir simulation equation, which relates the control inputs, states, and outputs of the system together. Equation (55) is the initial states of the reservoir, i.e. initial pressure and saturation. Equation (56) is the linear equality constraints of the control inputs. In the case that the water injectors are controlled by water injection rate and the producers are controlled by liquid production rate, the voidage replacement ratio constraint can be included via this constraint. Equation (57) is the lower bounds and upper bounds of the control inputs. The allowable range of control inputs can be imposed on the optimization via these constraints.

Implementation

For this research, similar to the model training procedure, production optimization is implemented in MATLAB®. The ‘fmincon’ function is used to perform the constrained minimization. In this case, the objective function, to be minimized, is modified to be the negative value of NPV. The initial guess is the control trajectory that each producer is controlled by the constant uniform flowing bottom-hole pressure. The

gradient of the objective function with respect to control trajectory is automatically obtained by numerical perturbation in the ‘fmincon’ function. The maximum number of iterations is set to be 100.

CASE STUDIES

To demonstrate the entire workflow from the model construction to the production optimization problem, the following synthetic reservoir models are used as full-order models.

Synthetic Reservoir Model 1

The first example is the inverted-5-spot waterflood in the synthetic 2D two-phase reservoir. The objective is to maximize the NPV of the project by varying the bottom-hole flowing pressure of each producer within 400 days of production. The information about the reservoir and fluid properties can be found in the Table 1. Location and basic information about each injector and producer can be found in Table 2, while fluid relative permeability and PVT data can be found in Table 3 and Table 4 respectively.

The map, shown in Figure 17, depicts the logarithmic value of the permeability of each grid block. Overall, it can be seen that the southwest region has the highest permeability, while the northeast region has the lowest permeability in this map.

Table 1: Synthetic model 1 – basic reservoir properties

Properties	Parameters	Value
Number of grid cells in x direction	N_x	51
Number of grid cells in y direction	N_y	51
Number of grid cells in z direction	N_z	1
Grid block size in x direction	Δx	32.808399 ft
Grid block size in y direction	Δy	32.808399 ft
Reservoir thickness	h	32.808399 ft
Permeability in x, y, z direction	k_x, k_y, k_z	Figure 17
Porosity (reference)	ϕ	20%
Rock compressibility (constant)	c_r	3×10^{-6}
Oil relative permeability	$k_{ro}(S_w)$	See Table 3
Water relative permeability	$k_{rw}(S_w)$	See Table 3
Oil viscosity	μ_o	See Table 4
Oil formation volume factor	B_o	See Table 4
Water viscosity	μ_w	See equation (58)
Water formation volume factor	B_w	See equation (59)
Oil compressibility	c_o	$1 \times 10^{-5} psi^{-1}$
Water compressibility	c_w	$3 \times 10^{-6} psi^{-1}$
Initial reservoir pressure (all block)	p_o	3000 psi
Initial water saturation (all block)	S_w	0.1

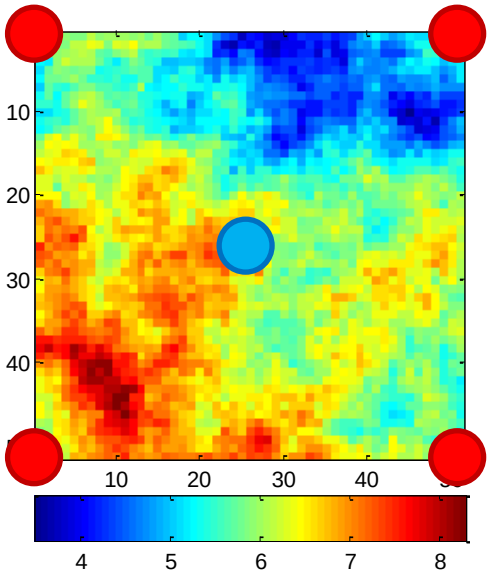

Figure 17: Synthetic model 1 – logarithmic value of permeability map

Table 2: Synthetic model 1 – basic information about the wells

Well no.	I location	J location	K location	Well radius (ft)	Skin factor
INJ1	26	26	1	0.583	0
PROD1	1	1	1	0.583	0
PROD2	1	51	1	0.583	0
PROD3	51	1	1	0.583	0
PROD4	51	51	1	0.583	0

Table 3: Water and oil relative permeability

Water saturation	Water relative permeability	Oil relative permeability
0	0	1
0.10	0.0001	1
0.20	0.0025	0.716
0.30	0.0230	0.4793
0.40	0.0842	0.2899
0.50	0.2115	0.1479
0.60	0.4319	0.0533
0.70	0.7740	0.0059
0.75	0.9999	0.0001
0.80	1.000	0
0.90	1.000	0
1.00	1.000	0

Table 4: Oil PVT and viscosity data

Oil phase pressure (psia)	Oil formation volume factor (RB/STB)	Oil viscosity (cp)
400	1.012	1.17
800	1.009	1.14
1200	1.005	1.11
1600	1.001	1.08
2000	0.996	1.06
2400	0.990	1.03
2800	0.988	1.00
3200	0.985	0.98
3600	0.980	0.95
4000	0.975	0.94
4400	0.970	0.92
4800	0.965	0.91
5200	0.960	0.90
5600	0.955	0.89
6000	0.950	0.88
6400	0.945	0.87
6800	0.940	0.86
7200	0.935	0.85
7600	0.930	0.84
8000	0.925	0.83
8400	0.920	0.82
8800	0.915	0.81
9200	0.910	0.80
9600	0.905	0.79
10000	0.900	0.78

The water formation volume factor is defined by equation (58).

$$B_w(p_w) = \frac{B_w(p_{ref})}{1 + X + X^2/2} \quad \textbf{(58)}$$

where

p_{ref} is the reference pressure, 2800 psi in this case

$B_w(p_{ref})$ is the formation volume factor at the reference pressure, 1 RB/STB in this case

$B_w(p_w)$ is the formation volume factor at the pressure of p_w

p_w is the water phase pressure

$X = c_w(p_w - p_{ref})$, where c_w is the water compressibility

Water viscosity can be calculated using equation (59).

$$\mu_w(p_w) = \frac{\mu_w(p_{ref})}{1 + Y + Y^2/2} \quad \textbf{(59)}$$

where

p_{ref} is the reference pressure, 2800 psi in this case

$\mu_w(p_{ref})$ is the water viscosity at the reference pressure, 1 cp in this case

$\mu_w(p_w)$ is the water viscosity at the pressure of p_w

$Y = -c_v(p_w - p_{ref})$, where $c_v$is water viscosibility, $c_v = 0\ psi^{-1}$in this case

Training Data

As mentioned previously, the flow network model needs to be calibrated to injection/production training data in order to be able to reproduce the response from the full-order model. The training data is generated from the full-order model using the following control trajectory.

As the production optimization would be performed for 400 days, the training data should be at least 400 days or more. In this case, 600 days of training data is used to ensure water breakthrough in every producer. The injector is controlled by a constant bottom-hole injection pressure of 3500 psi. Each producer is allowed to be operated between 2500 and 2900 psi. The whole production period is divided into 10 equal periods. Ten realizations of control trajectory are generated using L.H.S., and they are shown in Figure 18.

The full-order model responses are generated using ECLIPSE. The injection and production responses can be found as follows. Figure 19, Figure 20, and Figure 21 show water injection rate of injector and the oil production rate, water production rate of each producer respectively. Figure 22 shows the liquid production rate of each producer. It can be seen that the total liquid production rate and the total injection rate are about the same since the field is operated at the voidage replacement ratio of unity.

From the training data, each well has a different range of liquid production rates, which are dictated by the permeability heterogeneity. All producers have good amount of data after water-breakthrough as previously suggested. These responses are used as the observed data for the flow net work model calibration.

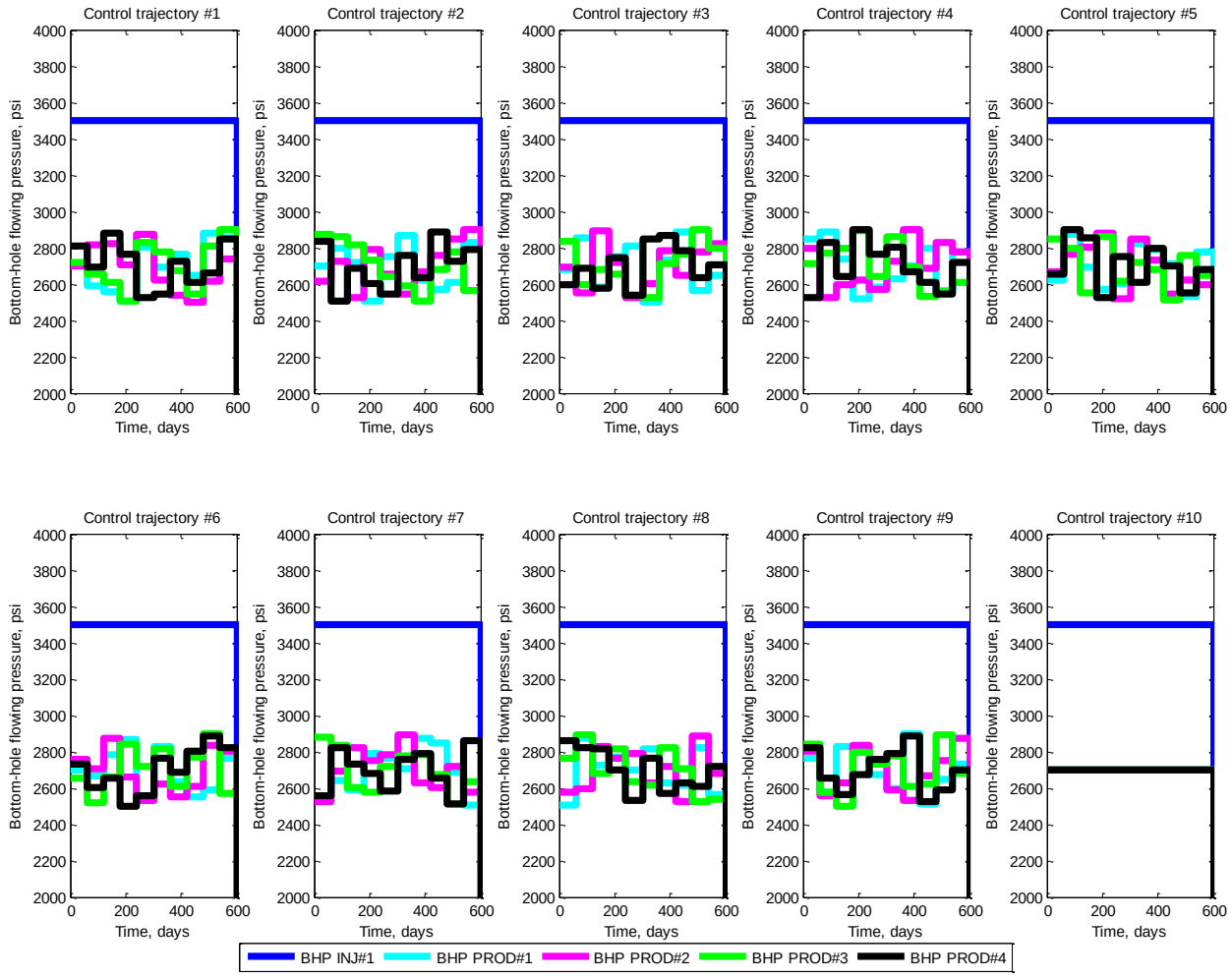

Figure 18: Synthetic model 1 – training control trajectories, bottom-hole flowing pressure of each well

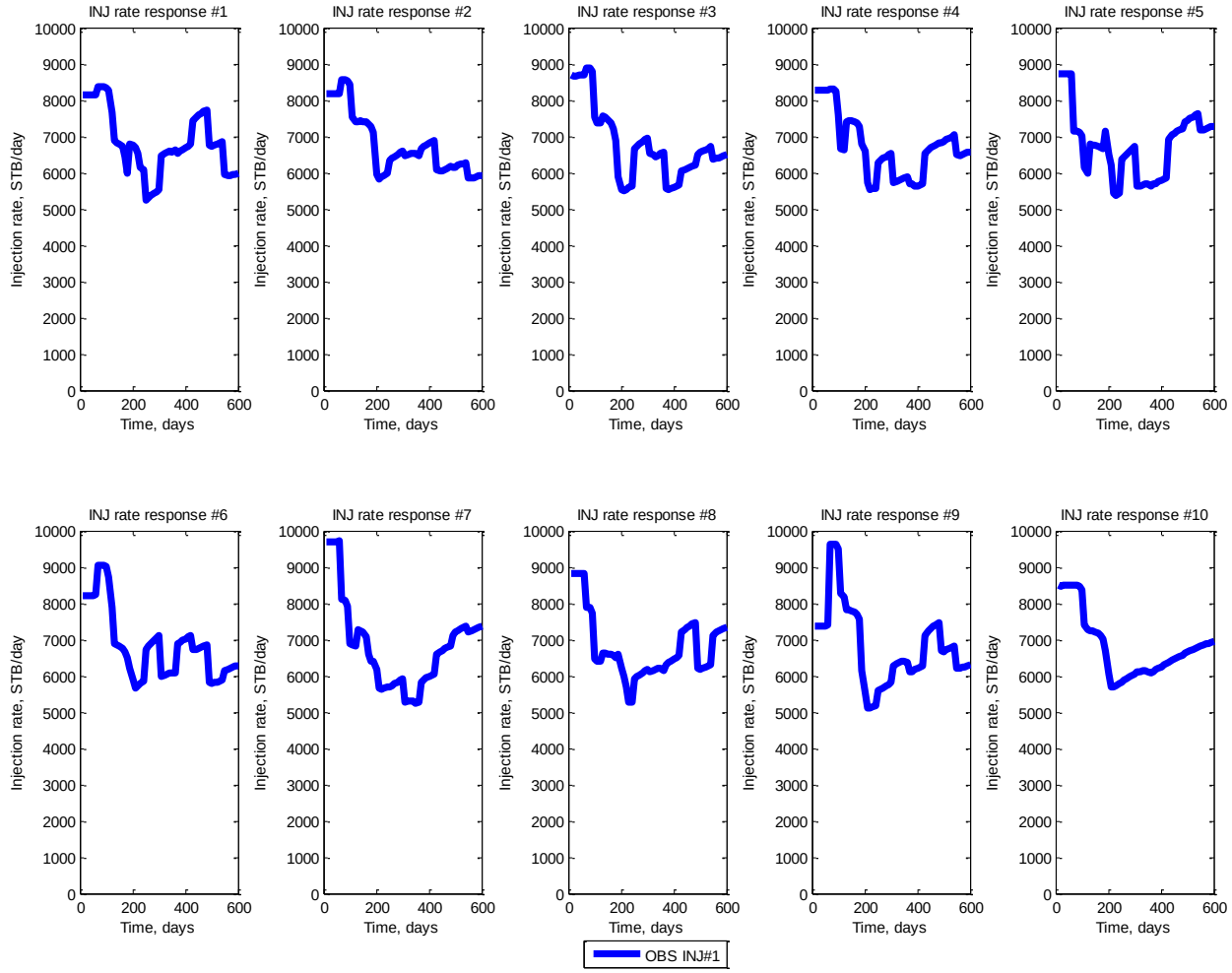

Figure 19: Synthetic model 1 – resulting water injection rate of injector

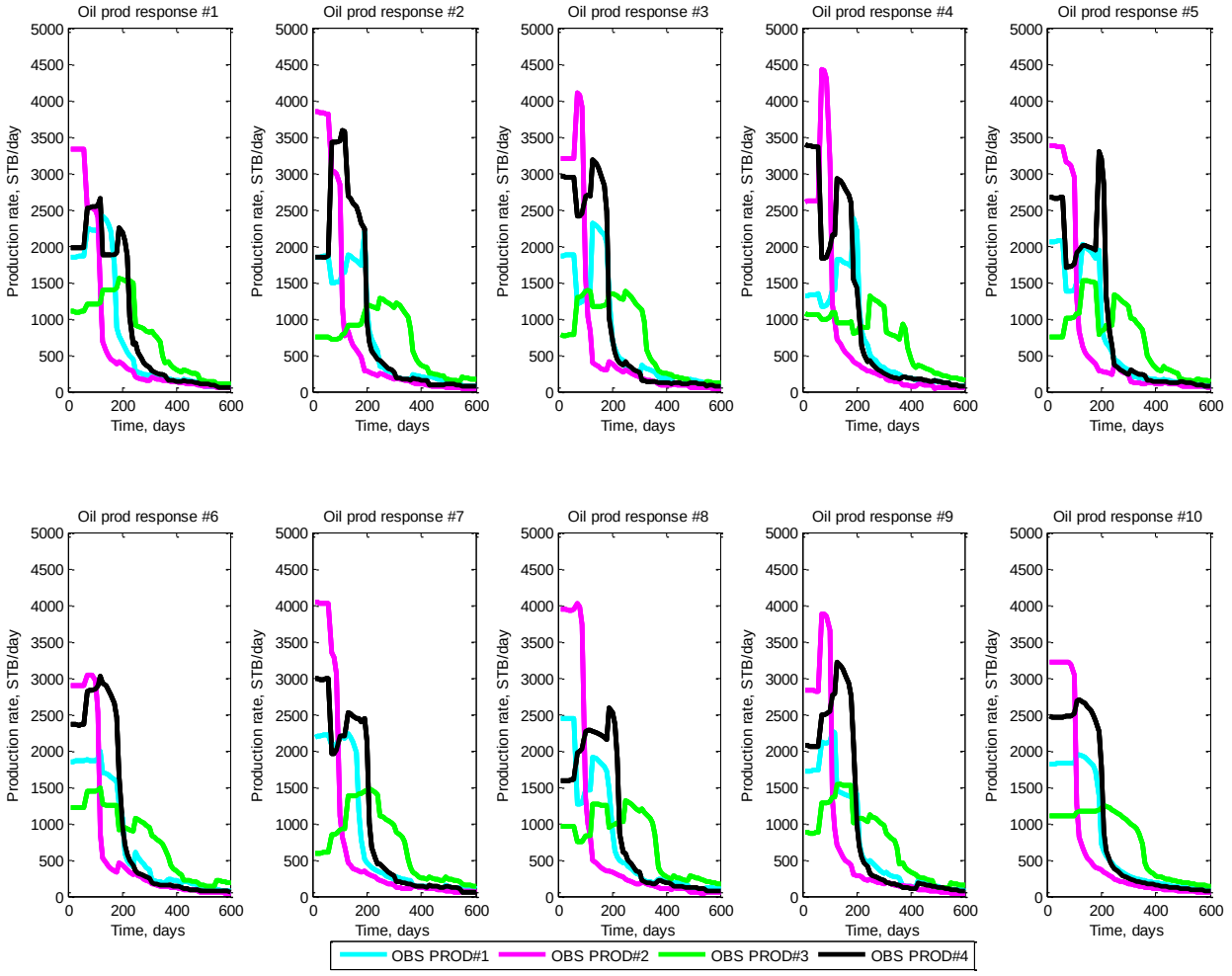

Figure 20: Synthetic model 1 – resulting oil production rate of each producer

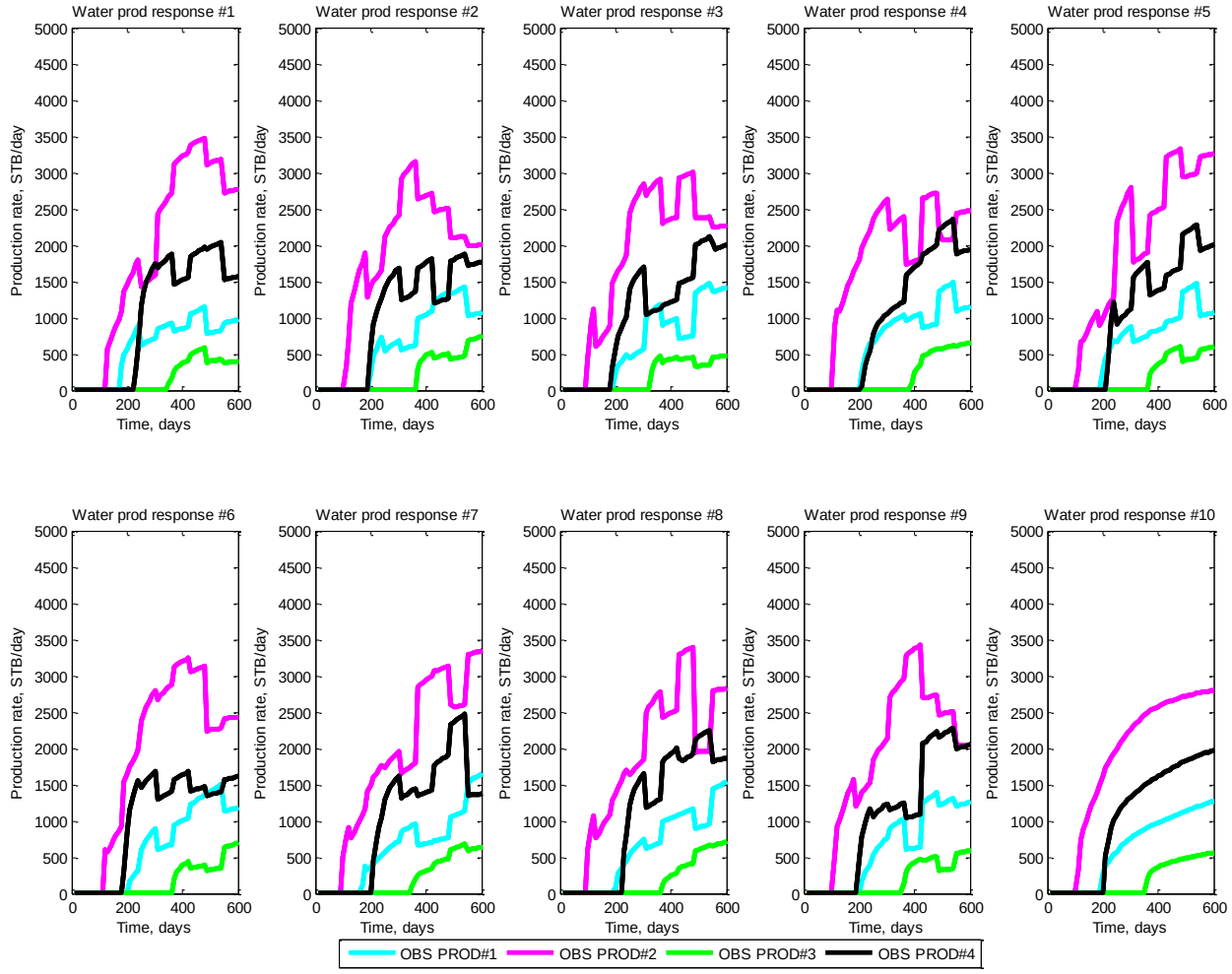

Figure 21: Synthetic model 1 – resulting water production rate of each producer

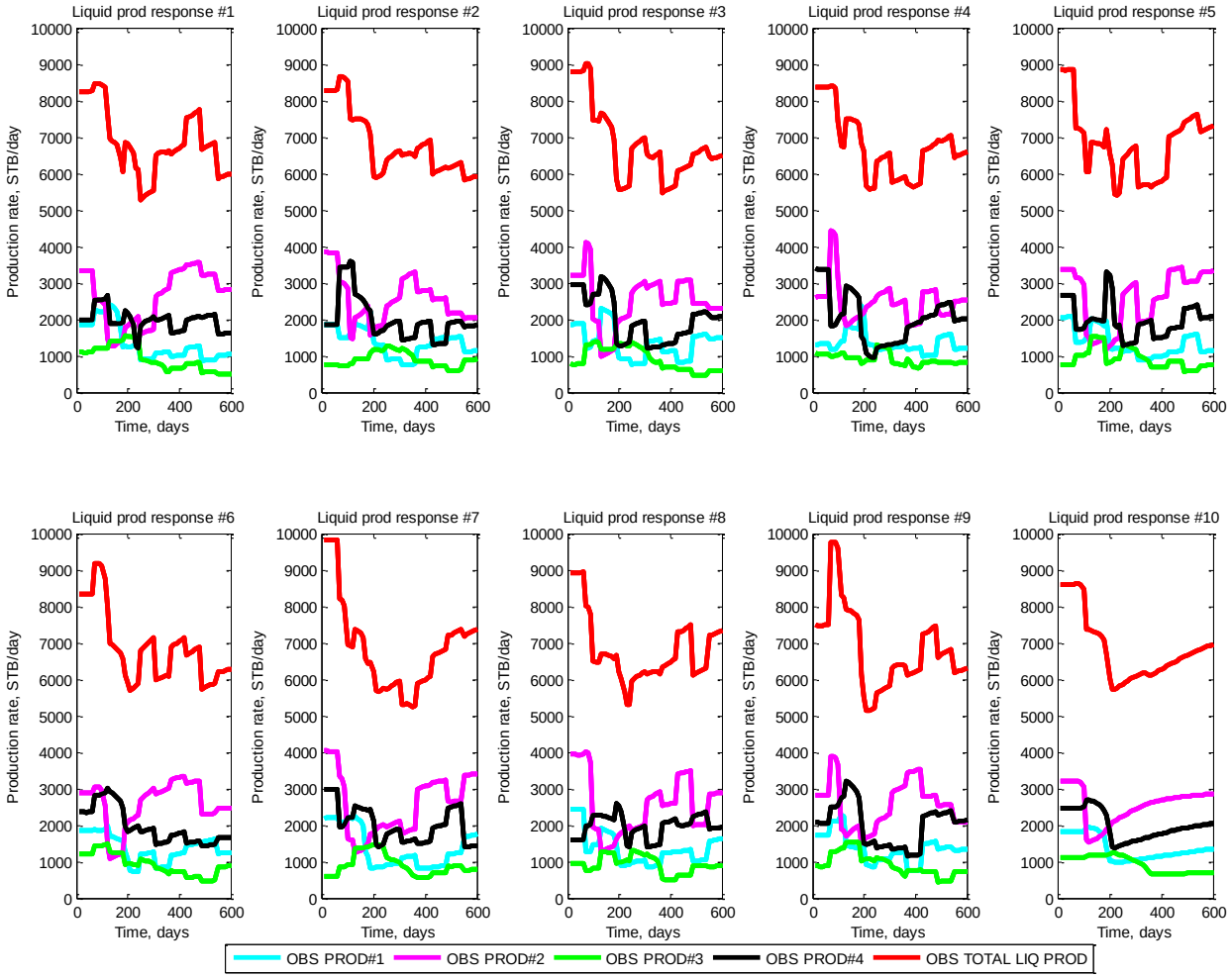

Figure 22: Synthetic model 1 – resulting liquid production rate of each producer

Calibration

As there are five wells in this problem, the matrix set-up would be exactly the same as the one given in previous sections. The model is initialized such that the total pore volume of the flow network model is the same as the original full-order model. In addition, to make sure that the calibrated flow network model would preserve the pore volume of the full-order model, a linear equality constraint is prescribed in the optimization algorithm. The lower bound of the grid dimension perpendicular to the flow direction, dy, is defined to be 10 ft. The initial guess of dy is designed such that 90% of the pore volume is contained in the connection between the injector and producers, which is a reasonable guess for this waterflood problem. The initial guess of permeability of each grid block is equal to the average permeability of the full-order model. The lower bound of the permeability value is defined to be 10 md. The minimization is performed using 'fmincon' in MATLAB®. The resulting calibrated flow network model parameters and the matches of each response are given as follows.

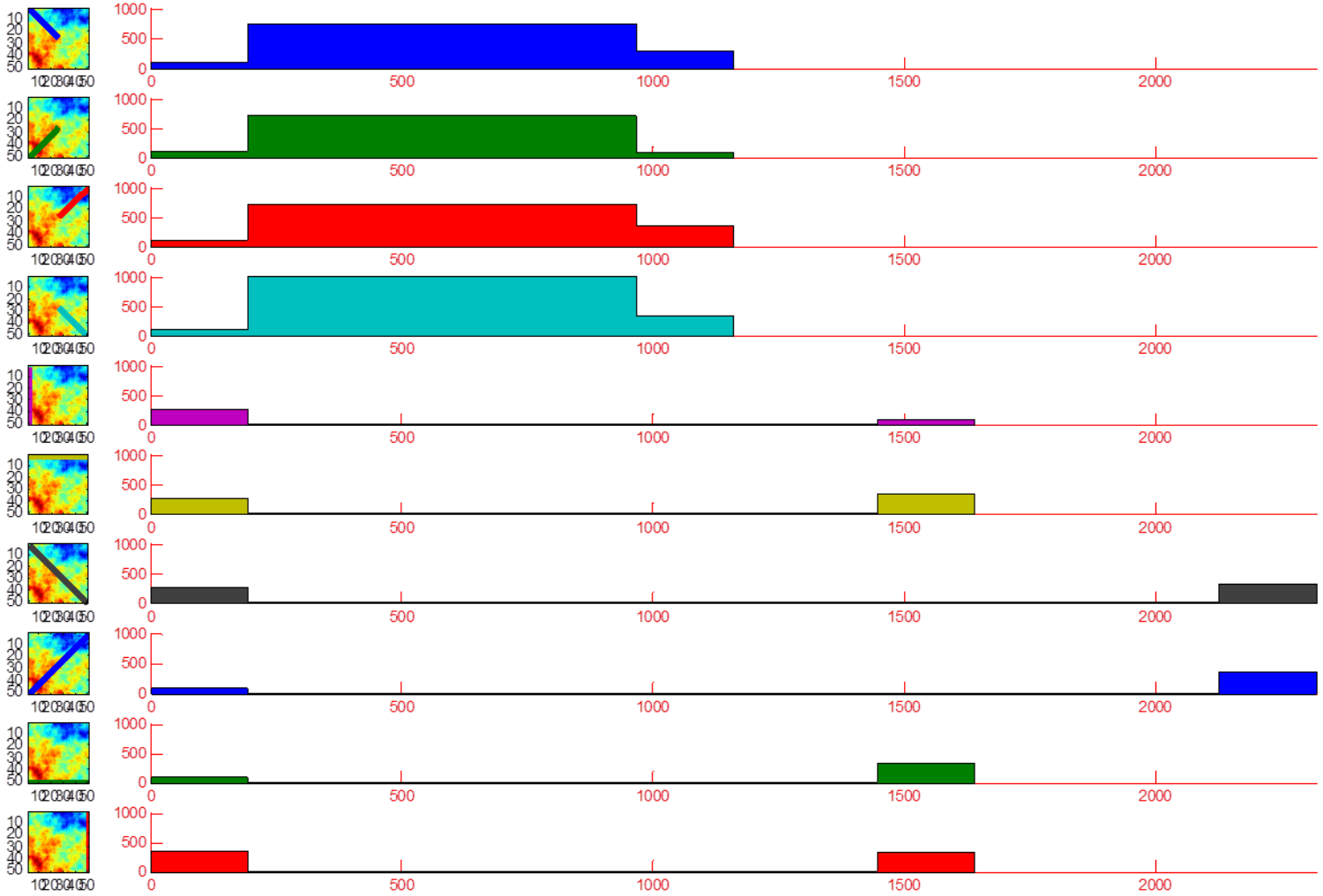

Figure 23: Synthetic model 1 – calibration result of grid dimension perpendicular to the flow path

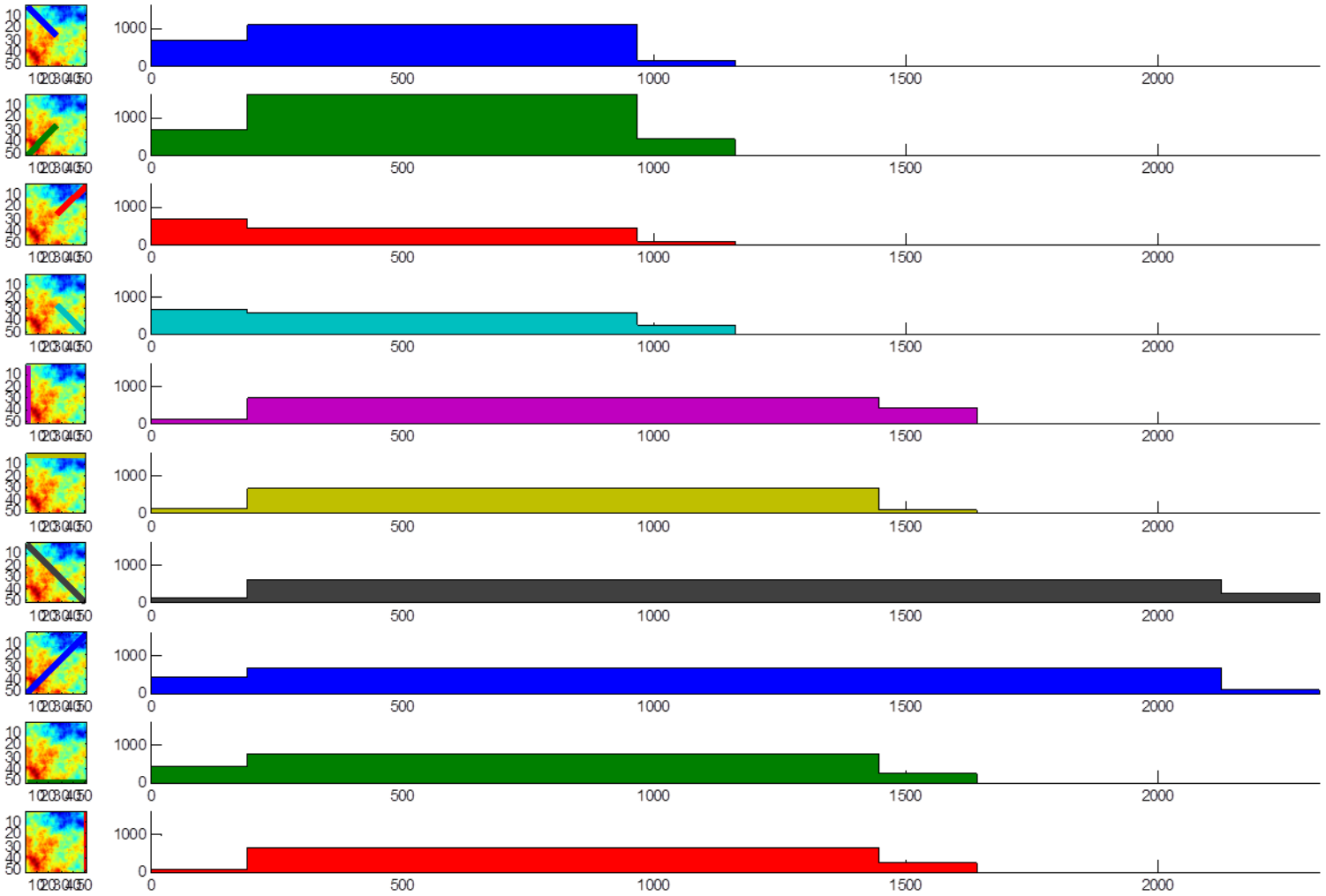

Figure 24: Synthetic model 1 – calibration result of grid permeability

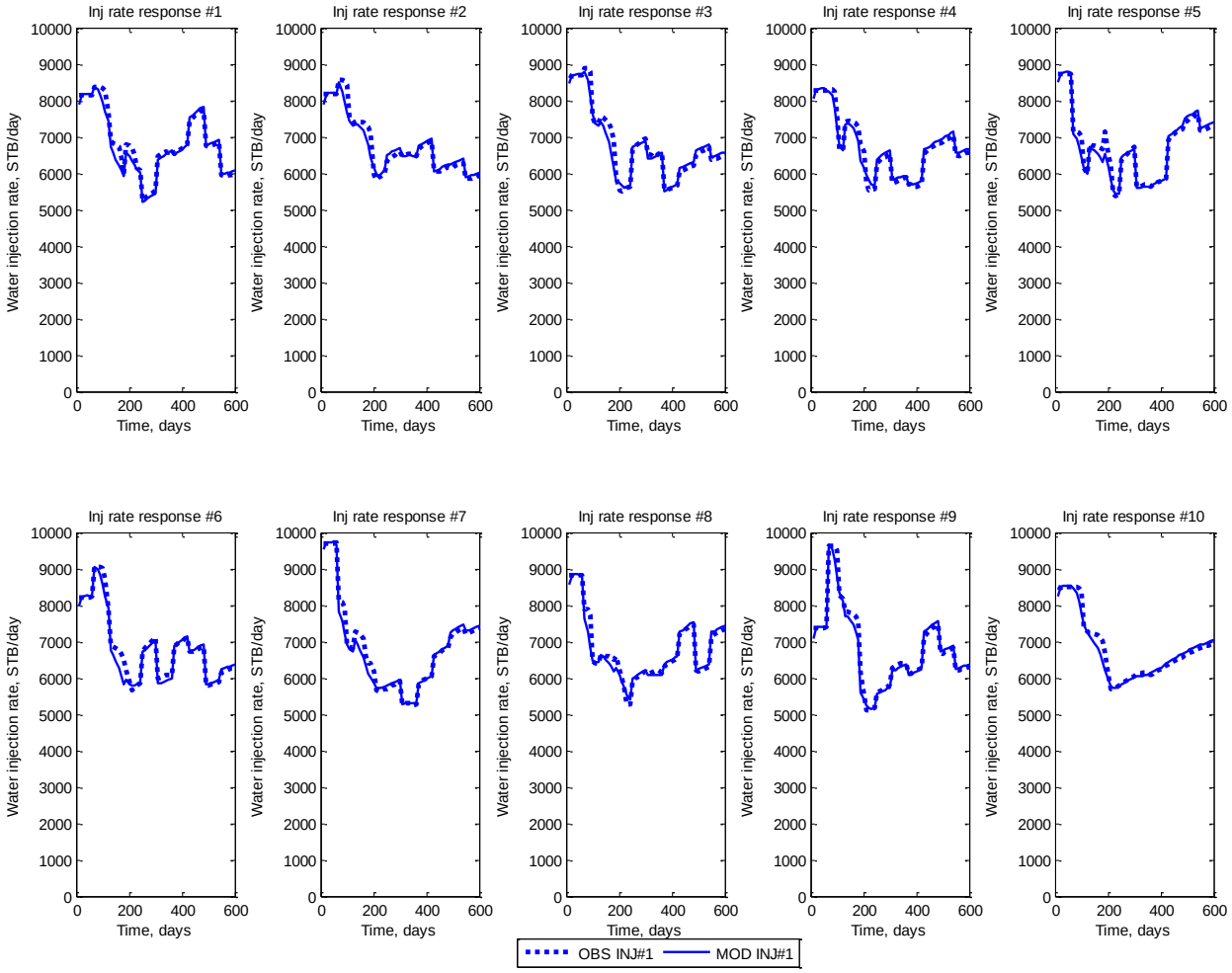

Figure 25: Synthetic model 1 – water injection rate match of the injector

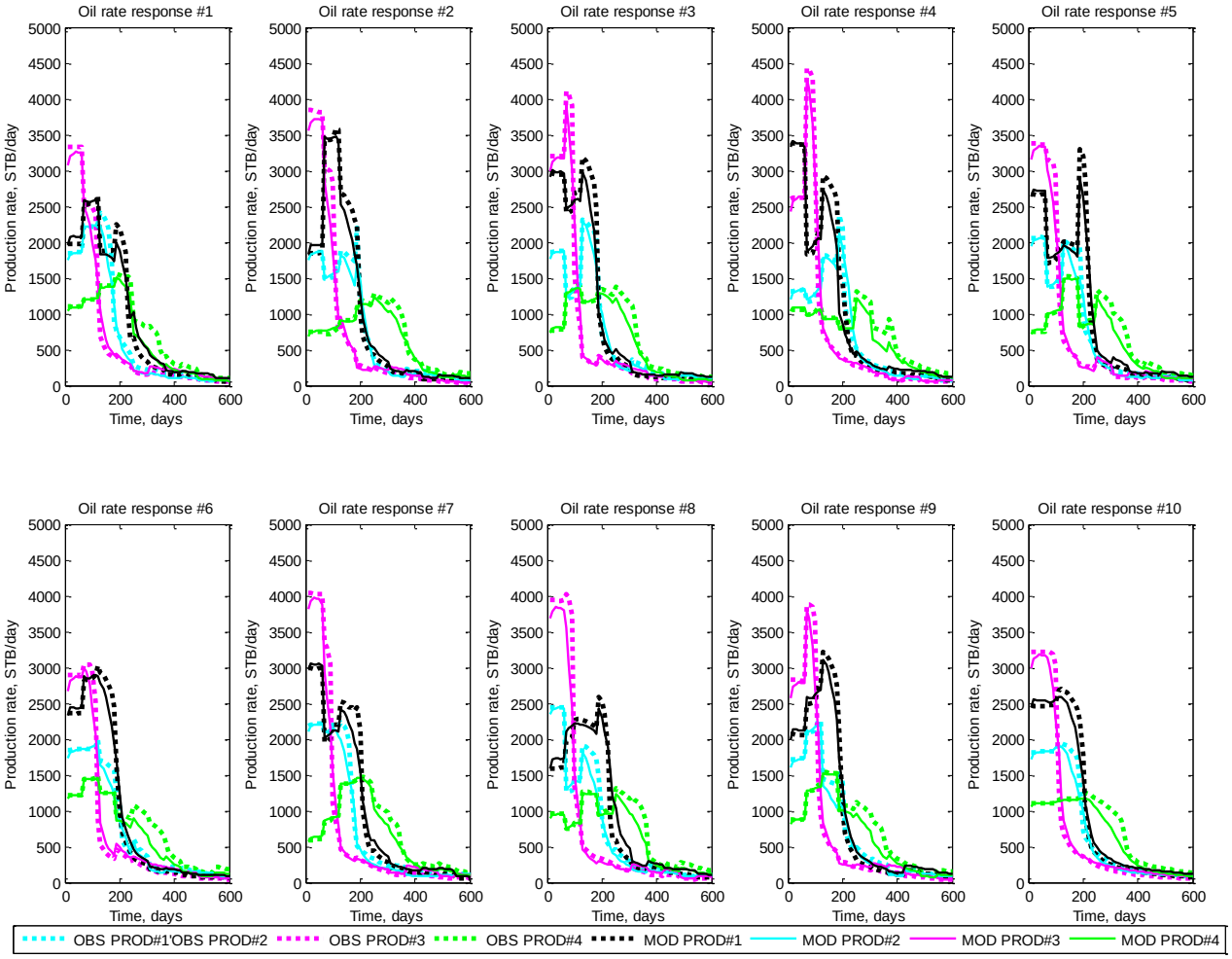

Figure 26: Synthetic model 1 – oil rate match of each producer

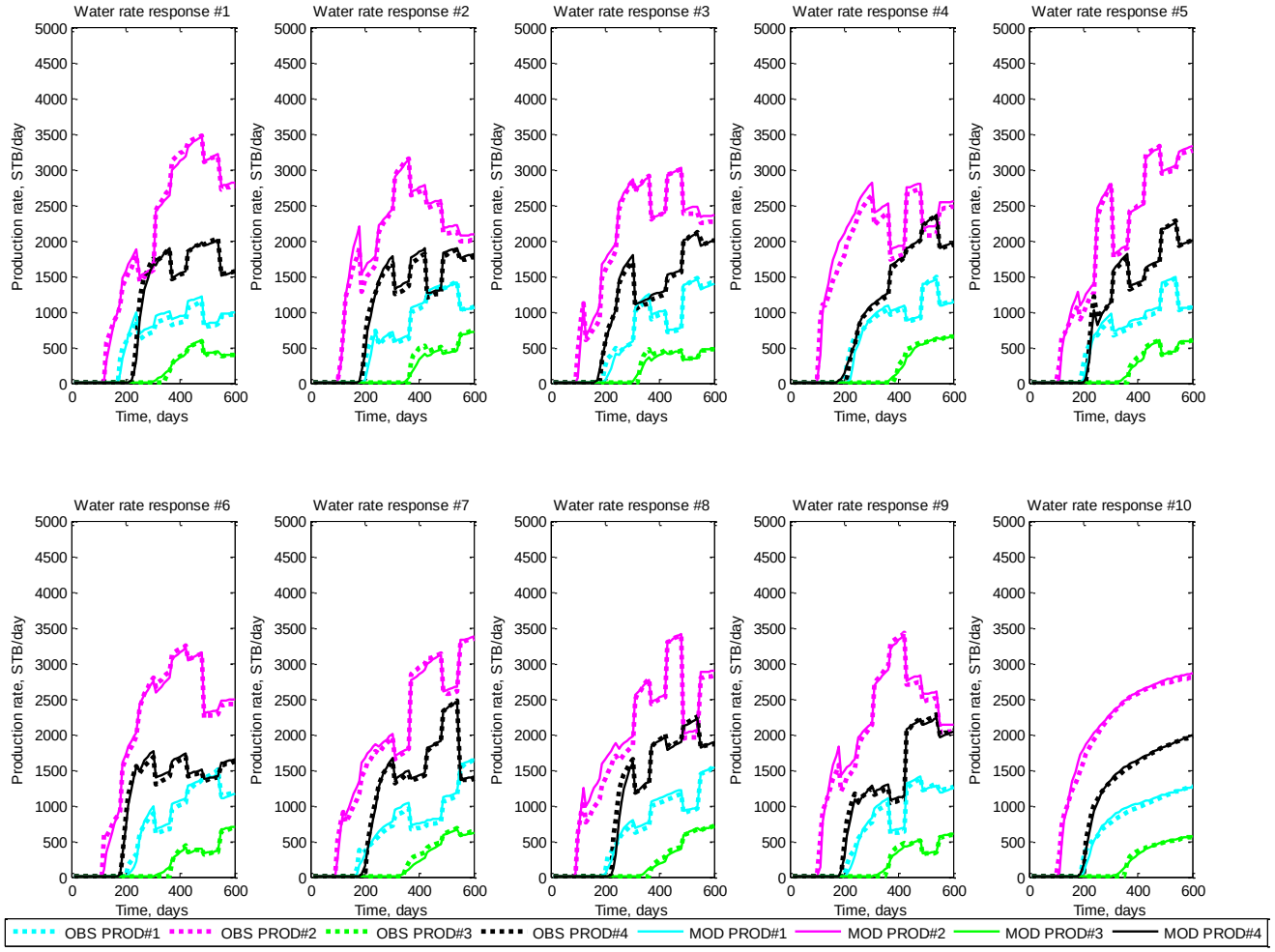

Figure 27: Synthetic model 1 – water rate match of each producer

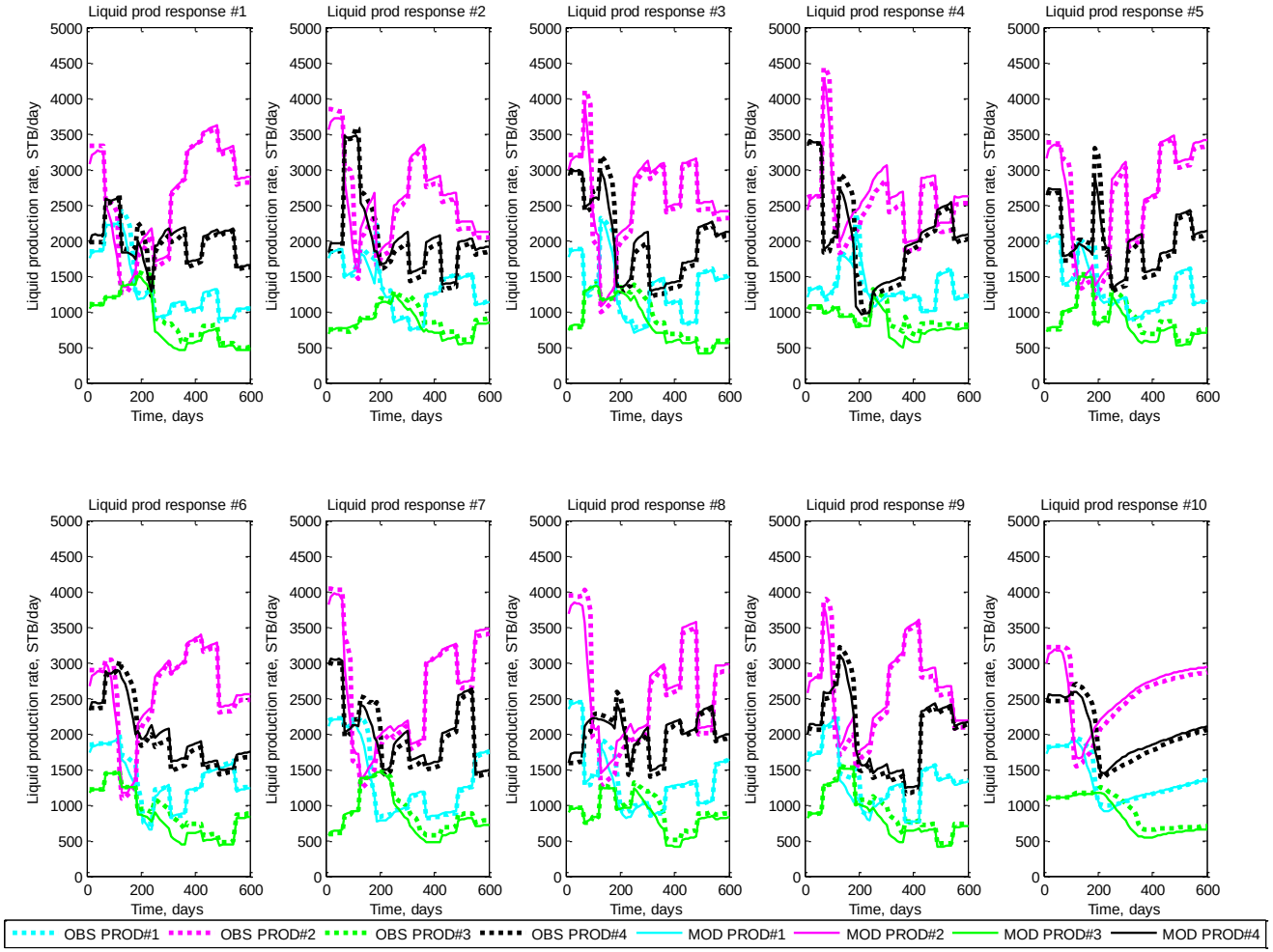

Figure 28: Synthetic model 1 – liquid production rate match of each producer

Figure 23 and Figure 24 show the calibrated grid dimension in the direction perpendicular to the flow path and the grid permeability, respectively. The small maps on the left hand side of each graph in both figures show the corresponding connection of each graph. In Figure 23, it can be seen that most of the fluid is really contained in the connection in between injector and producers, and only a minimal amount of fluid is contained in the producer-producer connection. This is expected for the waterflooding problem. In Figure 24, among these injector-producer connections, the permeability in the connection between INJ#1 and PROD#2 is the highest, while the lowest permeability in the network model is found between INJ#1 and PROD#3. This is corresponding to the original permeability map of the full-order 2D model.

Figure 25 to Figure 28 show the match of the observed data, generated from the full-order model, and the calibrated flow network model responses. Overall, it can be seen that the flow network model can capture and reproduce the trend of the response from the full-order 2D model, although it is not 100% matched.

To confirm the robustness of the resulting model from the robust training, the result is compared with the cases that the models are only calibrated against one single realization. In this case, eleven models are compared; ten of them are the results from normal calibration. The model#1 is calibrated against control trajectory#1, while model#2 is calibrated against control trajectory#2. Model#3 to model#10 are built in the same way. For model#11, it is calibrated against all the realizations simultaneously using robust training technique. All eleven models are prescribed with the 10 control trajectories used in robust training. For each model, the root mean square error (RMSE)

is calculated for each control trajectory. The cumulative probability density function (CDF) of RMSE for each model is plotted together on Figure 29.

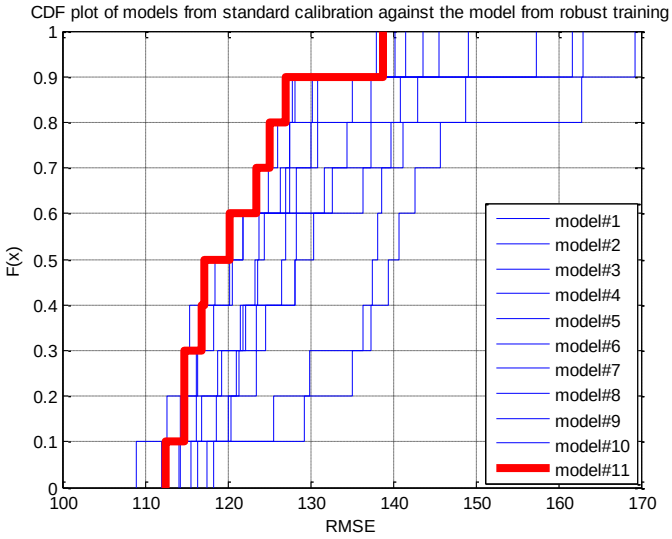

Figure 29: Synthetic model 1 – CDF plots of RMSE for eleven different models

As seen in Figure 29, RMSE distribution of the model obtained from robust training are smaller than the result of other models in the probabilistic sense. Although in some specific control trajectories, other models might yield less error, given that a wide range of control trajectories will be explored in the production optimization, it would be safer to use the robust training technique to calibrate the model.

Note that although the flow network model responses from these 10 control trajectories match well with the full-order model responses, the flow network model could lose its prediction capability if it is prescribed with a control trajectory that is totally different from ones in the training data set.

Production Optimization

In the previous section, the flow network model is calibrated against production data generated from the full-order model using the robust training technique. In this section, the predictive flow network model will be used as a surrogate model for production optimization. The main advantage of this idea is that the flow network model requires much less computational effort than the full-order model. Note that the full-order model has 51 by 51, that is 2601 grids in total, whereas the flow network model has only 45 grids.

The objective here is to maximize the net present value (NPV) of the project, based on the assumed oil price of $100 per STB, the cost to handle water production and water injection of $10 per STB, and a discount factor of zero. The producers' bottom-hole flowing pressure would be varied, while the water injector would be constantly injected at 3500 psi of bottom-hole injection pressure over 400 days. These allowable ranges of injector and producers bottom-hole pressure are the same as ones in the training data.

The initial guess is chosen to be the case in which every producer is controlled constantly at 2700 psi flowing bottom-hole pressure. The production optimization is also implemented by using 'fmincon' in MATLAB®. Figure 30 shows the bottom-hole flowing pressure of each producer in the initial guess control trajectory.

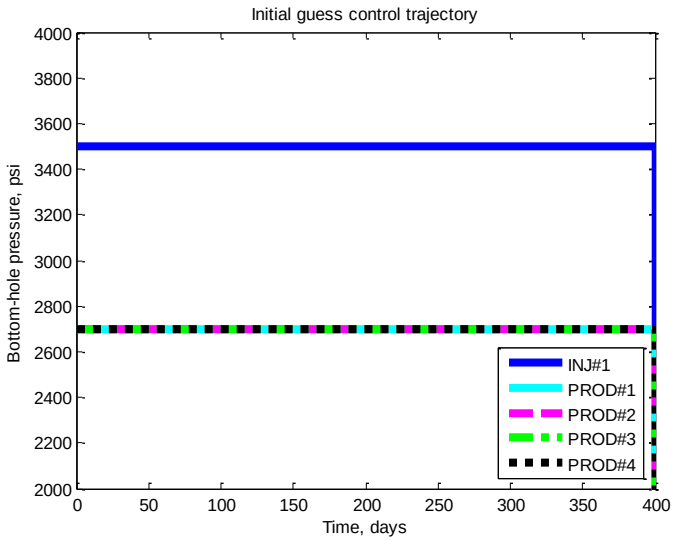

Figure 30: Synthetic model 1 – initial guess of bottom-hole pressure of each well

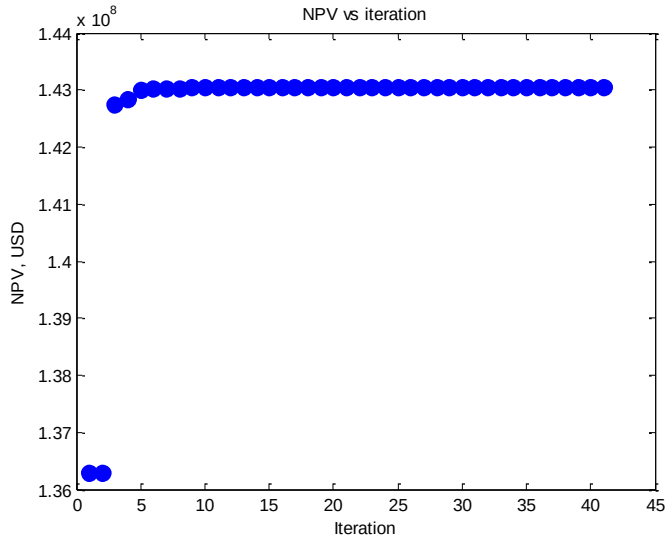

Figure 31: Synthetic model 1 – NPV vs iteration on the flow network model

The NPV in each iteration, calculated by flow network model, can be found in Figure 31. It can be seen that most of the improvement occurs in the very first few

iterations. The total NPV improvement is 4.96%. The result is summarized in Table 5 and the optimal control trajectory, i.e. the optimal bottom-hole flowing pressure of each producer, is shown in Figure 32.

Table 5: Synthetic model 1 – summary of production optimization on the flow network model

	Initial Guess	Optimal Control
Total oil production (MMSTB)	1.734	1.721
Total water production (MMSTB)	0.996	0.601
Total water injection (MMSTB)	2.712	2.304
NPV (MMUSD)	136.287	143.047

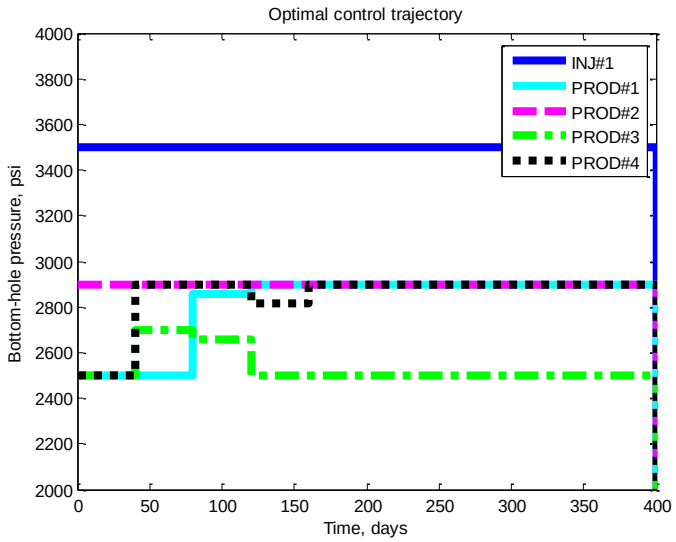

Figure 32: Synthetic model 1 – optimal bottom-hole flowing pressure of each well

To this end, one might question whether the optimal control trajectory obtained from production optimization using the flow network model would really improve the

production on the full-order model. There is a chance that the flow network model might lose its prediction capability during the optimization process, and yield a poor result.

The optimal control trajectory is verified against the full-order model. The resulting optimal control trajectory from production optimization using the flow network model is run on the full-order model, and the responses are compared as shown in Table 6. The results of the flow network model and full-order model are different in magnitude. The NPV improvement on the full-order model becomes 3.94%.

Although the resulting optimal control trajectory from the flow network model can really improve production in the full-order model, it might not be optimal in the full-order model. In this study, the optimality of optimal control in the full-order model is not checked, only comparison is given. Ideally, the process can be improved by implementing the 'nested approach' as suggested by van Doren et al. (2006).

Table 6: Synthetic model 1 – optimal responses from the flow network model on the flow network and the full order model

	Flow network model		Full order model	
	Initial guess	Optimal control	Initial guess	Optimal control
Total oil production (MMSTB)	1.734	1.721	1.822	1.805
Total water production (MMSTB)	0.996	0.601	0.960	0.598
Total water injection (MMSTB)	2.712	2.304	2.765	2.387
NPV (MMUSD)	136.287	143.047	144.933	150.650
Improvement	4.96%		3.94%	

The cumulative field oil and water production from the full-order model is shown in Figure 33. Overall, it can be seen that the NPV is mainly improved by reduction in

water production and injection in the optimal control case, while the oil production is relatively unchanged from the initial guess.

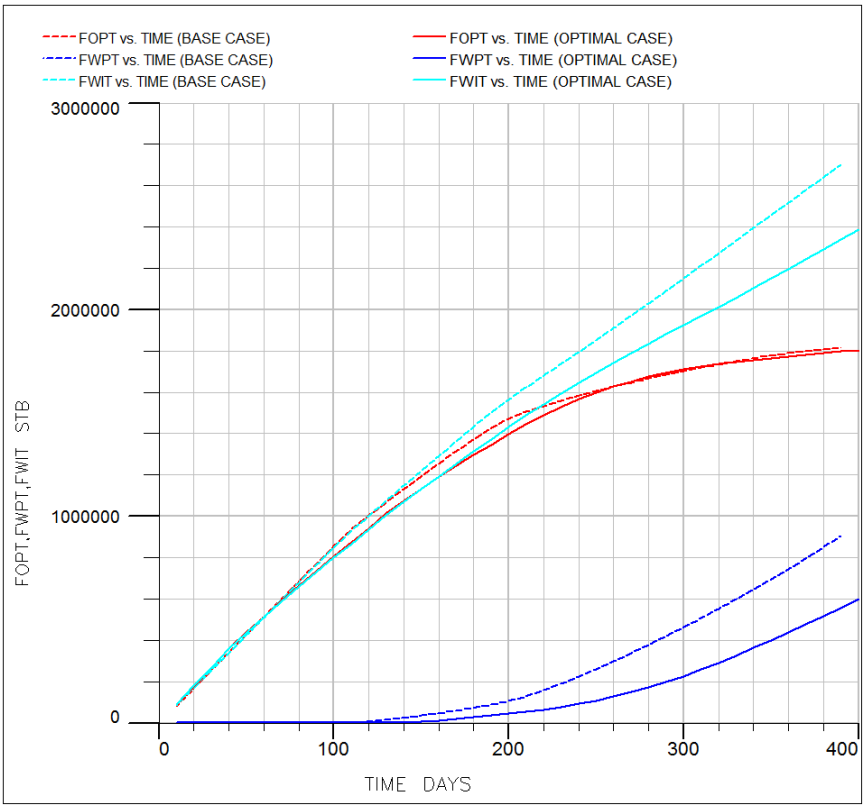

Figure 33: Synthetic model 1 – responses from the full-order model using the initial guess and the optimal control trajectory obtained from the flow network model

One might also question if the optimal control obtained by using this surrogate model is the same as when the full-order model is used. In this case, the production optimization is performed using the full-order model via implementation using the 'OPTIMIZE' module in ECLIPSE. The same constraints are applied. The result of optimization using the flow network and full-order model is compared in Table 7.

Table 7: Synthetic model 1 – comparison of production optimization using the full-order model and the flow network model

	Using flow network model	Using full-order model
Initial guess NPV (MMUSD)	144.933	144.933
Optimal NPV (MMUSD)	150.650	150.539
Improvement	3.94%	3.87%

The NPV improvements from the two processes are very similar. In addition, the responses from the full-order model optimization, shown in Figure 34, are very similar to the responses obtained by the flow network model, shown in Figure 33.

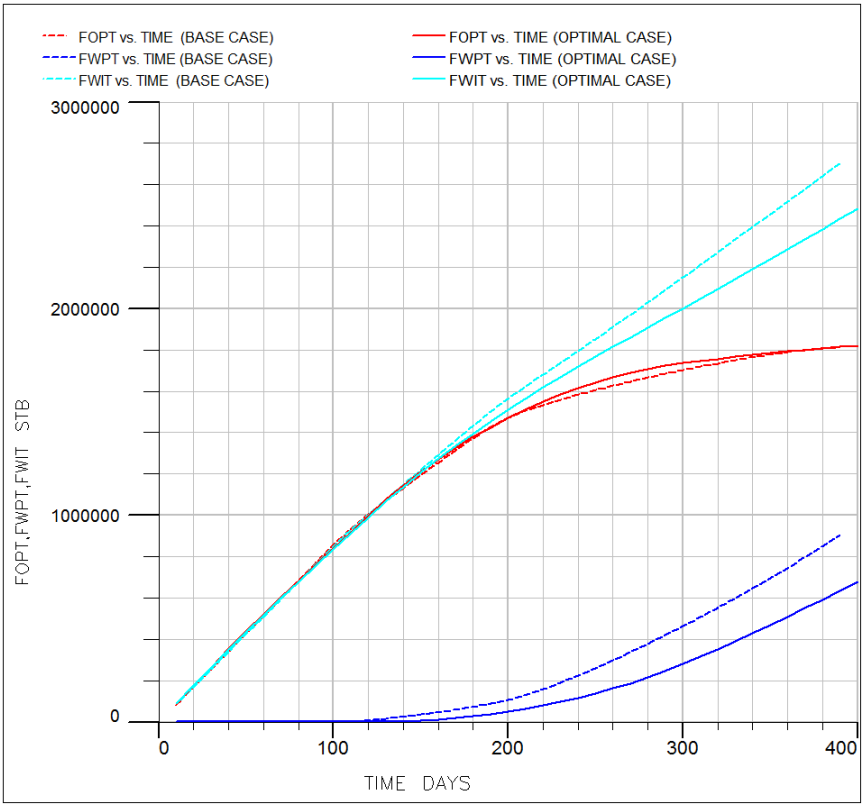

Figure 34: Synthetic model 1 – responses from the full-order model using the initial guess and the optimal control trajectory obtained from the full-order model

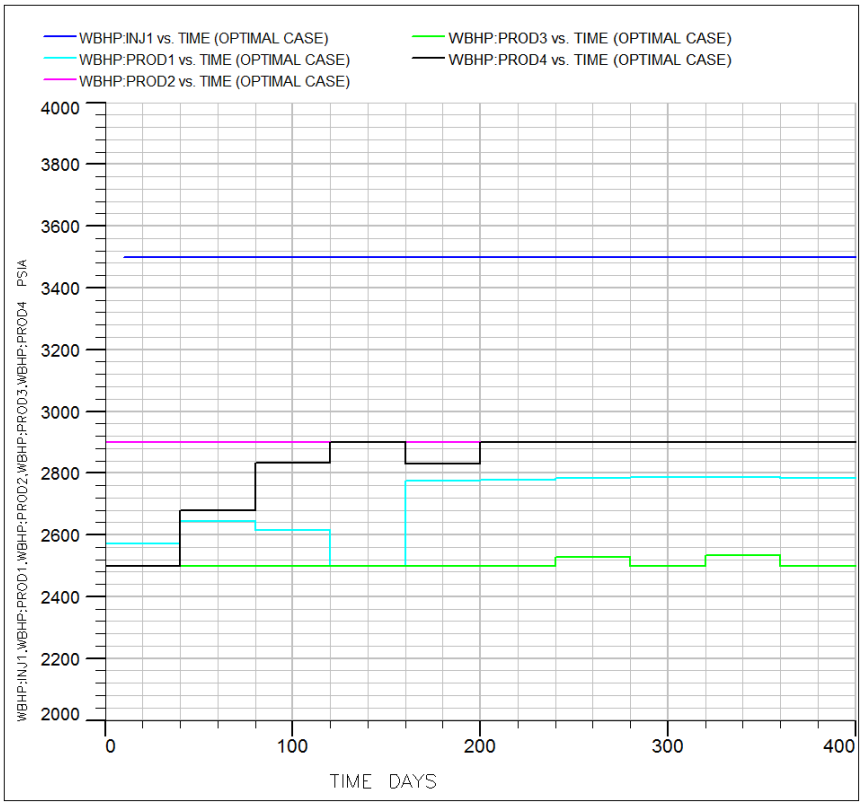

Figure 35: Synthetic model 1 – optimal control trajectory from the full-order model optimization

The optimal control obtained from the full-order model can be seen in Figure 35. It also gives a similar effect as the one obtained by the flow network model shown in the Figure 32. To be specific, in the later time, PROD#3 is fully open, while the others are choked to promote more sweep efficiency in the low permeability area in the northeast region of the reservoir.

Speed-Up

One of the most interesting issues about using the flow network model instead of the full-order model to perform production optimization is how much speed-up can be

obtained. To investigate this issue, a few aspects have to be clarified. First of all, what should be compared are the full-order model production optimization and the flow network model production optimization.

For the full-order model production optimization, ECLIPSE is used as the full-order reservoir simulator. ECLIPSE is a famous reservoir simulator that is well-known in the industry. The code is maturely developed, and hence it is considered to be very efficient. The simulation runs are defined using fully implicit formulation. Production optimization is performed using the 'OPTIMIZE' module in ECLIPSE, which is the gradient-based optimizer. The gradient is evaluated using the adjoint method, which is considered to be less expensive than the numerical perturbation method.

For the flow network model production optimization, the flow network model is developed on MATLAB®. Basically, it is the finite difference reservoir simulation model that is developed on the semi-implicit, or the lagging coefficients, formulation. The time-stepping is user defined, compared to automatic time-stepping implemented in ECLIPSE. The flow network model is developed mainly to study the concept. It is by no means optimal at this stage. In addition, although MATLAB® is very powerful and very versatile, especially to prototype the code, it is not as fast as FORTRAN, which ECLIPSE utilizes. For the production optimization using the flow network model, the gradient-based method is also used. However, the gradient is determined by the numerical perturbation method. It is required to run the flow network model as many times as the number of control input parameters, allowed to be varied during production optimization.

The main point that makes the flow network model faster than the full-order model is the significant reduction in the number of grid blocks. Considering the above differences in the status of the full-order model production optimization, which is implemented in the maturely developed ECLIPSE, and the flow network model production optimization, which is not optimal, it is unfair to compare the computational efficiency.

However, to give some idea of how fast the flow network model is, comparison of elapsed time of the full-order model runs and the flow network model runs on the same control trajectories are investigated as shown in Figure 36.

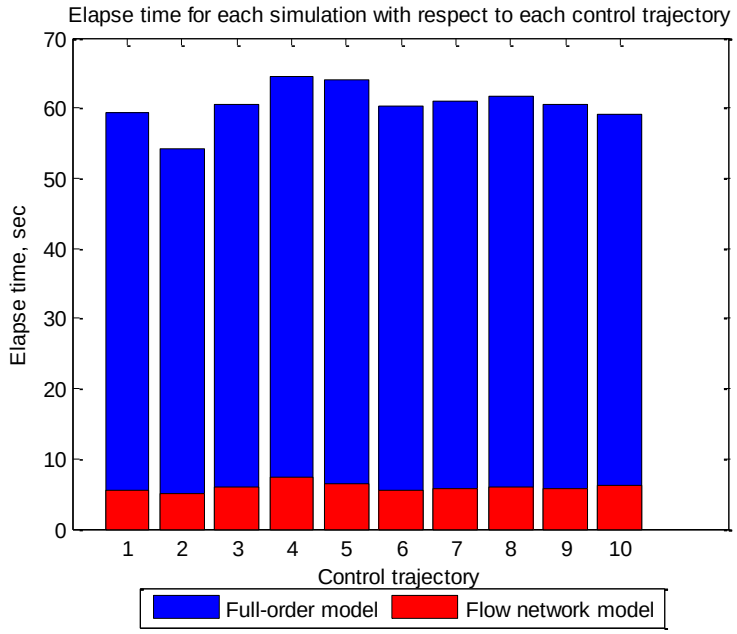

Figure 36: Synthetic model 1 – elapse time of the full-order and the flow network model on the control trajectories used to train the flow network model

From Figure 36, the flow network model is approximately 10 times faster than the full-order model. Although the flow network model code is not optimized, it is still faster than the full-order model run on ECLIPSE. This speed-up is mainly caused by considerable reduction in the number of grid blocks, from 2601 to 45 grids (58 times).

It must be emphasized that this is not the comprehensive comparison; it is very specific to the problem and the reduction in the number of grids.

Synthetic Reservoir Model 2

The inverted-5-spot waterflood problem is previously shown in the synthetic model number 1. This example demonstrates the methodology on the more complex problem, i.e. more wells and a more complex geological scenario. The synthetic reservoir permeability and porosity distributions were chosen from the top layer of the SPE10 reservoir model (Christie and Blunt 2001). The magnitude of porosity and permeability is scaled as shown in Figure 37 and Figure 38, respectively. General information about the model can be found in Table 8. Location and basic information about each injector and producer can be found in Table 9. The fluid relative permeability and PVT data are exactly the same as the previous problem and are summarized in Table 3 and Table 4, respectively.

The maps, shown in Figure 37 and Figure 38, depict the logarithmic value of the permeability and porosity of each grid block in the reservoir model, respectively. Overall, it can be seen that the two producers in the western area are isolated from the other part of the reservoir by the low porosity and permeability zone.

Table 8: Synthetic model 2 – basic reservoir properties

Properties	Parameters	Value
Number of grid cells in x direction	N_x	60
Number of grid cells in y direction	N_y	220
Number of grid cells in z direction	N_z	1
Grid block size in x direction	Δx	32.808399 ft
Grid block size in y direction	Δy	32.808399 ft
Reservoir thickness	h	32.808399 ft
Permeability in x, y, z direction	k_x, k_y, k_z	Figure 37
Porosity (reference)	ϕ	Figure 38
Rock compressibility (constant)	c_r	3×10^{-6}
Oil relative permeability	$k_{ro}(S_w)$	See Table 3
Water relative permeability	$k_{rw}(S_w)$	See Table 3
Oil viscosity	μ_o	See Table 4
Oil formation volume factor	B_o	See Table 4
Water viscosity	μ_w	See equation (58)
Water formation volume factor	B_w	See equation (59)
Oil compressibility	c_o	$1 \times 10^{-5} psi^{-1}$
Water compressibility	c_w	$3 \times 10^{-6} psi^{-1}$
Initial reservoir pressure (all block)	p_o	3000 psi
Initial water saturation (all block)	S_w	0.1

Table 9: Synthetic model 2 – basic information about the wells

Well no.	I location	J location	K location	Well radius (ft)	Skin factor
INJ1	30	55	1	0.583	0
INJ2	30	165	1	0.583	0
PROD1	1	1	1	0.583	0
PROD2	1	110	1	0.583	0
PROD3	1	220	1	0.583	0
PROD4	60	1	1	0.583	0
PROD5	60	110	1	0.583	0
PROD6	60	220	1	0.583	0

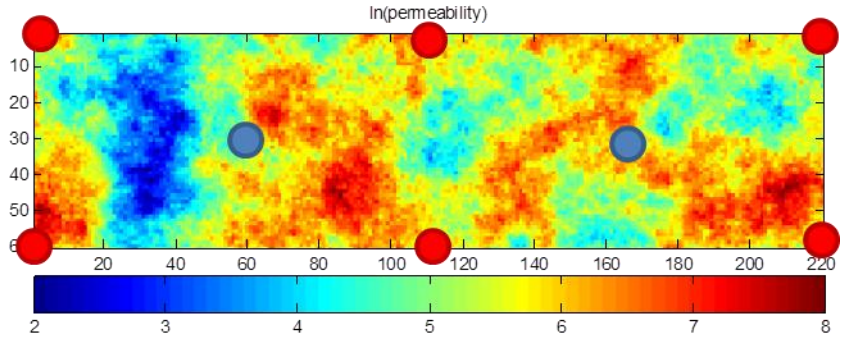

Figure 37: Synthetic model 2 – the logarithmic value of permeability map

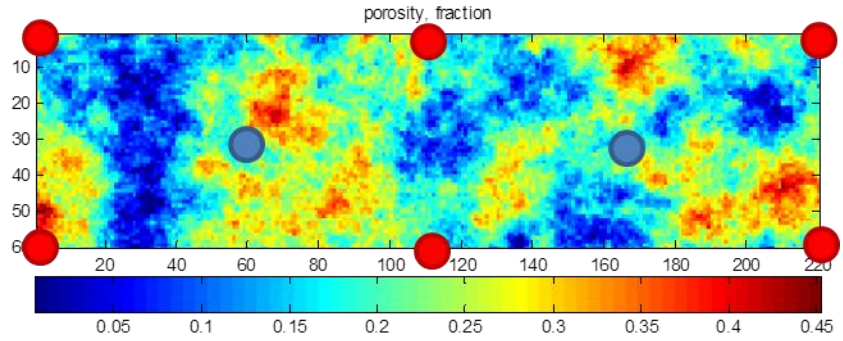

Figure 38: Synthetic model 2 – porosity map and well location

Training Data

The training data are generated from the allowable range of the well operating condition. Each injector is allowed to be operated between 5000 and 6000 psi, while each producer is allowed to be operated between 2000 and 2900 psi. The reservoir would be optimized for 400 days; the training data is thus generated for 600 days. Eleven control trajectories are generated and shown in Figure 39. This includes the uniform control, used as an initial guess for production optimization. The full-order model responses with respect to each control trajectory are shown in Figure 40 to Figure 43.

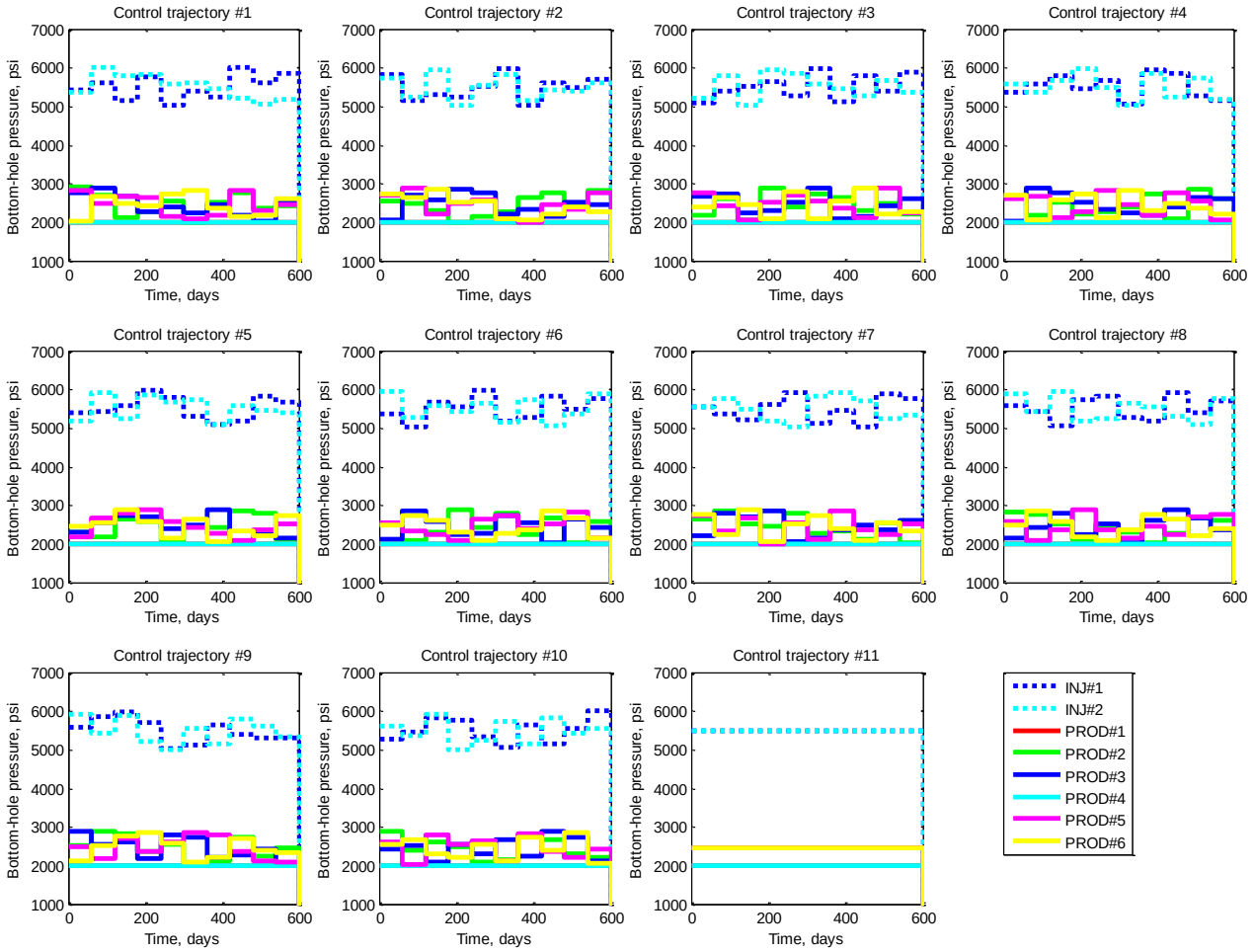

Figure 39: Synthetic model 2 – training control trajectories, bottom-hole flowing pressure of each well

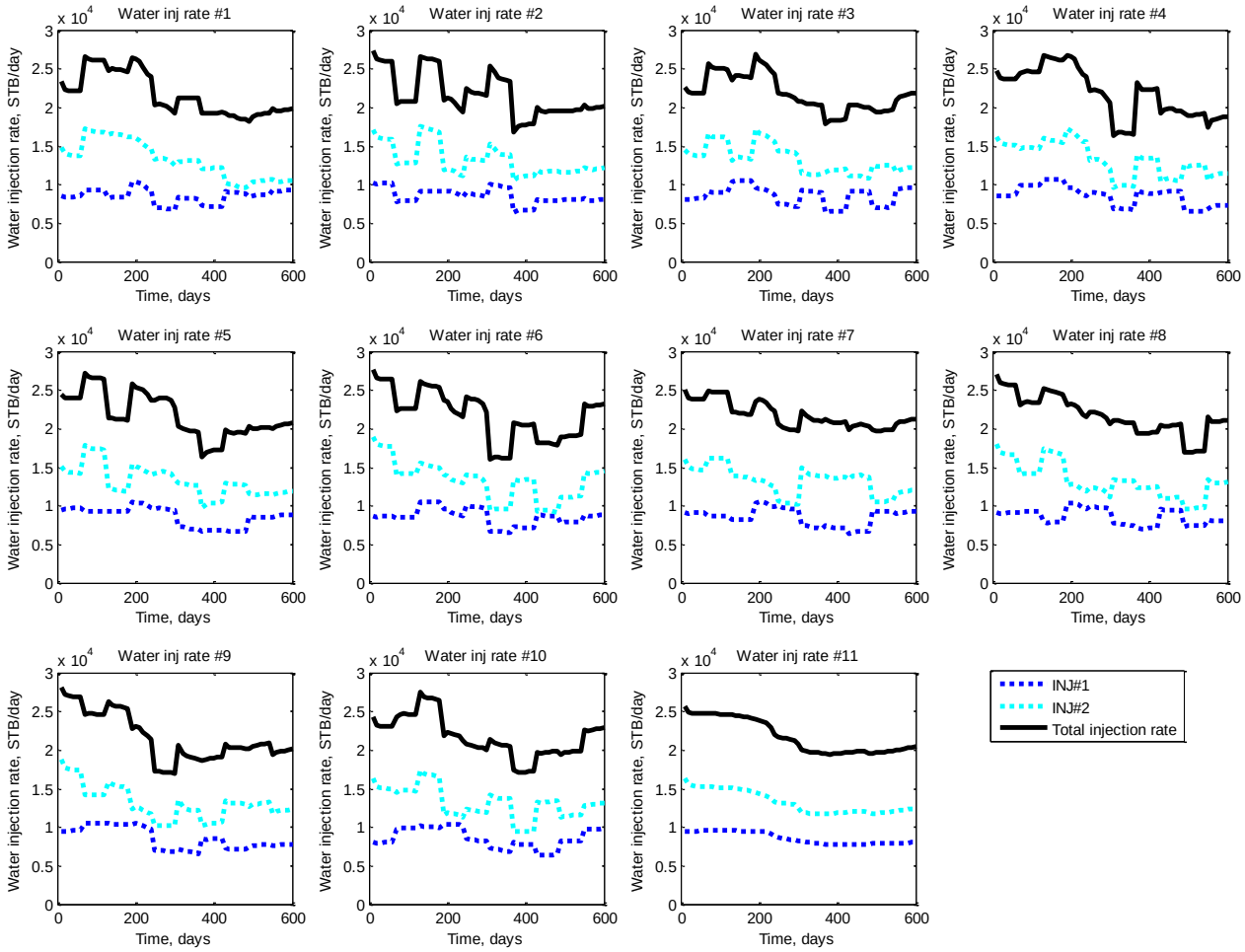

Figure 40: Synthetic model 2 – resulting water injection rate of injector

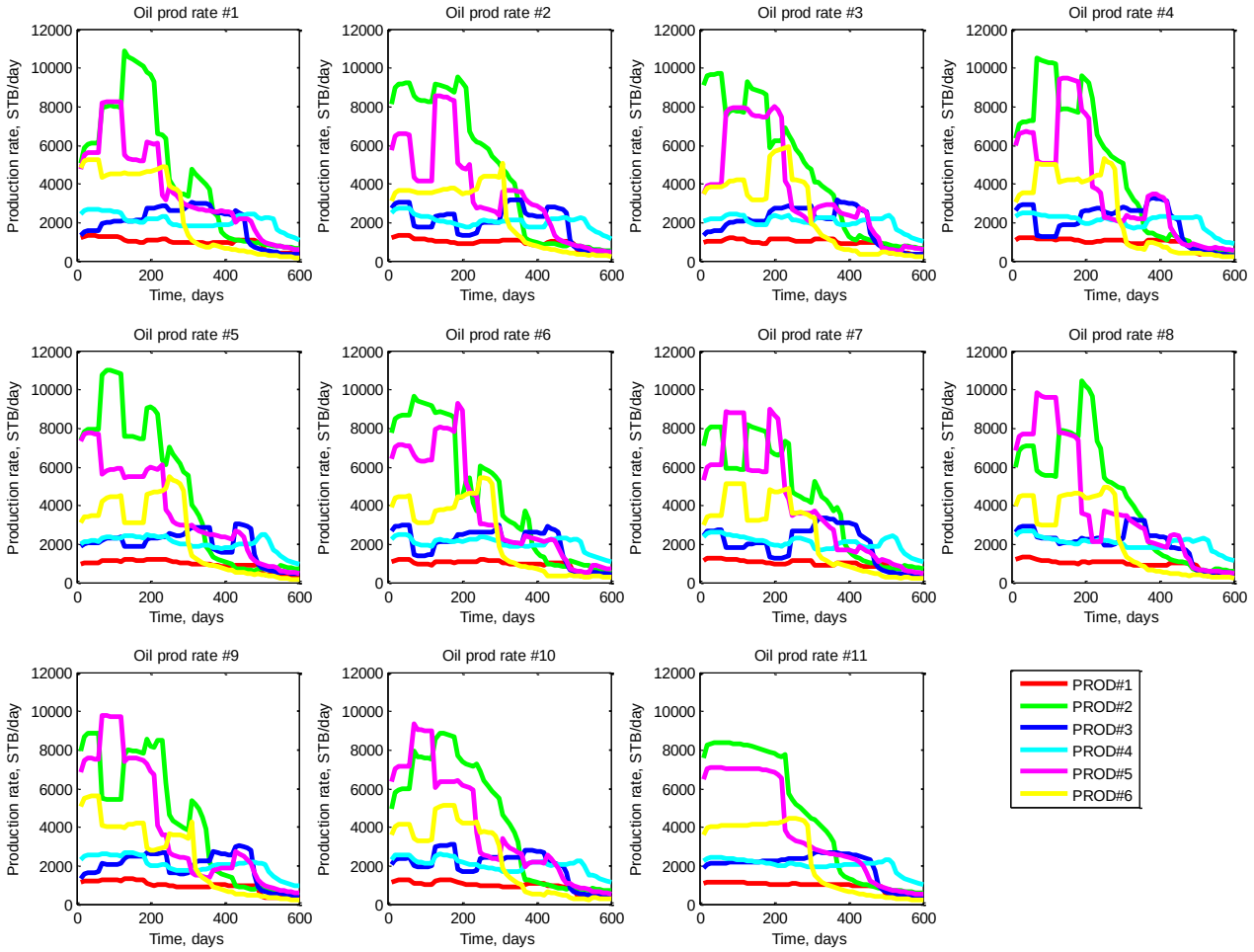

Figure 41: Synthetic model 2 – resulting oil production rate of each producer

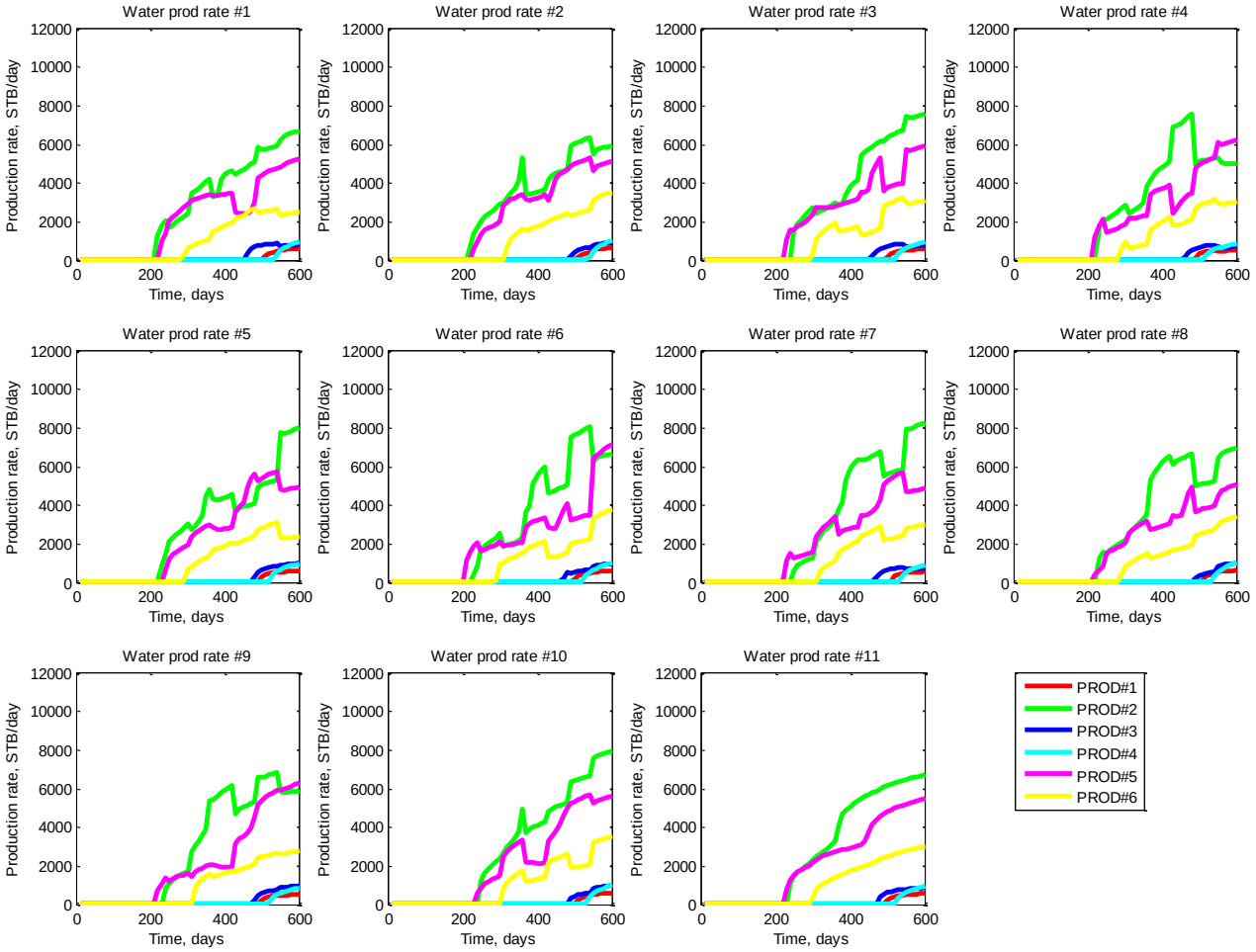

Figure 42: Synthetic model 2 – resulting water production rate of each producer

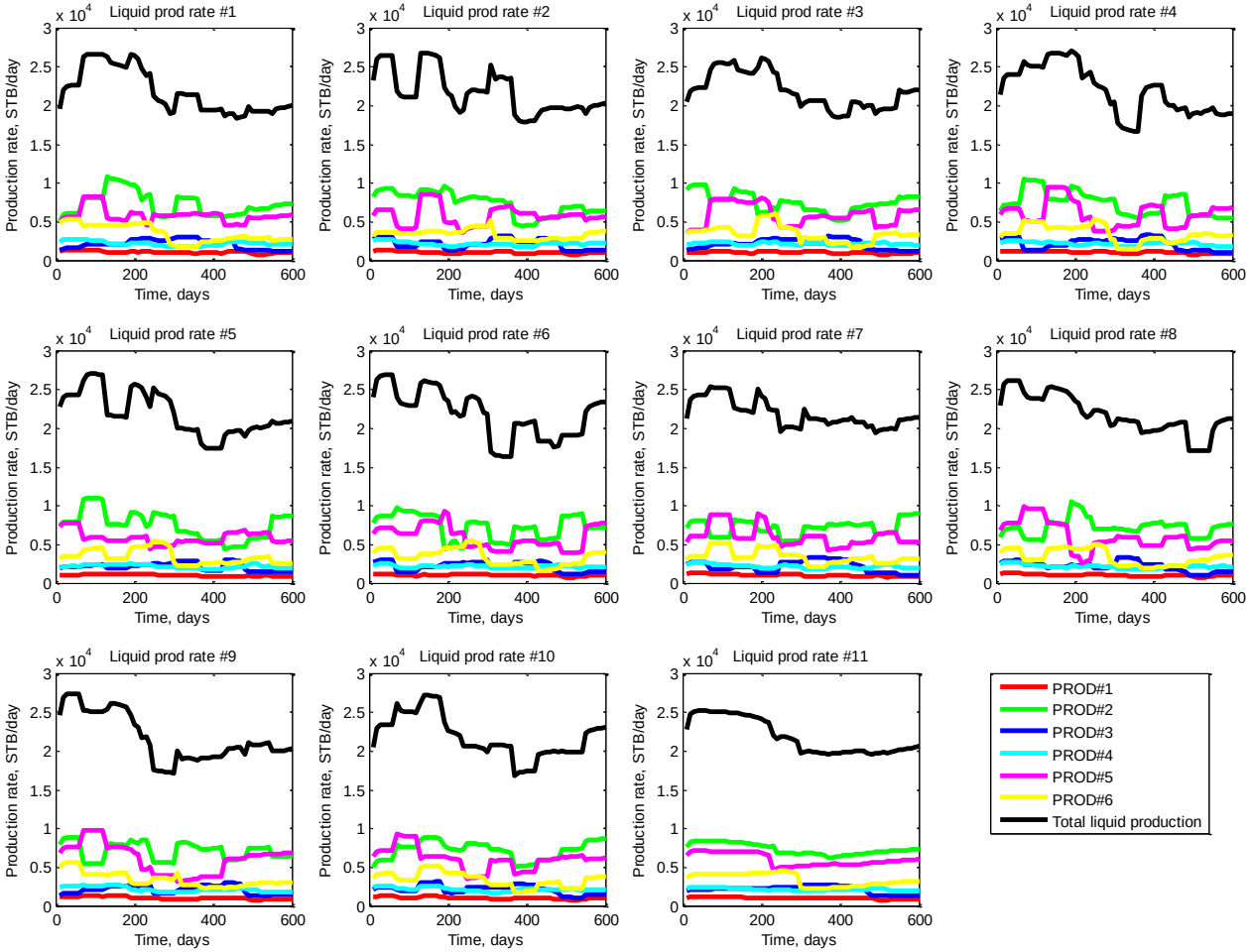

Figure 43: Synthetic model 2 – resulting liquid production rate of each producer

Calibration

Similar to the previous problem, the calibration is initialized such that the total pore volume of the flow network model is the same as the full-order model. It is included via the linear equality constraint in the minimization. The lower bound of the grid block dimension perpendicular to the flow direction, dy, is defined as 10 ft. The initial guess of dy is designed such that 90% of the pore volume is contained in the connection between the producers and the nearby injectors. The initial guess of permeability of each grid is equal to the average permeability of the full-order model. The lower bound of the permeability is 10 md. The minimization is performed using 'fmincon' in MATLAB®. The calibrated parameters of the flow network model, i.e. dy and permeability, can be found in Figure 44 and Figure 45. The calibrated flow network model responses are compared to the full-order model responses in Figure 46 to Figure 49.

From the results, most of the fluid is still contained in the injector-producer connections. Although the permeability result is more difficult to interpret, the most important thing is that the flow network model can capture the fluctuation of the full-order model responses quite well.

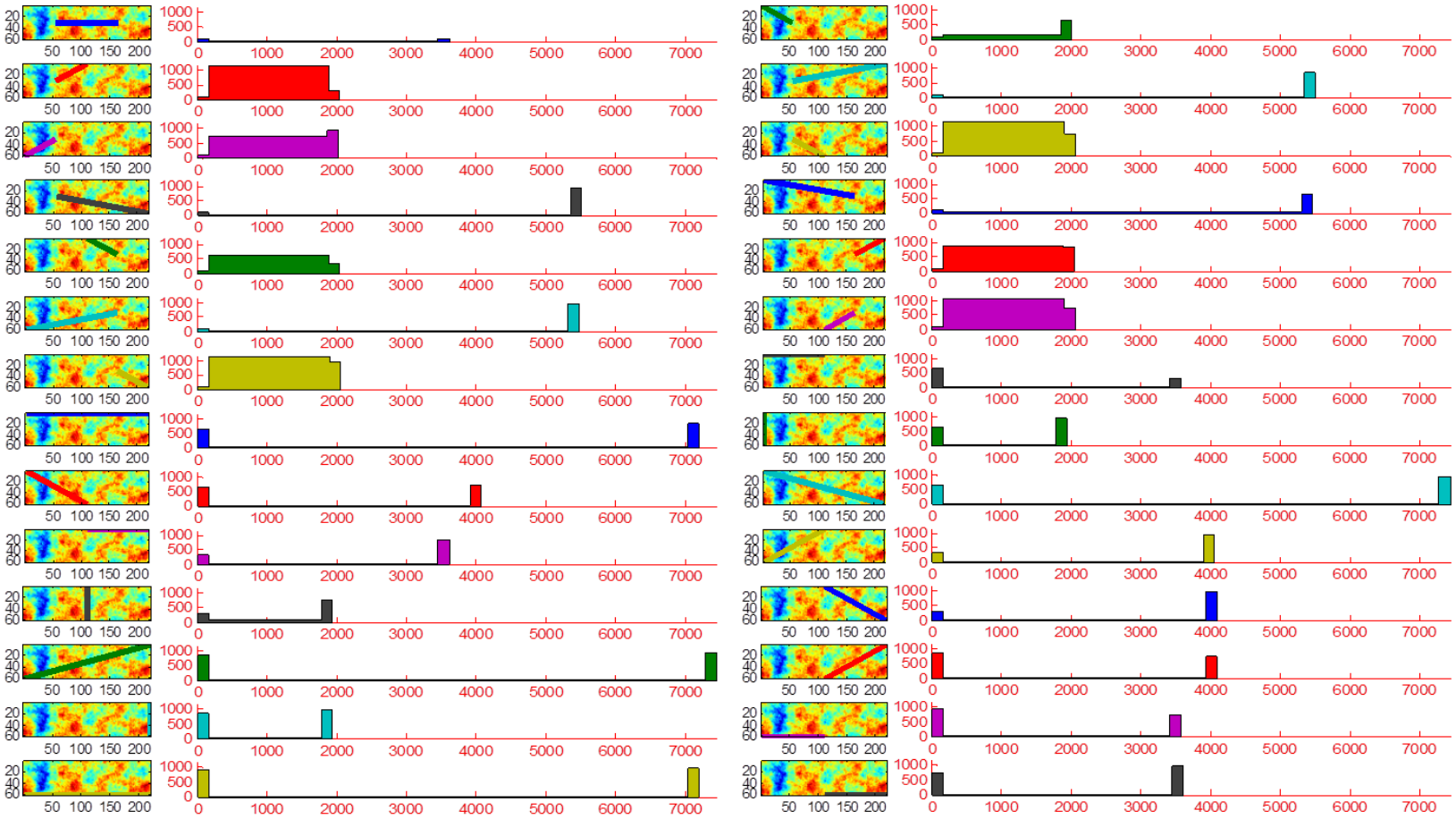

Figure 44: Synthetic model 2 – calibration result of grid dimension perpendicular to the flow path

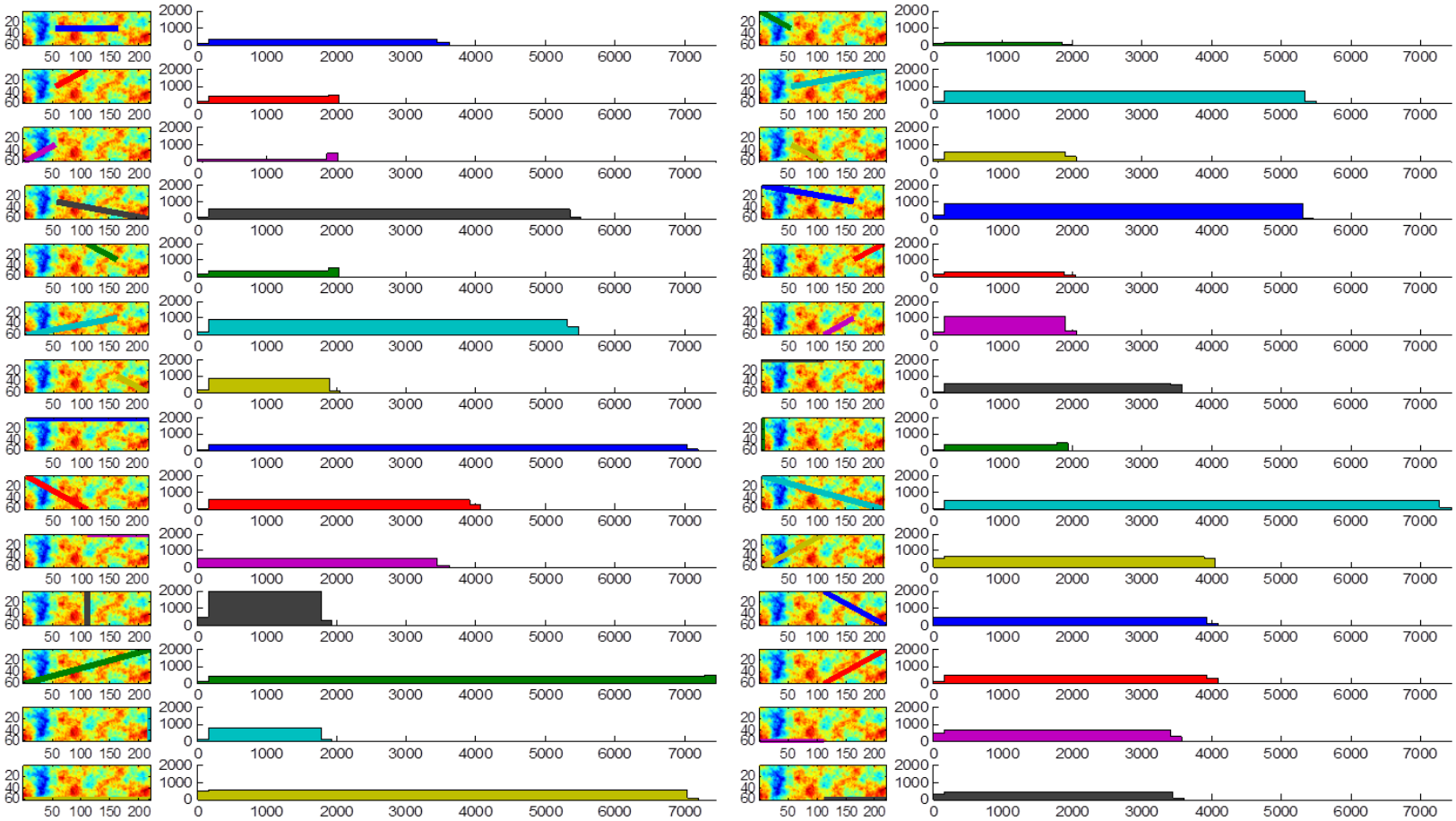

Figure 45: Synthetic model 2 – calibration result of grid permeability

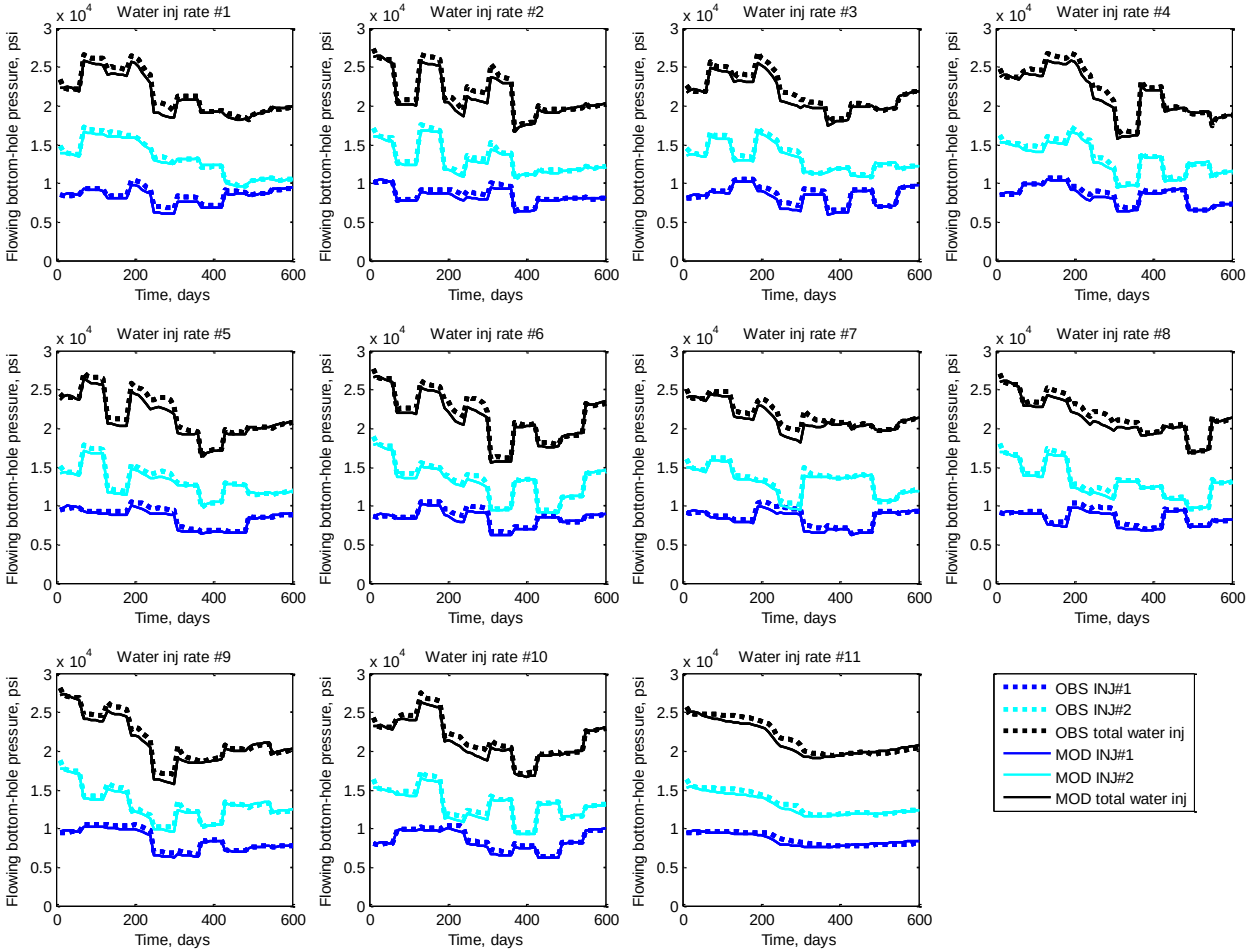

Figure 46: Synthetic model 2 – water injection rate match of each injector

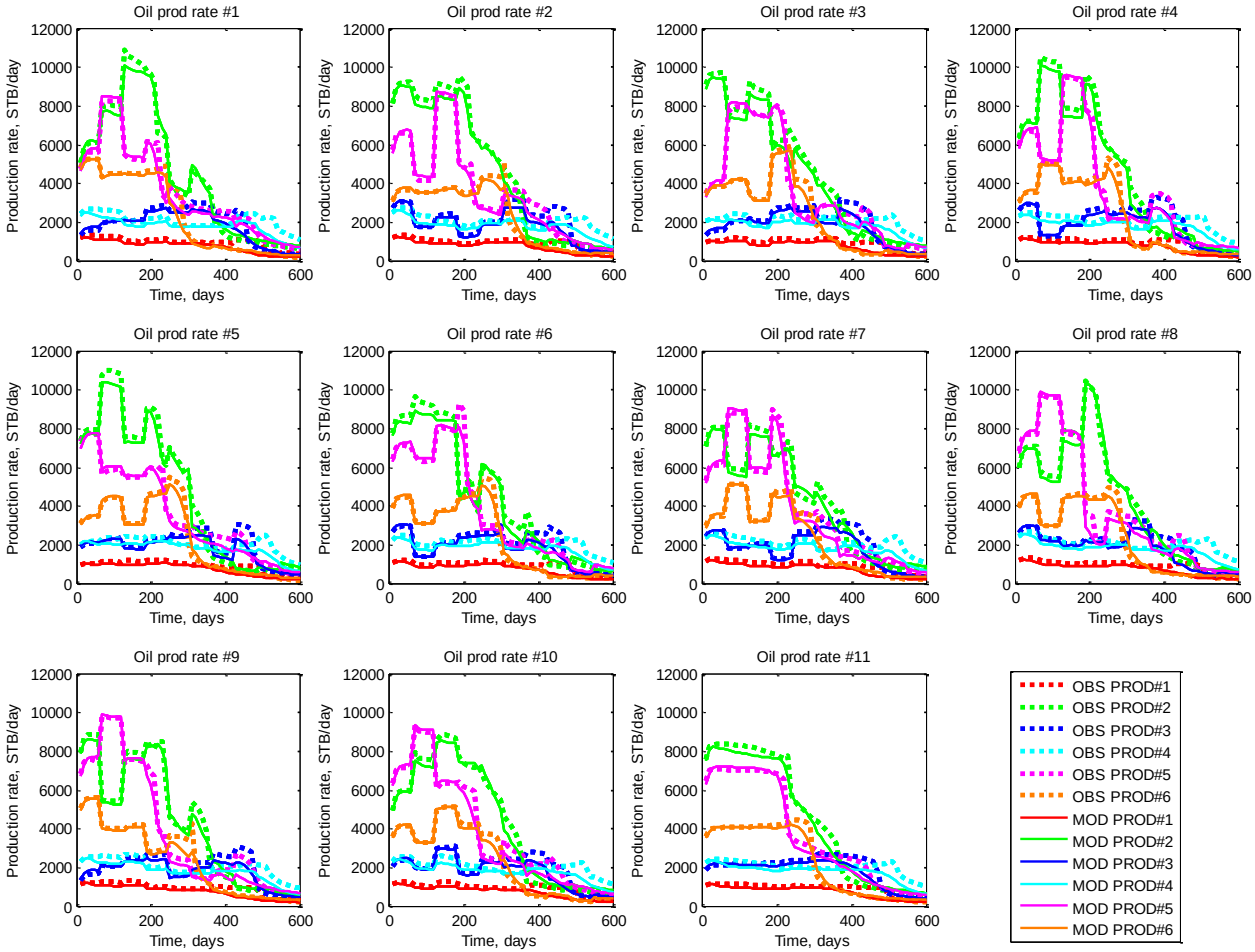

Figure 47: Synthetic model 2 – oil rate match of each producer

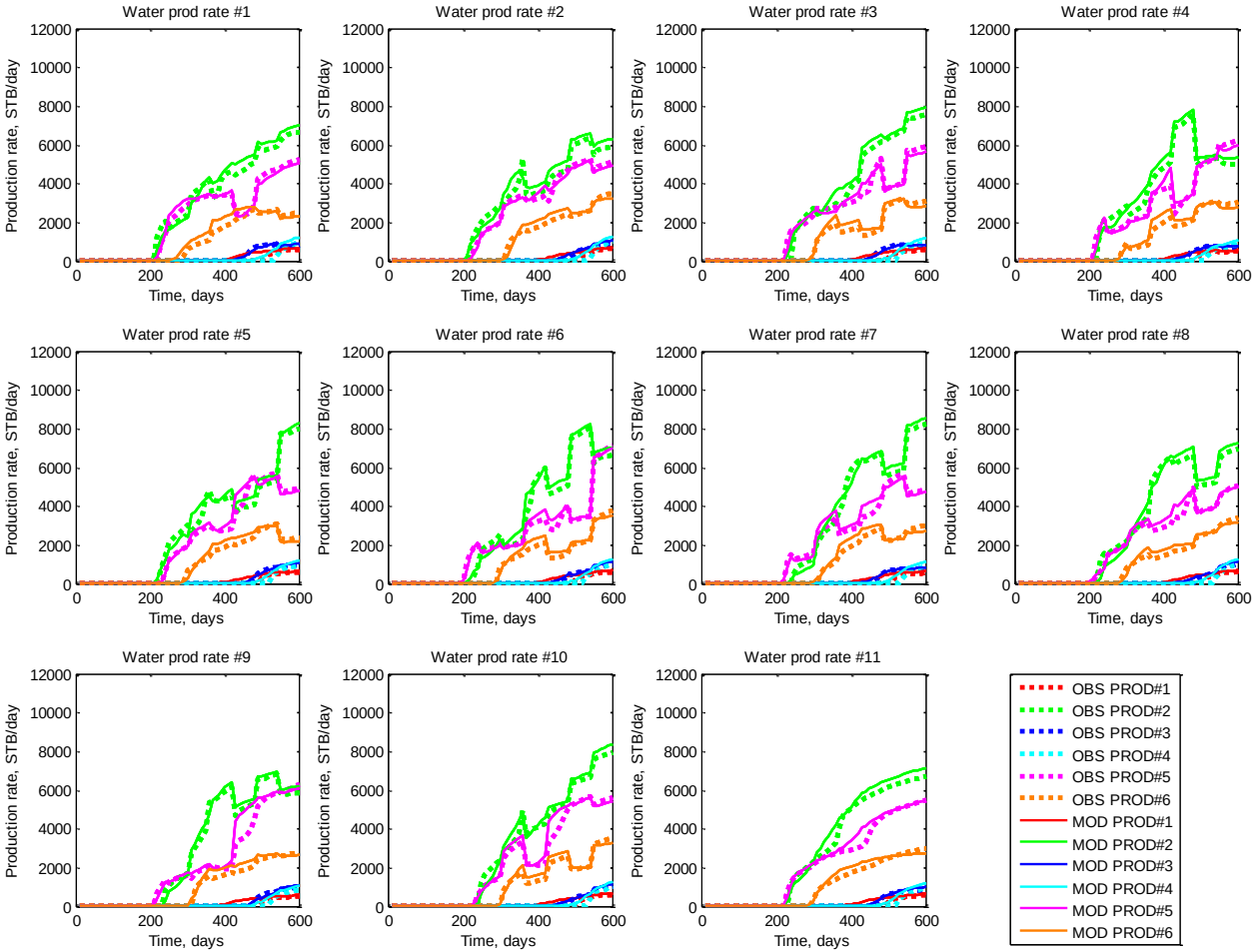

Figure 48: Synthetic model 2 – water rate match of each producer

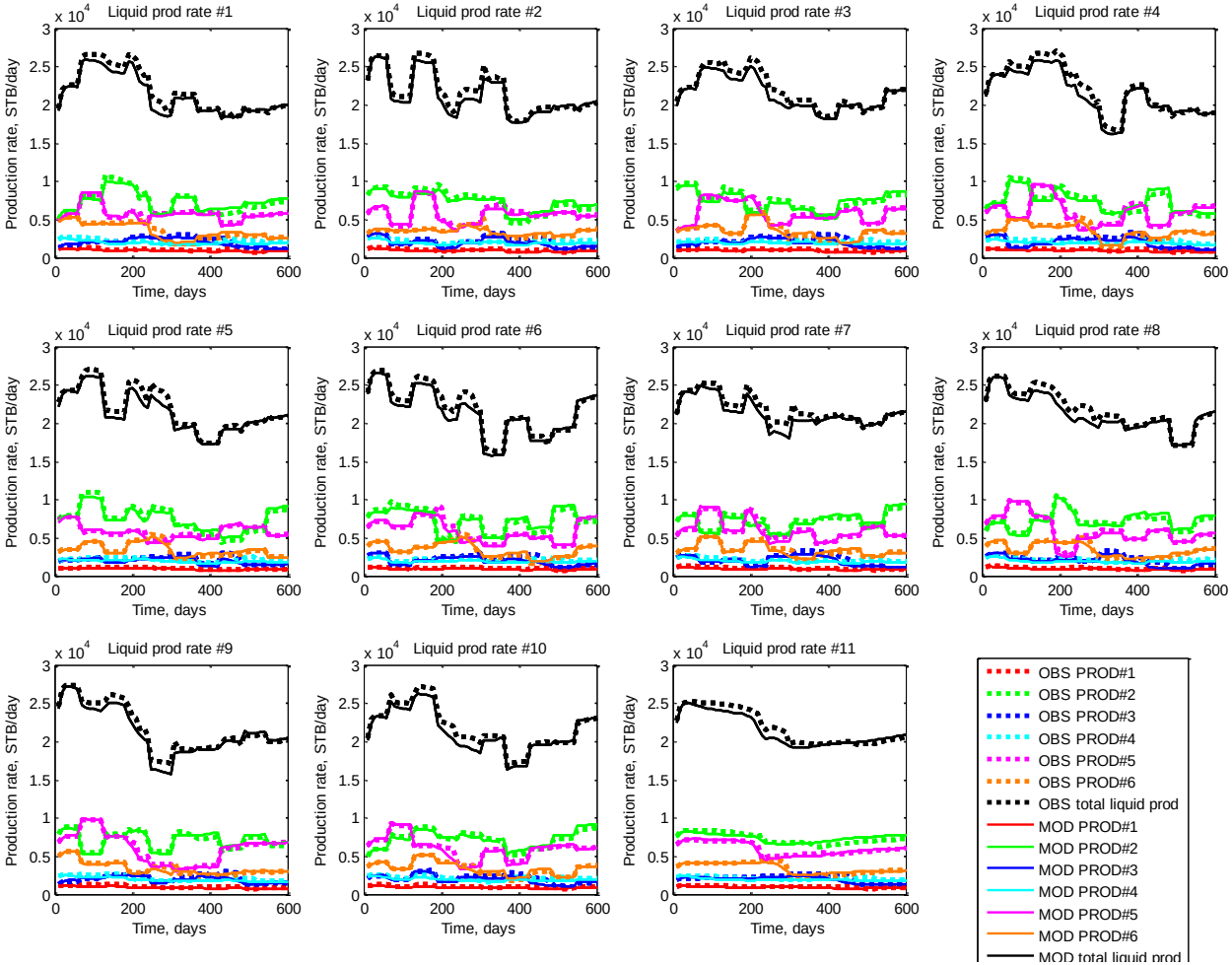

Figure 49: Synthetic model 2 – liquid production rate match of each producer

Production Optimization

The calibrated flow network model is generated using the robust training technique. With the same economical assumption previously applied to the synthetic model 1, production optimization is performed to maximize the project NPV for 400 days of production.

The initial guess is designed such that both injectors are constantly operated at 5500 psi, while each producer is constantly operated at 2450 psi, except PROD#1 and PROD#4, which are operated at 2000 psi constantly to promote more sweep efficiency.

The optimization parameters for this synthetic model are injection pressure for both injectors. They are allowed to be varied between 5000 and 6000 psi. In addition, each producer, except PROD#1 and PROD#4, is allowed to be operated between 2000 and 2900 psi.

The results are illustrated as follows. Figure 50 shows the bottom-hole flowing pressure of each producer in the initial guess control trajectory. NPV improvement and result of production optimization can be found in Table 10. The total NPV improvement is 5.24%. The optimal control trajectory, i.e. the optimal bottom-hole flowing pressure of each injector and producer is shown in Figure 51.

Table 10: Synthetic model 2 – summary of production optimization on the flow network model

	Initial Guess	Optimal Control
Total oil production (MMSTB)	7.669	8.097
Total water production (MMSTB)	1.111	1.295
Total water injection (MMSTB)	8.781	9.394
NPV (MMUSD)	669.122	704.209

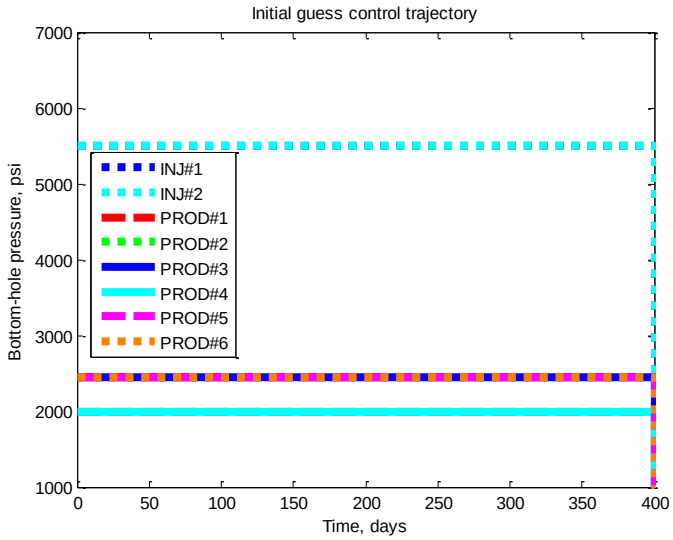

Figure 50: Synthetic model 2 – initial guess of bottom-hole pressure of each well

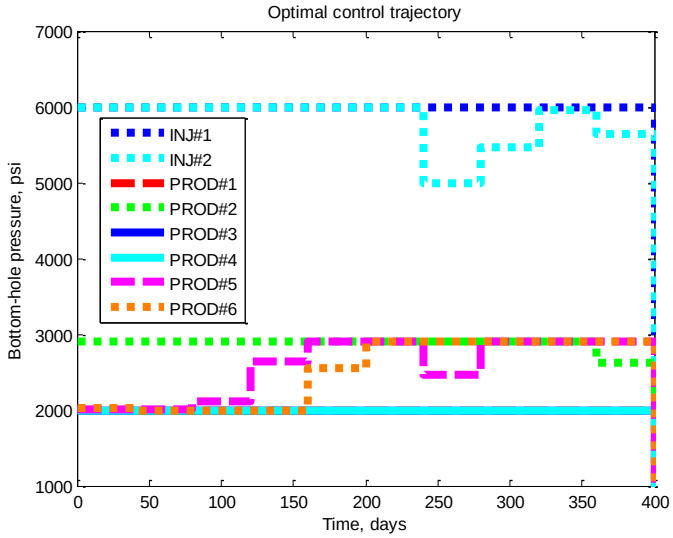

Figure 51: Synthetic model 2 – optimal bottom-hole flowing pressure of each well

The optimal control trajectory is verified with the full order model and the result is compared in the Table 11. It can be seen that the actual NPV improvement is 6.46%

Table 11: Synthetic model 2 – optimal response from the flow network model on the flow network and the full order model

	Flow network model		Full order model	
	Initial guess	Optimal control	Initial guess	Optimal control
Total oil production (MMSTB)	7.669	8.097	8.128	8.665
Total water production (MMSTB)	1.111	1.295	0.968	1.064
Total water injection (MMSTB)	8.781	9.394	9.103	9.770
NPV (MMUSD)	669.122	704.209	712.103	758.139
Improvement	5.24%		6.46%	

The field cumulative injection and production from the full-order model is shown in Figure 52. Overall, it can be seen that the NPV is mainly improved by increases in oil production, although the water injection and production is also increased.

The optimal control obtained by using this surrogate model is compared with the optimal control obtained from the full-order model production optimization in Table 12. It can be seen that the NPV improvement is very similar, although the cumulative injection/production responses are a bit different. The injection/production responses from the full-order optimization, shown in Figure 53, also have a similar trend as the one obtained by flow-network model, shown in Figure 52.

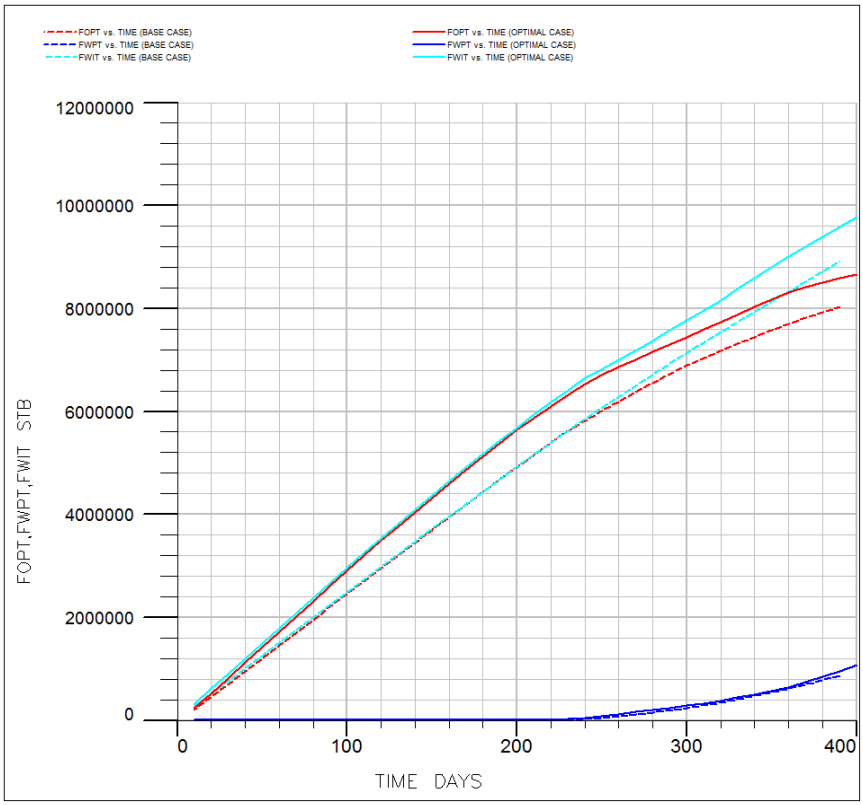

Figure 52: Synthetic model 2 – responses from the full-order model using the initial guess and the optimal control trajectory obtained from the flow network model

Table 12: Synthetic model 2 – comparison of production optimization using the full-order model and the flow network model

	Using flow network model	Using full-order model
Initial guess NPV (MMUSD)	712.103	712.103
Optimal NPV (MMUSD)	758.139	757.068
Improvement	6.46%	6.31%

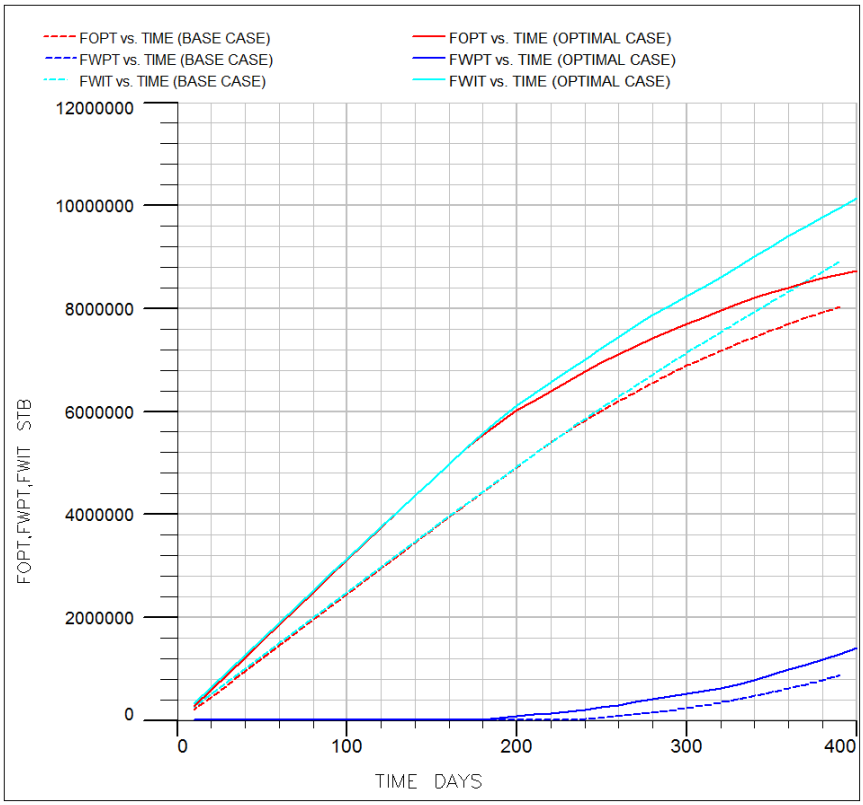

Figure 53: Synthetic model 2 – response from the full-order model using the initial guess and the optimal control trajectory obtained from the full-order model

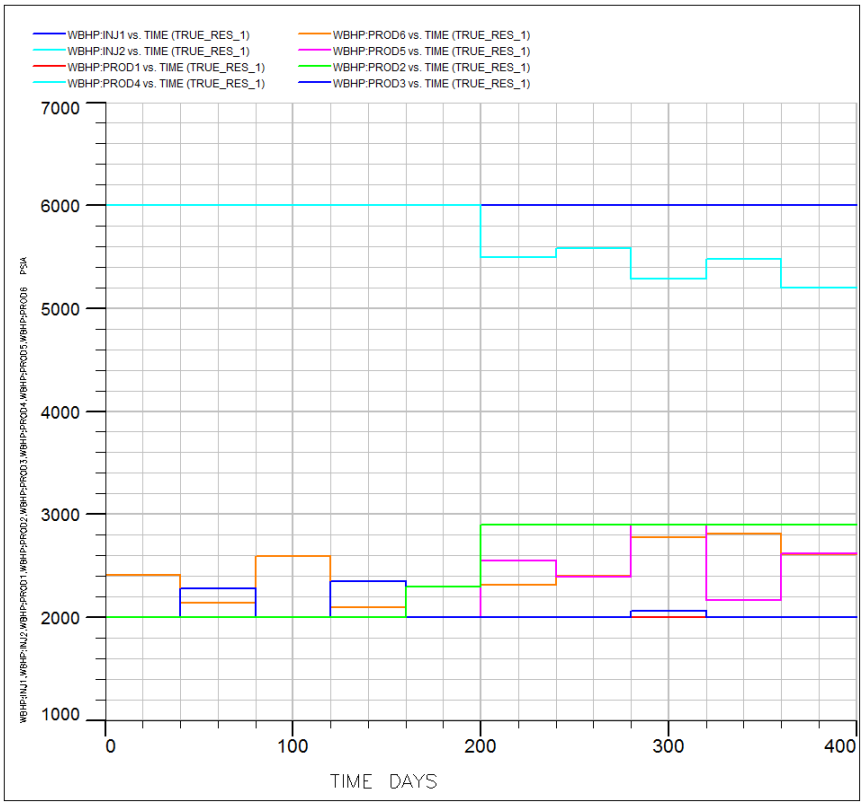

Figure 54: Synthetic model 2 – optimal control trajectory from full-order model optimization

From Figure 51 and Figure 54, the optimal control obtained from both the full-order and flow network models are very similar. The well INJ#2 has lower bottom-hole pressure, and PROD#2, PROD#5, and PROD#6 are operated at higher bottom-hole pressure.

Speed-Up

Similar to the comparison given in the synthetic model number 1, the elapsed time for each simulation, both the full-order and flow network models, with respect to different training control trajectories for synthetic model number 2 is given in Figure 55.

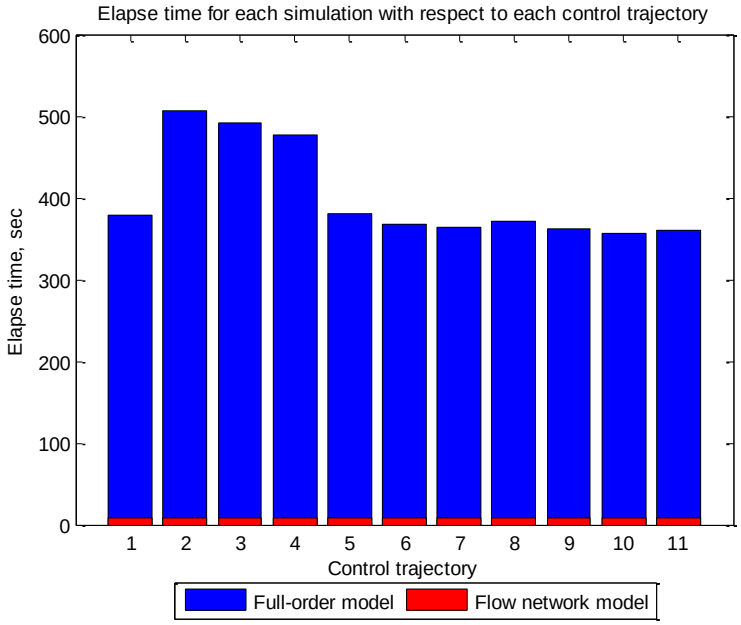

Figure 55: Synthetic model 2 – elapse time of the full-order and the flow network model on the control trajectories used to train the flow network model

From Figure 55, the flow network model is approximately 45 times faster than the full-order model. This is even better than the speed-up found in the synthetic model number 1. This is mainly because the synthetic model number 2 has a larger reduction in the number of grid blocks. In this model, the number of grids is reduced from 13200 to 120 grids, which is a 110 times reduction.

FUTURE RESEARCH

This research demonstrates that the flow network modeling can be used for the given examples; however, many related issues were discovered in the model development process.

The first issue is the modeling error introduced by dimension reduction. The main idea of the flow network model is to transform the multi-dimensional flow into the network of one-dimensional flow. This may be similar to trying to use one single streamline to approximate the flow which would not be an accurate representation. It has been tested that the flow network model cannot reproduce the response, generated from the homogeneous quarter of the 5-spot waterflood problem, perfectly. The possible solution for this is to use dynamic pseudo relative permeability or to use more than one connection between each pair of wells.

Secondly, the discretization error would be small when the grid size is very small. On the other hand, the flow network model is constructed using a small number of grids in each connection. Hence, each grid would be relatively big, causing the numerical dispersion. The possible solution for this is to use the pseudo relative permeability to control numerical dispersion.

In addition, it is sometimes difficult to calibrate the model to some specific responses from some specific geological models. This is especially pronounced when the producers are controlled by flow rate. The flow network model is built based on the dynamic properties of the model, i.e. the drainage area and the quality of the reservoir in

the corresponding flow area. In some cases, when the dynamics of the problem changes drastically, we may not be able to match the response with one single flow network model. This is very similar to the streamline simulation; we have to update the streamline once the pressure field is altered significantly.

In this research, the objective function in the model calibration does not contain any information about the prior knowledge of the reservoir. Although it is not required that the flow network model must have a good agreement to the full-order model in terms of the geological and dynamic interpretation, a flow network model with more similar properties to the full-order model might be considered to be a better model. It might be achieved by designing the initial guess of the flow network model parameters using the prior knowledge from the full-order model. The connection linking any two wells with high permeability could be initialized with high permeability values. In addition, one can penalize the mismatch between the desired parameters, designed from the prior knowledge, and the parameters in each iteration. This would make the model in-line with the prior geological knowledge and might be more predictive.

In the production optimization aspect, the optimal production strategy obtained from the flow network model might not be optimal in the full-order model. It would be better to verify the optimality of the obtained control on the full-order model. If it is optimal, then it can be used directly; otherwise, the flow network model might need to be re-trained with the optimal control, previously obtained, and the production optimization can be repeated. We can implement this in the iterative manner until the

real optimal solution is found. This is called the ‘nested approach’, proposed by van Doren et al. (2006).

This research also demonstrates that the flow network model can be used to perform production optimization for the rate allocation problem. However, because there is no spatial interpretation in the flow network model, it might not be used to specify the well location for further development. The full-order model is still required for the well placement problem.

In the implementation aspect, the semi-implicit formulation is used in this research. We sometimes experienced the numerical stability problem, especially in the calibration process, where the grid dimension and grid permeability is changed during the iterations. Another possible improvement is to implement the fully implicit formulation with the Newton-Raphson technique; this would make the flow network model more stable, and hence make the process more robust. In addition, automatic time-stepping should also be implemented. Once the code is optimized, we can then measure how much speed-up we gain with this kind of model.

In the application aspect, only two-phase two-dimensional waterflood problem has been tested. The flow network model might be applied to the more complex problem, e.g. three-phase flow problems and three-dimensional problems. In this case, the flow network model parameters would need to be modified to capture the required additional physics governing the flow.

In this research, the objective is to utilize the flow network model as a surrogate model for production optimization. The full-order model is assumed to be known.

However, regardless of the prediction capability, the flow network model can be built by using only the input and output relationships, i.e. injection/production data and how each well is controlled. Therefore, it is possible to utilize the flow network model as a standalone model, which could even be more beneficial and more computationally efficient. Note that the other prior knowledge of the reservoir like estimated porosity, permeability, initial fluid in place, and the well configuration can still be included to guide the model calibration.

CONCLUSION

In this thesis, the use of reduced-order modeling is investigated in order to mitigate the high computational effort associated with the production optimization process in large-scale reservoir simulation models. Many reduced-order modeling techniques have been proposed and utilized in the industry. Some of these techniques may involve complex mathematical manipulations, whereas some of them may use too simplified physics, and hence lose the long term prediction capability. This thesis proposes the flow network model as an alternative reduced-order modeling technique to be used particularly in the production optimization framework.

The flow network model is constructed to capture the input and output response of the wells/reservoirs, i.e. injection and production data. Every well in the system is connected to one another by one-dimensional finite difference reservoir simulation models, which are standard in the industry. The multi-dimensional flow domains are reduced to the network of one-dimensional flow system.

The flow network model is built and trained by the injection and production data, generated from the full-order model, using the robust training technique. This yields a model that is less sensitive to the control trajectory, and hence more suitable for the production optimization process.

The proposed flow network model provides a useful and fast tool for characterizing inter-well connectivity, estimating drainage volume between each pair of

wells and predicting reservoir production over an extended period of time for optimization purposes.

This new concept is demonstrated using the synthetic waterflood problems from model construction to production optimization. The resulting optimal control trajectory is compared with the full-order model production optimization result. Note that although the optimality of the control trajectory, obtained from the flow network model optimization, is not verified in the full-order model, the most important thing is that the NPV is improved from the initial guess, and the result is very similar to the production optimization using the full-order model.

The bottom line is a computationally demanding process like production optimization could be done much more efficiently. The full-order model is only required to generate the training data for the flow network model calibration and to verify the optimal control obtained from production optimization. Most of the calculation is performed using the flow network model.

All in all, the flow network modeling developed here is a promising technique to mitigate the computational burden associated with production optimization, which involves several forward simulation runs of large-scale reservoir models. It adds to the portfolio of similar methods developed elsewhere. Considering that this research is the first step towards an innovative methodology to develop and utilize the flow network model, further study can be made to gain more insights on both theoretical and practical aspects of the flow network model in various applications.

REFERENCES

Alhuthali, A., Oyerinde, D., and Datta-Gupta, A. 2007. Optimal Waterflood Management Using Rate Control. *SPE Reservoir Eval & Eng* **10** (5): 539-551. SPE-102478-PA. http://dx.doi.org/10.2118/102478-PA.

Aziz, K. and Settari, A. 1979. *Petroleum Reservoir Simulation*. London: Applied Science Publishers.

Brouwer, D.R. and Jansen, J.D. 2002. Dynamic Optimization of Water Flooding with Smart Wells Using Optimal Control Theory. Paper SPE 78278 presented at the European Petroleum Conference, Aberdeen, United Kingdom, 29-31 October. http://dx.doi.org/10.2118/78278-MS.

Cardoso, M.A. and Durlofsky, L.J. 2010. Use of Reduced-Order Modeling Procedures for Production Optimization. *SPE J.* **15**(2): 426-435. SPE-119057-PA. http://dx.doi.org/10.2118/119057-PA.

Christie, M.A. and Blunt, M.J. 2001. Tenth Spe Comparative Solution Project: A Comparison of Upscaling Techniques. Paper SPE 66599 presented at the SPE Reservoir Simulation Symposium, Houston, Texas, 11-14 February. http://dx.doi.org/10.2118/66599-MS.

ECLIPSE Reservoir Engineering Software. 2011. Schlumberger, http://www.slb.com/services/software/reseng/eclipse.aspx.

Ertekin, T., Abou-Kassem, J.H., and King, G.R. 2001. *Basic Applied Reservoir Simulation*. Richardson, Texas: Textbook Series, SPE.

Griva, I., Nash, S.G., and Sofer, A. 2009. *Linear and Nonlinear Optimization*. Philadelphia, Pennsylvania: Society for Industrial and Applied Mathematics.

Jansen, J.D., Brouwer, D.R., Naevdal, G. et al. 2005. Closed Loop Reservoir Management. *First Break* **1**(23): 43-48.

Jansen, J.D., Bosgra, O.H., and Van den Hof, P.M.J. 2008. Model-Based Control of Multiphase Flow in Subsurface Oil Reservoirs. *Journal of Process Control* **18** (9): 846-855. http://dx.doi.org/10.1016/j.jprocont.2008.06.011.

MATLAB®, version 7.12.0.635. 2011. Natick, Massachusetts: The Mathworks, Inc.

Peaceman, D.W. 1983. Interpretation of Well-Block Pressures in Numerical Reservoir Simulation With Nonsquare Grid Blocks and Anisotropic Permeability. *SPE J.* **23**(3): 531-543. SPE-10528-PA. http://dx.doi.org/10.2118/10528-PA

Sayarpour, M. 2008. Development and Application of Capacitance-Resistive Models to Water/CO_2 Floods. PhD dissertation, University of Texas at Austin, Austin, Texas (August 2008).

van Doren, J., Markovinović, R., and Jansen, J.D. 2006. Reduced-Order Optimal Control of Water Flooding Using Proper Orthogonal Decomposition. *Computational Geosciences* **10** (1): 137-158. http://dx.doi.org/10.1007/s10596-005-9014-2.

van Essen, G.M., Zandvliet, M.J., Van den Hof, P.M.J. et al. 2006. Robust Waterflooding Optimization of Multiple Geological Scenarios. Paper SPE 102913 presented at the SPE Annual Technical Conference and Exhibition, San Antonio, Texas, 24-27 September. http://dx.doi.org/10.2118/102913-MS.

Weber, D.B. 2009. The Use of Capacitance-Resistance Models to Optimize Injection Allocation and Well Location in Water Floods. PhD dissertation, University of Texas at Austin, Austin, Texas (August 2009).

VITA

Pongsathorn Lerlertpakdee received his Bachelor of Engineering degree in Petroleum Engineering with 1st class honors from Chulalongkorn University, Thailand, in 2006. He has been working for PTT Exploration and Production Public Company Limited, Thai national company, since then. His work involves both reservoir engineering and production engineering aspects. He entered the Petroleum Engineering graduate program at Texas A&M University in September 2010, sponsored by his employer. His research interests include production optimization and closed loop reservoir management. He graduated with the degree of Master of Science in Petroleum Engineering from Texas A&M University in August 2012.

Mr. Pongsathorn may be reached at Harold Vance Department of Petroleum Engineering, Texas A&M University, 3116 TAMU – 407 Richardson Building, College Station, Texas 77843-3116. His email is pongsathornl@gmail.com.